UNIVERSITA' VITA-SALUTE SAN RAFFAELE

CORSO DI DOTTORATO DI RICERCA INTERNAZIONALE IN MEDICINA MOLECOLARE

Curriculum in Basic and Applied Immunology and Oncology

DISSECTING THE ROLE OF CLPP IN MULTIPLE MYELOMA

DoS: Dr. Simone Cenci
Second Supervisor: Dr. Nikhil C. Munshi

Tesi di DOTTORATO di RICERCA di Tommaso Perini
matr. 013904
Ciclo di dottorato XXXIV
SSD: BIO/13, MED/06, MED/15

Anno Accademico 2020/2021

Allegato 2

CONSULTAZIONE TESI DI DOTTORATO DI RICERCA

Il/la sottoscritto/*I* TOMMASO PERINI

Matricola / *registration number* 013904

natO a/ *born at* BUSSOLENGO (VR)

il/*on* 10/06/1987

autore della tesi di Dottorato di ricerca dal titolo / *author of the PhD Thesis titled*

Dissecting the role of ClpP in Multiple Myeloma

☐ AUTORIZZA la Consultazione della tesi / AUTHORIZES *the public release of the thesis*

☒ NON AUTORIZZA la Consultazione della tesi per 12 mesi /DOES NOT AUTHORIZE *the public release of the thesis for* 12 *months*

a partire dalla data di conseguimento del titolo e precisamente / *from the PhD thesis date, specifically*

Dal / *from* 02/03/2022 Al / *to* 02/03/2023

Poiché /*because*:

☐ l'intera ricerca o parti di essa sono potenzialmente soggette a brevettabilità/ *The whole project or part of it might be subject to patentability;*

☑ ci sono parti di tesi che sono già state sottoposte a un editore o sono in attesa di pubblicazione/ *Parts of the thesis have been or are being submitted to a publisher or are in press;*

☐ la tesi è finanziata da enti esterni che vantano dei diritti su di esse e sulla loro pubblicazione/ *the thesis project is financed by external bodies that have rights over it and on its publication.*

Data /Date 31/01/2022 Firma /Signature

DECLARATION

This thesis has been composed by myself and has not been used in any previous application for a degree. Throughout the text I use both “I” and “We” interchangeably.

All the results presented here were obtained by myself, except for:

1. RNA sequencing data of primary samples of patients were generated by the laboratory of Dr. Nikhil Munshi (Dana Farber Cancer Institute, Boston, MA, USA). RNA-seq analysis (Results, figure 10, figure 11, figure 15B) was performed in collaboration with Dr. Mehmet Samur (Dana Farber Cancer Institute, Boston, MA, USA).
2. Immunohistochemistry of bone marrow biopsies (Results, figure 15A) was performed by Dr. Maurilio Ponzoni (Department of Pathology, San Raffaele Scientific Institute, Milan, Italy).
3. Seahorse experiments (Results, figure 18A, figure 19) were performed in collaboration with Dr. Laura Cassina (Laboratory of Molecular basis of cystic kidney disorders, Division of Genetics and Cell Biology, San Raffaele Scientific Institute, Milan, Italy).
4. Polysome profiling (Results, figure 25A-B) was performed in collaboration with Dr. Massimo Resnati (Laboratory of Age Related Diseases, San Raffaele Scientific Institute, Milan, Italy).
5. RNA-sequencing of MM cell lines (Results, figure 30, figure 31) was performed by the Center for Omic Sciences (COSR, San Raffaele Scientific Institute, Milan, Italy). Data analysis was performed in collaboration with Dr. Eugenia Bezzecchi (COSR, San Raffaele Scientific Institute, Milan, Italy).
6. Metabolomics experiments (Results, figure 33, figure 34) were performed in collaboration with Dr. Davide Stefanoni (Department of Biochemistry and Molecular Genetics, University of Colorado Anschutz Medical Campus, Aurora, CO, United States).

All sources of information are acknowledged by means of reference.

Abstract

Despite the efficacy of targeted treatments, multiple myeloma (MM) is still incurable, urging to identify novel vulnerabilities to design more effective therapies. Mitochondria are emerging therapeutic targets in oncology for their crucial role not only as cellular powerhouses, but also in signalling, redox homeostasis, initiation of apoptosis, production of metabolites, and supply of biosynthetic precursors.

Owing to intensive immunoglobulin production, myeloma cells are heavily reliant on protein homeostasis and experience significant exposure to mitochondrial stressors. We hypothesized that myeloma cells depend on the prototypical mitochondrial stress-adaptive pathway, the mitochondrial unfolded protein response (UPR^{mt}), for their fitness and survival. We tested its activation status and its manipulation as a possible tool against myeloma. We found that while a clear upregulation of the UPR^{mt} signature is evident in MM, its regulation is independent of the master transcription factor ATF5, so far believed to mediate the mammalian UPR^{mt}.

One of the key players of the UPR^{mt} and gatekeeper of mitochondrial homeostasis is ClpP, a resident mitochondrial protease suggested to maintain oxidative phosphorylation efficiency. Prompted by its distinctive expression in malignant plasma cells, we investigated the role of ClpP in multiple myeloma cells and tested it as a possible anti-myeloma target. We found that ClpP downregulation leads to disappearance of MM cells from culture due to apoptosis or cell cycle arrest. Surprisingly, toxicity extends to glycolytic cell lines and we demonstrated that ClpP knockdown has no effects on mitochondrial oxygen consumption by MM cells, thus unveiling an energy-independent vulnerability. By combining RNA-seq, proteomics, and metabolomics we identified unprecedented and unexpected cellular features regulated by ClpP, including protein translation both in the cytosol and in mitochondria, impairment of fatty acid metabolism with accumulation of acyl-carnitines and long chain unsaturated fatty acids, deregulation of the polyamine pathway with depletion of spermine, spermidine and putrescine. Intriguingly, we also detected a strong impact on interferon-regulated pathways, hinting at mitochondria and ClpP as possible tools to manipulate MM immunogenicity.

Our data suggest that ClpP is vital to MM cells due to a novel non-bioenergetic function, and pave the way for its further evaluation as a therapeutic target.

Table of contents

Acronyms and abbreviations

ADEPs: acyldepsipeptides
$ATF5^{kd}$: ATF knockdown
BM: bone marrow
CCLE: Cancer Cell Line Encyclopedia
CI / CII: complex I / complex II (of the electron transport chain)
$ClpP^{kd}$: ClpP knockdown
$ClpP^{WT\text{-}FLAG}$ / $ClpP^{MUT\text{-}FLAG}$: (cells expressing a) wild type /mutant FLAG tagged ClpP
ClpX: Caseinolytic Mitochondrial Matrix Peptidase Chaperone Subunit X
CoASH: coenzyme A
CRAB: hypercalcemia, renal failure, anemia, bone lesions
CRISPR: clustered regularly interspaced short palindromic repeats
GRA: glycolytic rate assay
GSEA: Gene Set Enrichment Analysis
hClpP: (human) ATP-dependent Clp protease proteolytic subunit
HMM: hyperdiploid multiple myeloma
IFN: interferon
Ig: immunoglobulins
IPTG: isopropil-β-D-1-tiogalattopiranoside
ISG: interferon stimulated genes
ISR: integrated stress response
LC-MS/MS: liquid chromatography-tandem mass spectrometry
LNGFR: low affinity nerve growth factor
MM: multiple myeloma
mtDNA: mitochondrial DNA
MTS: mitochondrial targeting sequence
OCR: oxygen consumption rate
OTC: ornithine transcarbamylase
OXPHOS: oxidative phosphorylation
PCA: principal component analysis
PCs: plasma cells
PUFA: poly-unsaturated fatty acids
RNA-seq: RNA sequencing
ROS: reactive oxygen species
TAILS: terminal amine isotope labeling of substrates
TCA cycle: tricarboxylic acid cycle
UPR: unfolded protein response
UPR^{mt} : mitochondrial unfolded protein response

List of figures and tables

Introduction

Multiple Myeloma

Multiple myeloma (MM) is an incurable malignancy originating from differentiated plasma cells (Siegel *et al*, 2016). It accounts for 10%–15% of all hematological cancers, with a worldwide incidence of around 160000 cases and 100 000 deaths per year (Ludwig *et al*, 2020). Even with the use of high-dose chemotherapy and the development of novel therapeutic agents (proteasome inhibitors, immunomodulatory agents and immunotherapies), this diseases remains incurable, with only a minority of patients reaching long term remission (S.K. Kumar *et al.* 2014). In fact, while median overall survival of MM patients has reached 10 years, approximately 25% of patients will die within 3 years from diagnosis (Kristinsson *et al*, 2014). Therefore, the complexity and challenge of MM treatment still urge us to identify novel cellular vulnerabilities to devise new treatments and strategies aimed to deliver the *coup de grâce* to this still incurable cancer (Gulla & Anderson, 2020).

[The following paragraph on MM pathogenesis was previously published in the manuscript "The immunity-malignancy equilibrium in multiple myeloma: lessons from oncogenic events in plasma cells" of which I am first author].

Plasma cells (PCs) are postmitotic, or infrequently dividing, cells, originated as terminal effectors of activated B cells within the germinal center reaction. PCs are responsible for immunoglobulin (Ig) production and are localized in the spleen, gut, and bone marrow (BM) (Tellier & Nutt, 2019; Nutt *et al*, 2015). A small subset of long-lived PCs survives for years in the BM niche and is responsible for individual serological memory. In healthy individuals, long-lived PCs account for less than 1% of BM cellularity. During the development of precursor conditions and then progression to overt MM, a clone of PCs accumulates several genomic hits, acquires a proliferative advantage, and colonizes the BM in multiple foci (Kumar *et al*, 2017; Bergsagel & Kuehl, 2005). Genomic alterations at the basis of MM pathogenesis do not appear in a linear process but rather in a heterogeneous and branched scheme, adding complexity to the disease and favoring the emergence of drug-resistant subclones (Maura *et al*, 2019; Morgan *et al*,

2012). The initial transformation is not caused by specific mutations in single genes but rather by large chromosomal events like translocations or copy number variations. Indeed, 50%–60% of MM cases are hyperdiploid multiple myeloma (HMM), characterized by trisomies of odd numbered chromosomes (3, 5, 7, 9, 11, 15, 19, and 21), while non-HMM are characterized by translocations involving the IgH locus (chromosome 14) and MMSET/FGFR3 t(4;14) (11%); CCND1 t(11;14) (15%); CCND3 t(6;14) (<1%); MAF t(14;16) (3%); or MAFB t(14;20) (1.5%) (Kumar *et al*, 2017; Bergsagel & Kuehl, 2005). A common consequence in both HMM and non-HMM is cell cycle deregulation hallmarked by overex- pression of cyclin D (CCND) family members and activation of NF-kB and MAPK signaling pathways (Morgan *et al*, 2012; Bergsagel *et al*, 2005; Hurt *et al*, 2004). During disease evolution and progression, secondary and late events accumulate, showing diversity both in genes involved and pathways affected. Of note, MYC is a crucial driver of MM evolution and is affected by copy number variation or translocations juxtaposing its gene to the IgH, IgK, and IgL loci or to the super-enhancer of genes like FAM46C and TXNDC5 (Hurt *et al*, 2004; Walker *et al*, 2014; Affer *et al*, 2014; Avet-Loiseau *et al*, 2001; Shou *et al*, 2000). Other secondary events include copy number variations, specific gene mutations, loss of heterozygosity, and epigenetic changes. The most common copy number variations are gain of 1q, and deletions of 1p (involving FAM46C and CDKN2C), 13p (RB1), and 17p (TP53). Other deletions have been identified in genes modulating NF-kB signaling pathway (TRAF3, CYLD, BIRC2, and BIRC3) (Morgan *et al*, 2012).

Myeloma cells start growing within the bone marrow, and mostly retain their ability to secrete a monoclonal immunoglobulin (Ig). Known as M-spike, this easily measurable serum parameter is most useful for diagnosis and monitoring. Deregulated growth and continued Ig production progressively lead to bone marrow failure and end-organ damage, giving rise to the typical MM symptoms (hypercalcaemia, renal insufficiency, anemia, bone disease with lytic lesions or pathological fractures, which are collectively known as CRAB features) (Kumar *et al*, 2017). MM is usually preceded by a premalignant condition called monoclonal gammopathy of undetermined significance (MGUS), which is characterized by the infiltration of clonal plasma cells into the bone marrow and the secretion of monoclonal protein, but no end-organ damage. Historically,

treatment was started at the appearance of CRAB features: with new biomarkers that can identify patients at very high risk of progression to active disease, the diagnostic criteria for monoclonal gammopathies have undergone revisions and allow some patients to commence treatment earlier (Rajkumar *et al*, 2014).

Improved understanding of the biology of myeloma marked the start of an effort to design therapies to address signaling pathways relevant for MM growth and survival (Bianchi & Ghobrial, 2013). However, despite all the scientific efforts to decipher MM biology, very little of current therapy of MM is informed by our understanding of the molecular mechanisms and timing of disease evolution. Indeed, the first two classes of molecules that showed high efficacy, namely proteasome inhibitors and immunomodulatory drugs, have been by far more effective than approaches based on high-quality basic/translational research. Even more surprising, all the genomic characterization on myelomagenesis gave very little insight on to why these drugs should be active in MM. In fact, sensitivity of MM to current treatments does not stem from genetic events specific of malignant cells, but from features of normal plasma cells that are retained during transformation (Boise *et al*, 2014). For this reason, looking for non-oncogene addictions and actionable targets intrinsic to MM biology holds promise against this disease, even independently of its enormous genomic heterogeneity.

Mitochondria in cancer

Mitochondria have been considered damaged in cancer for a long time. This stemmed from the seminal observation by Otto Warburg that cancer cells undergo aerobic glycolysis even in presence of oxygen, and from his inference that this was due to damaged mitochondrial respiration (Warburg, 1956; Weinhouse, 1956). While the ‘‘Warburg effect’’ is a recognized feature of the majority (but not all) of cancer cells, we now know that in most cases cancer cells possess intact mitochondrial respiration, with some cancer types even depending on oxidative phosphorylation (OXPHOS) for survival (Vyas *et al*, 2016). Moreover, in the past few decades our understanding of mitochondria biology and roles extended well beyond the classical “powerhouse of the cell’’ idea. In fact, mitochondria have pleiotropic functions in both physiology and pathology, including the generation of reactive oxygen species (ROS), redox molecules and metabolites,

regulation of cell signaling and cell death, and biosynthetic metabolism. Indeed, among non-energetic functions of ATP, mitochondrial functions implicated in tumor biology include biogenesis, turnover, fission and fusion dynamics, cell death, oxidative stress, metabolism and bioenergetics, signaling, and mtDNA maintenance (**Fig.1**). There is no universal rule for mitochondrial functions in cancer, but the field of mitochondrial biology in malignant cells is rapidly expanding and already showed how they can act as cellular stress sensors guiding cellular adaptation to nutrient depletion and hypoxia during tumorigenesis, or can drive survival during cancer treatment (Vyas *et al*, 2016).

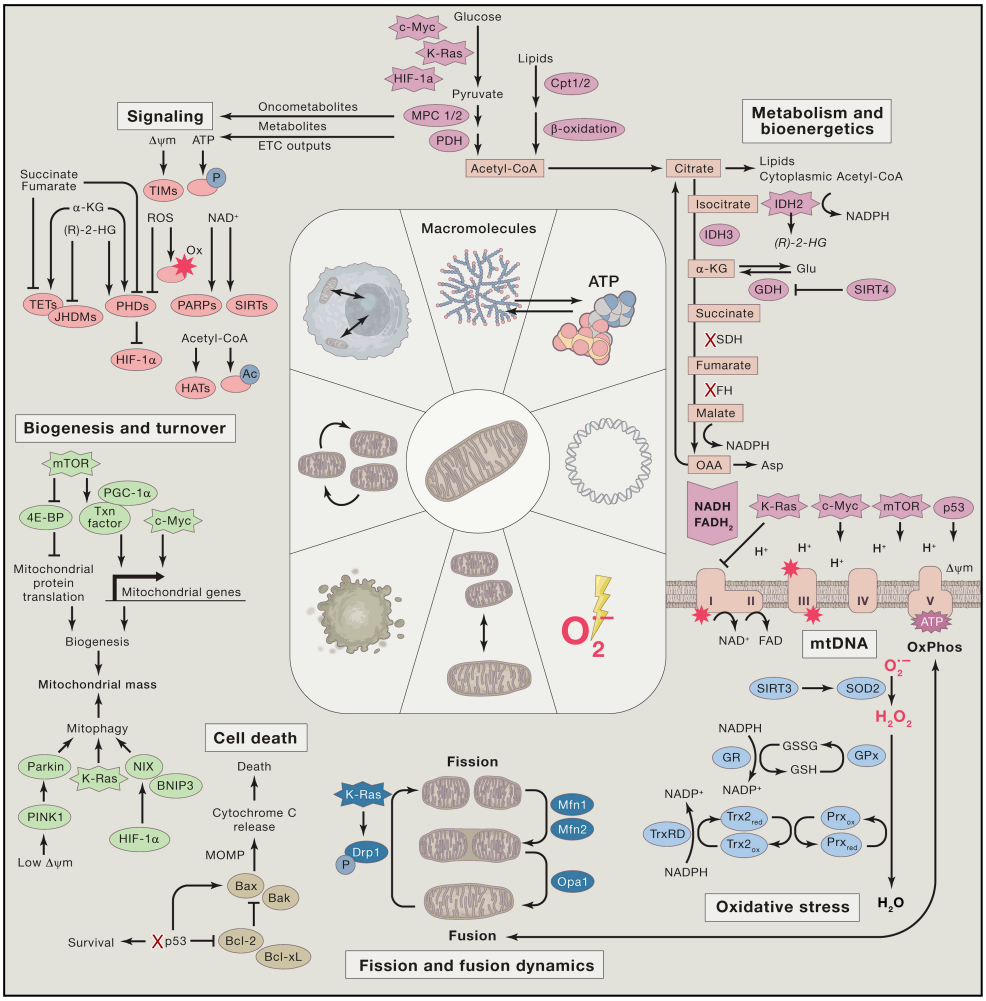

Figure 2. Mitochondrial roles in cancer. *Different mitochondrial functions have been involved in regulation of several apsects of cacncer cell biology, including metabolism and energy production, signalling and production of oncometbolites, regulation of oxidative stress and cell death. From Vyas et al, Cell 2016. (License number 5227611189966)*

Of particular interest in the context of stress sensing are mitochondrial retrograde signals, that render mitochondria crucial signaling hubs able to integrate a variety of information and generate an output that influences the whole cell and are aimed at maintaining mitochondrial homeostasis. Many intermediates of TCA cycle, β-oxidation and of the electron transport chain itself can affect gene transcription via chromatin modification or regulation of cytosolic signaling ways. α-ketoglutarate and acetyl-CoA are the two most notable examples, able to regulate broad transcriptional programs and crucial cellular functions (Carey *et al*, 2014; Lee *et al*, 2014; Wellen *et al*, 2009). A special mention in the landscape of mitochondrial signaling is needed for oncometabolites. These are metabolites produced by oncogenic mutations in IDH enxymes (IDH1 and IDH2) or in enzymes succinate dehydrogenase (SDH) and fumarate hydratase (FH). The subsequent accumulation of (R)-2-hydroxyglutarate, succinate and fumarate is a major tumorigenic event due to their ability to act as competitive inhibitors of α-KG-dependent chromatin-modifying enzymes (Dang *et al*, 2009; Nowicki & Gottlieb, 2015). The relevance of retrograde signaling is also demonstrated by the effects of mitochondrial calcium fluxes: any reduction in mitochondrial membrane potential reduces calcium import into mitochondria, thus increasing its cytosolic concentration. This mainly affects calcineurin, with effects on NF-kB activity and AKT phosphorylation (Wallace, 2012), leading transcriptional upregulation of more than 120 proteins, involved in several cellular homeostatic functions and regulation of tissue invasiveness and tumorigenesis (such as cathepsin L, AKT1, TGF-β, p53) (Guha *et al*, 2007, 2010). Similarly, increased ROS production by dysfunctional mitochondria can promote neoplastic transformation by affecting HIF1α, FOS-JUN and the MAPK pathway (Weinberg *et al*, 2010; Chandel *et al*, 2000; Liu *et al*, 2005).

Mitochondrial UPR

Recently, a specific response to accumulation of misfolded proteins in the mitochondrial matrix has been identified, termed mitochondrial unfolded protein response (UPR^{mt}) because of its similarities with the better-characterized endoplasmic reticulum unfolded protein response (UPR) (Yun & Finkel, 2014). Originally identified in response to expression of a mutant form of the mitochondrial protein ornithine transcarbamylase (OTC), activation of UPR^{mt} leads to upregulation of a number of

mitochondrial-specific protein chaperones (Zhao *et al*, 2002). However, recent works have highlighted that the effects of UPR^{mt} are much broader and drive metabolic shifts towards glycolysis, mitochondrial biogenesis and upregulation of innate immune responses (Pellegrino *et al*, 2014; Nargund *et al*, 2015). In line with these widespread effects, UPR^{mt} has been implicated in regulation of development, aging, cardioprotection and cancer (Yun & Finkel, 2014).

A detailed understanding of activation of this response is now available in lower organisms like *C. elegans*, where a single transcription factor (activating transcription factor associated with Stress-1 (ATFS-1)) has been identified as the main activator. ATFS-1 exhibit both a nuclear and a mild mitochondrial targeting sequence (MTS): when mitochondria are healthy and transmembrane potential is normal, ATFS-1 is constantly imported into mitochondria and degraded. In cases of loss of mitochondrial potential, ATFS-1 MTS is too weak to allow import, and the protein is translocated to the nucleus (Nargund AM, Pellegrino MW, 2012; Yun & Finkel, 2014). Indeed, a number of challenges and damages impacting mitochondrial potential can activate this response beyond accumulation of misfolded proteins, including mtDNA depletion, OXPHOS defects, inhibition of mitochondrial protein synthesis, mtDNA mutations, reactive oxygen species, hypoxia, as well as pathogenic bacteria that target mitochondria (**Fig.2**) (Deng & Haynes, 2017).

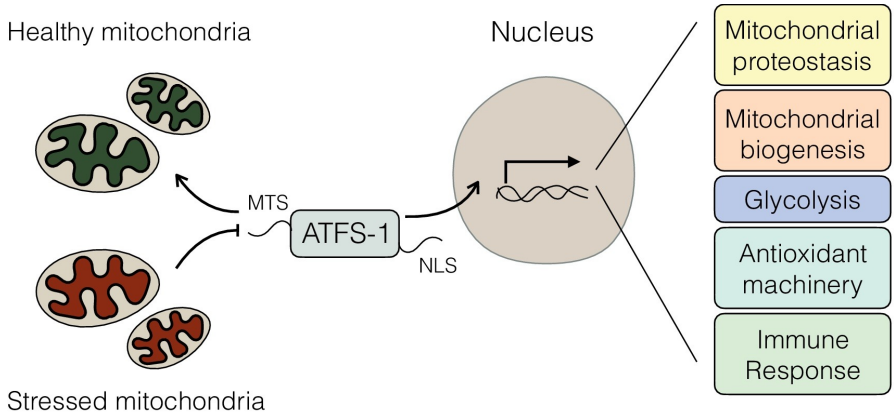

Figure 2. UPR^{mt} signaling in C. elegans*. In presence of mitochondrial dysfunction, ATFS-1 is no longer imported into mitochondria and degraded but rather transcolcates to the nucleus and drives wide transcpritional programs. From Deng and Haynes, Semin Canc Biol, 2017. (License number 5231400864776)*

More recently, an elegant work has proposed the bZip transcription factor ATF5 as the mammalian homologue of ATFS-1. In fact, ATF5 has structural similarities with ATFS-1 (including a weak MTS), induces a similar transcriptional response and has a similar mito-nuclear trafficking. Notably, ATF5 can rescue UPR^{mt} signaling in *atfs-1*-deficient worms and mammalian cells require ATF5 to maintain mitochondrial activity during mitochondrial stress and promote organelle recovery (Fiorese *et al*, 2016). However, other studies are emerging suggesting that UPR^{mt} in mammals is more elaborate not only requires phosphorylation of stress kinase GCN2 but also involves at least CHOP and ATF4 in addition to ATF5, connecting this transcriptional response with a broader activation of the integrated stress response (ISR) **(Fig.3)** (Deng & Haynes, 2017; Horibe & Hoogenraad, 2007; Zhao *et al*, 2002; Zhou *et al*, 2008; Shpilka & Haynes, 2018) .

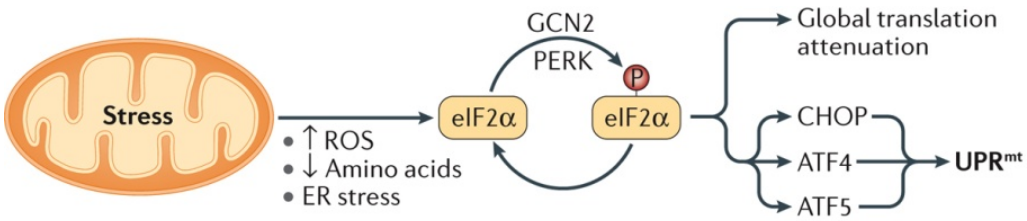

Figure 3. Activation of the mammalian UPR^{mt}. *In mammals ATF5 activity requires activation of eIF2α by the eIF2α kinase GCN2 (and PERK), which results in reduced protein synthesis and the preferential translation of mRNAs harbouring open reading frames in the 5′ untranslated region, such as CHOP, ATF4 and ATF5. From Shpilka and Haynes, Nat rev Mol Cell Biol 2017. (License number 5233690505067)*

UPR^{mt} and cancer

Not surprisingly, recent studies have suggested that the UPR^{mt} might have a role in cancer cell growth and survival **(Fig.4)**. First of all, CHOP, ATF4 and ATF5 are all contributing to tumorigenesis (Kim *et al*, 2000, 2002; Ye *et al*, 2010; Bobrovnikova-Marjon *et al*, 2010; Greene *et al*, 2009; Zhao *et al*, 2002). In particular, ATF5 has been found highly expressed and essential for growth and survival of several cancers from a variety of tissues, including breast, thyroid, colon, pancreas, glia, ovaries and both myeloid and lymphoid cells (Sheng *et al*, 2010; Chen *et al*, 2012; Bisikirska *et al*, 2016; Nukuda *et al*, 2016; Dluzen *et al*, 2011; Angelastro *et al*, 2006; Li *et al*, 2011).

Accordingly, CP-d/n-ATF5-S1, a specific ATF5 inhibitory peptide, is able to induce growth arrest and apoptosis both in cell culture and in xenograft models of prostate cancer, glioblastoma, melanoma and triple-negative breast cancer (Monaco *et al*, 2007; Karpel-Massler *et al*, 2016).

Many UPR^{mt}-induced genes and ATF5 targets are also upregulated and essential in cancer, such as mitochondrial chaperones and proteases. Mitochondrial HSP60 (*HSPD1*), for example, is associated with growth of prostate cancer and differentiation of colorectal cancer (Castilla *et al*, 2010; Hamelin *et al*, 2011). mtHSP70 (*HSPA9*) also promotes tumor cell growth by regulation of p53 and PI3K-Akt in breast and hepatocellular carcinoma (Wadhwa *et al*, 2006; Na *et al*, 2016; Ryu *et al*, 2014; Yi *et al*, 2008). Similarly, the proteases of the mitochondrial matrix LONP1 and ClpP have been described to be upregulated in several malignant cells and to be important in cancer due to their role in the maintenance of mitochondrial activities (Gibellini *et al*, 2014; Quirós *et al*, 2015; Di *et al*, 2016; Cole *et al*, 2015). Overall, inhibition of different steps of the UPR^{mt} is now getting attention as a possible way to interphere with tumor biology and cancer growth.

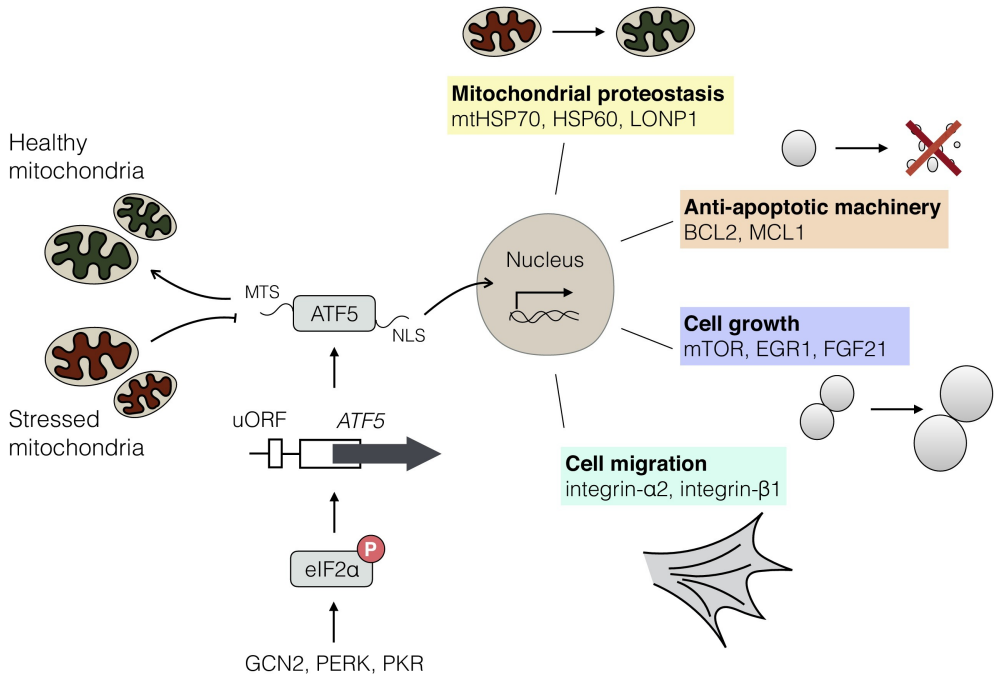

Figure 4. ATF5 role in cancer. *Activation of UPR^{mt} drives a broad protumoral transcpriptional programs that increases mitochondrial fitness and regulates apoptosis, cell growth and migration. From Deng and Haynes, Semin Canc Biol, 2017. (License number 5231400864776)*

Mitochondrial proteases

Beyond their role in responding to mitochondrial stress by increasing degradation of misfolded proteins, mitochondrial proteases (mitoproteases) are essential in maintaining mitochondrial homeostasis and functions in every aspect of cellular life (Quirós *et al*, 2015). Initial studies of turnover of mitochondrial proteome suggested that large-scale processes (namely autophagy) would be responsible for protein degradation, but soon it became clear that both organelle-scale and single-protein scale degradation exist. Indeed, mitochondria are made of both short- and long-lived proteins, with heterogeneous turnover mediated by both intra- and extra-mitochondrial mechanisms (Szczepanowska & Trifunovic, 2021a, 2021b; Rabinowitz, 1973; Fletcher & Sanadi, 1961; Snider *et al*, 2019). In fact, mitoproteases are a potent quality control system involved in the degradation of misfolded and damaged proteins, but also in the physiological processing of nuclear encoded proteins that are imported into mitochondria (Koppen & Langer, 2007). Moreover, they are able to regulate and sometimes deeply alter almost all essential biochemical functions in mitochondria by proteolytic processing of substrates or by degradation of short-lived regulatory proteins. Finally, the activity of mitoproteases also influencese mitochondrial fusion and fission, mitophagy and apoptosis (Anand *et al*, 2013). Mitoproteases have been classified in intrinsic, extrinsic and pseudo-mitoproteases **(Fig.5)**. Intrinsic mitoproteases are a group of twenty proteins that reside in the different mitochondrial compartments or both in the cytosol and mitochondria but work mainly in mitochondria. The five pseudoproteases are structurally similar to proteases but lack catalytic activity and usually regulate their homologous proteases to perform different functions. Finally, at least twenty transient mitoproteases can be identified, that only temporarily translocate to mitochondria to perform specific proteolytic activities (e.g. caspases) (Quirós *et al*, 2015; Szczepanowska & Trifunovic, 2021a).

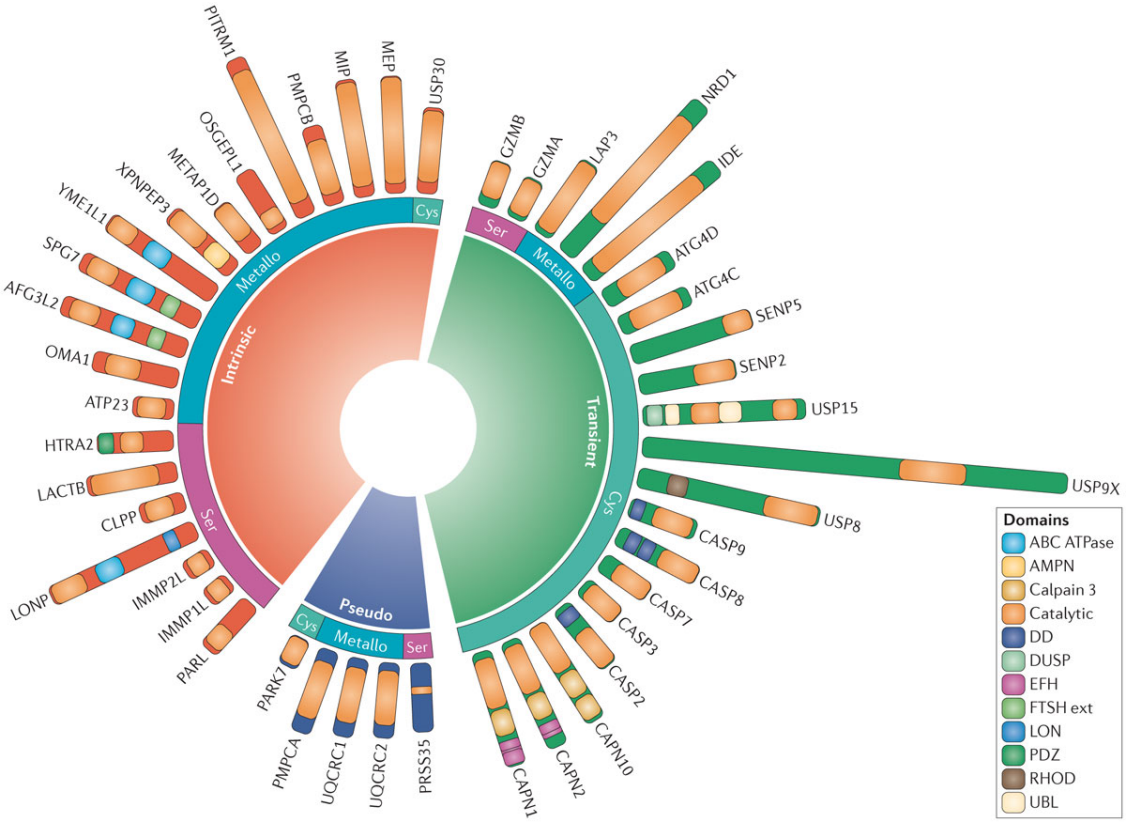

Figure 5. Classification of mitochondrial proteases. *Human mitoproteases are classified into 'intrinsic mitoproteases' that function mainly in the mitochondrion; 'pseudo-mitoproteases' that have structural similarity but lack catalytic activity and 'transient mitoproteases' that translocate to mitochondria for additional proteolytic activities. Each category is also divided into three different subcategories depending on catalytic class. From Quirós et al, Nat Rev Mol Cell Biol, 2015. (License number 5231910909960)*

The majority of quality control inside mitochondria is performed by two oligopeptidases (PITRM1, also known as HPREP and MEP, also known as neurolysin) and four intrinsic AAA+ (ATPases associated with various cellular activities) proteases **(Fig.6)**. These are two membrane integrated metalloproteases (iAAA protease, oriented towards intermembrane space and mAAA protease oriented towards the matrix) and two soluble matrix proteases, namely LONP1 and ClpXP (formed by ClpP and the separate chaperon ClpX) (Quirós *et al*, 2015; Szczepanowska & Trifunovic, 2021a). While both afford potent defenses against proteotoxic insults, recent evidence supports their further role in intramitochondrial gene expression, OXPHOS bioenergetics, metabolism and cofactor biosynthesis. For the purpose of this work, we will focus more in detail on the mitochondrial protease ClpP.

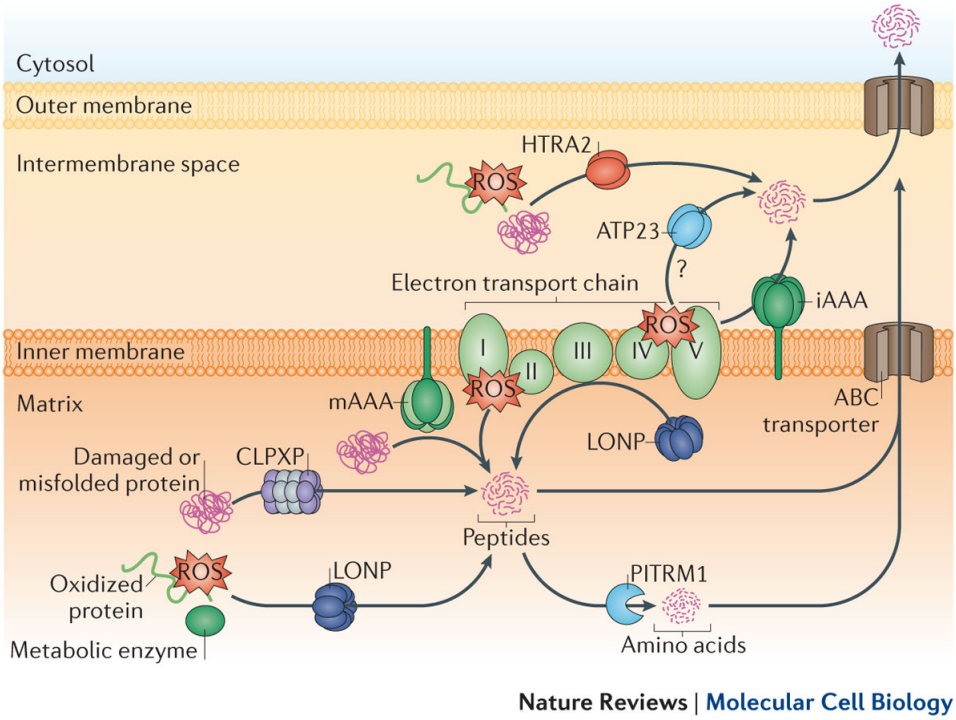

Figure 6. Role of matrix proteases. *Mitoproteases degrade defective proteins in different mitochondrial compartments. ClpXP and LONP take care of the degradation of misfolded, damaged and oxidized proteins in the matrix. From Quirós et al, Nat Rev Mol Cell Biol, 2015. (License number 5231910909960)*

ClpXP

Human ClpP (hClpP, Ser protease ATP-dependent Clp protease proteolytic subunit) assembles in a stable heptameric ring, but has no proteolytic activity and very low peptidase activity by itself. In presence of ATP, it interacts with ATPase chaperone ClpX and assembles in a tetradecamer, forming the proteolytic active complex ClpXP. Structural studies have revealed that ClpXP is made of two heptameric rings of ClpP joined face-to-face with active sites facing the inner chamber and an hexameric ring of hClpX on each end (Kang *et al*, 2005), forming a structure that resembles the cytosolic proteasome **(Fig.7)**. The ClpX ring is responsible for ATP-dependent unfolding and translocation into the catalytic core, and it is needed for substrate recognition (Lowth *et al*, 2012). Most of our understating of ClpXP biology comes from its bacterial homologues, highly identical to eukaryotic counterparts, but the precise impact of this protease on mitochondrial biology is still largely unknown (Liu *et al*, 2014). In bacteria ClpXP regulates viability, growth and cell cycle (Damerau & St. John, 1993; Jenal &

Fuchs, 1998). In humans, ClpP deficiency leads to Perrault syndrome, a recessive pathology characterized by hearing loss and ovarian failure (Jenkinson *et al*, 2013). A mouse model of ClpP deficiency, effectively recapitulates human pathology (Gispert *et al*, 2013).

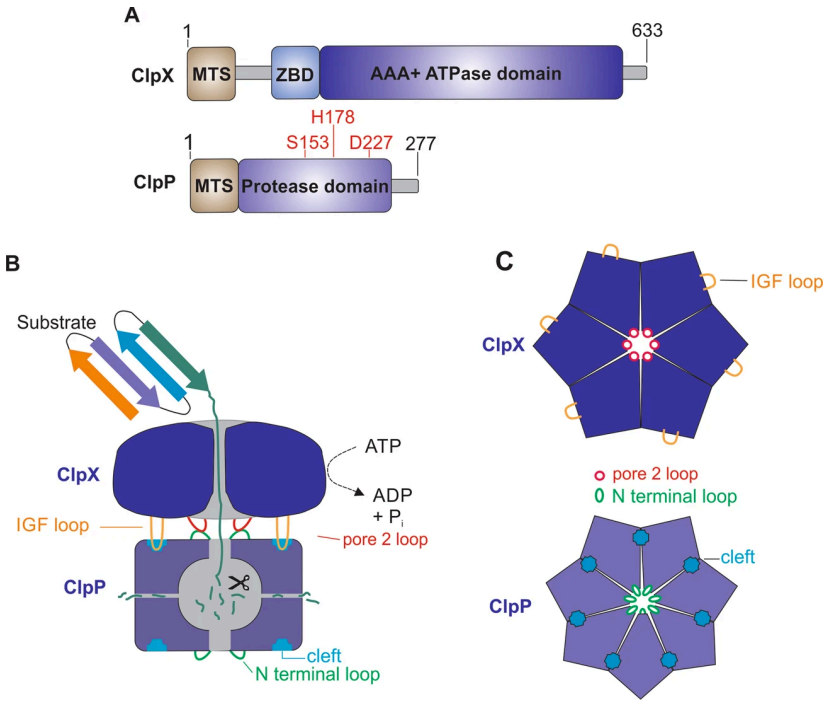

Figure 7. Structure of hClpP*. A) Domain organization of ClpX (top) and ClpP (bottom) with catalytic residues of Ser153, His178, and Asp227. MTS mitochondrial targeting sequence, ZBD zinc-binding domain; AAA+, ATPases associated with diverse cellular activities. B) Schematic representation of the ClpX and ClpP interaction and proteolytic cycle. C) Top view of hexameric ClpX (top) and heptameric ClpP (bottom). From Nouri et al, Cell Death Dis, 2020. (Open access article distributed under the terms of the Creative Commons CC BY license)*

Insights in the role of hClpX are emerging from studies of the effects of ClpP ablation and of ClpP substrates. Identification of ClpP substrates has been attempted with different methods and in different cell types **(Fig.8)**. The first study was performed in leukemic cells and was based on biotinylation of proteins close to ClpP thanks to a chimera of affinity-tagged ClpP and the *E.coli* biotin protein ligase BirA, followed by pulldown and mass spectrometry (Cole *et al*, 2015). In a complementary study, pharmacological activation of ClpP was added to identify proteins whose degradation led to apoptosis of leukemia cells (Ishizawa *et al*, 2019). Two different approaches were used to

charachterize ClpP substrates in mice. First, trapping experiments used a catalytically inactive ClpP harboring the mutation of an active site serine to alanine: the ClpP tetradecamer is formed but entraps the substrates that are inserted in the barrel (Fischer *et al*, 2015; Szczepanowska *et al*, 2016). Finally, a novel proteomic approach named terminal amine isotope labeling of substrates (TAILS) was used to label either light or heavy isotopes protein N-termini and follow their differential accumulation in wild-type and *CLPP* knockout mouse mitochondria (Hofsetz *et al*, 2020). These experiments yielded only partially overlapping results, likely due to differences in techniques and in cell types, but suggest an overall involvement of ClpP in OXPHOS, mitochondrial translation and metabolism.

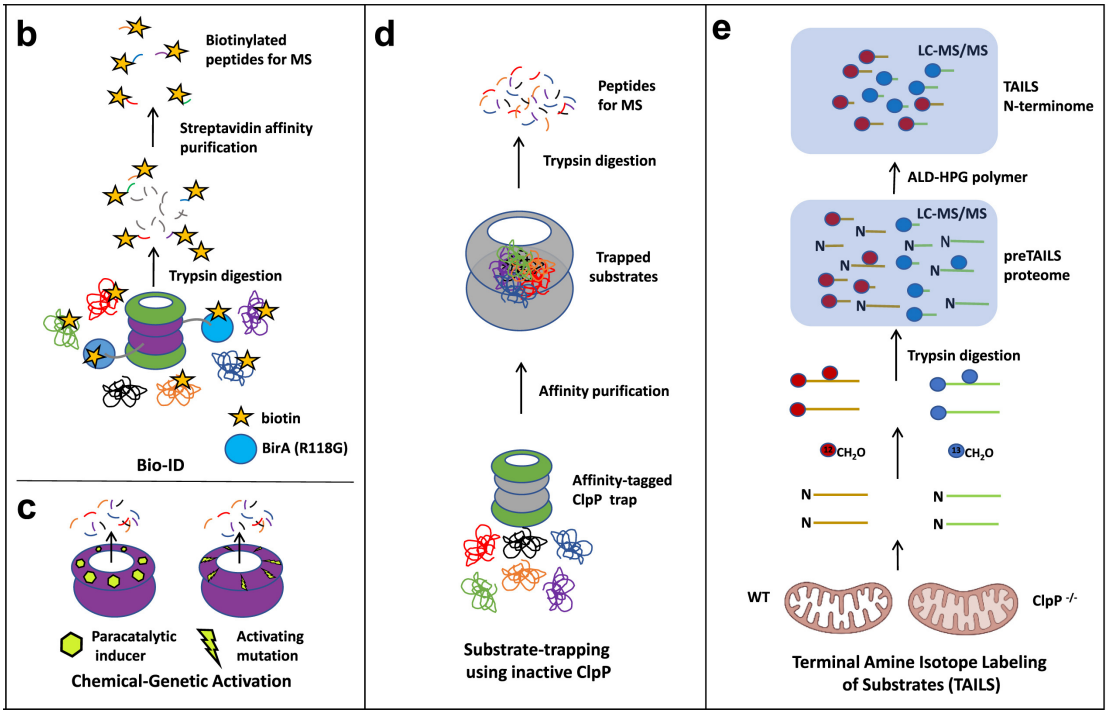

Figure 8. Proteomic methods for identification of ClpP interactors and substrates*. B) Bio-ID of ClpP interactors using a genetic fusion of affinity-tagged ClpP and the E. coli biotinylating enzyme, BirA mutant (R118G). C) Bio-ID of ClpP interactors combined with chemical activation of ClpP with imipridone ONC201. D) Substrate trapping using inactive ClpP (gray double barre) and proteomic means after trypsin digestion. E) Terminal amine isotope labeling of substrates (TAILS) for identifying primary and secondary ClpP substrates via N-terminome analysis. From Mabanglo et al, Curr Opin Chem Biol, 2021. (License number 5226510814117)*

In line with many subunits of respiratory complexes being *bona fide* ClpP substrates, ClpXP deficiency models are associated with a respiratory deficiency in yeast and in

mammals (Fischer *et al*, 2013; Szczepanowska *et al*, 2016; Hofsetz *et al*, 2020). In particular, ClpP has been suggested to exert quality control on the CI catalytic core through a salvage pathway that allows a specific turnover of these subunit to guarantee highly functional CI (Szczepanowska *et al*, 2020). Other commonly identified ClpP substrates include components of CII SDHA and SDHB. In myeloid leukemia cells ClpP knockdown causes accumulation of misfolded SDHA and supposedly impacts OXPHOS efficiency (Cole *et al*, 2015). Further components of the electron transport chain have also been suggested as ClpP substrates, including UQCRC1 and subunits of ATP synthase, but complete validation of these data is still missing (Szczepanowska & Trifunovic, 2021a) **(Fig.9)**.

A less expected role of ClpP is regulation of mitochondrial translation. While all the aforementioned studies identified different subunits of mitochondrial ribosomes as possible substrates of ClpP, an elegant work in knockout mice fibroblasts defined degradation of era-like 12S mitochondrial rRNA chaperone 1 (ERAL1) by ClpP as an essential step in assembly of 28S small ribosomal subunit. Very convincing data support the importance of this mechanism in affecting mitochondrial translation, even if its relevance in mediating cellular phenotypes of ClpP manipulation is unknown (Szczepanowska *et al*, 2016) **(Fig.9)**.

Since mitochondria host an enormous variety of metabolic processes, it is not surprising that ClpXP is suggested to degrade enzymes involved in these processes and therefore influence the metabolic status of cells. A clear example is the ability of ClpXP to degrade enzymes involved in fatty acid metabolism. ACADVL, an acyl-CoA dehydrogenase mediating the beta-oxidation of very-long-chain fatty acids, has been suggested as a preferential substrate of ClpP in mice, but other enzymes have been identified as well, including ACADS, ACADM, ACADSB, ACAT1, DECR1, ECHS1 and HADH (Szczepanowska *et al*, 2016; Fischer *et al*, 2013). Of note, ClpP knockout mice have defects in fatty acid oxidation and thermogenesis, but are protected against metabolic syndrome (Becker *et al*, 2018). Among ClpXP putative substrates are enzymes involved in pyruvate metabolism (PDH1A, PDHB, PDHX, PC) and the enzyme ornithine aminotransferase (OAT), that controls synthesis of proline and glutamate metabolism (Szczepanowska *et al*, 2016; Fischer *et al*, 2013) **(Fig.9)**. However, the impact of ClpP manipulation on these metabolic pathways is unknown.

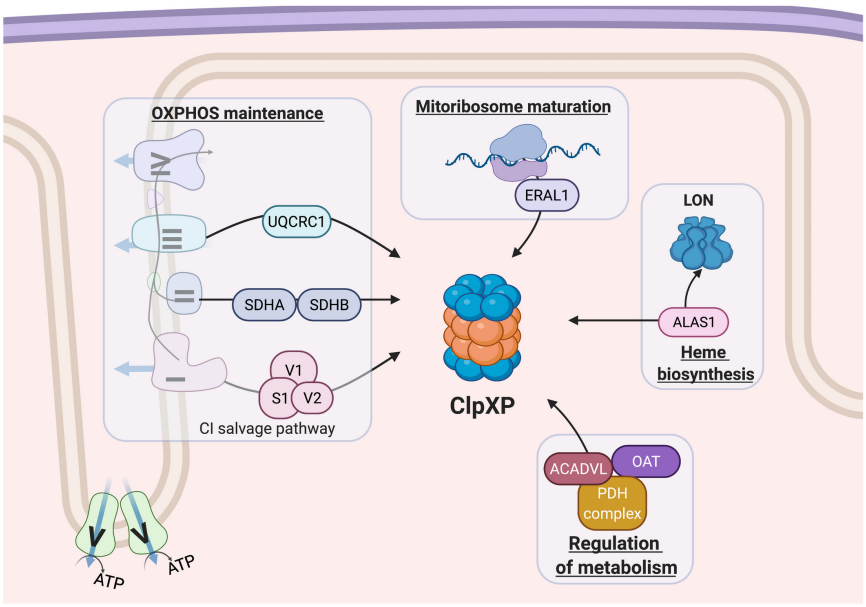

Figure 9. Mammalian ClpXP protease substrates. *ClpXP regulates maturation of mitochondrial ribosomes, degrades several subunits of OXPHOS complexes and metabolic enzymes. From Szczepanowska & Trifunovic, FEBS J, 2021. (License number 5234150724665)*

ClpP and its inhibition in cancer

As previously mentioned, ClpP has been recently recognized as possible target in cancer in a strategy to target tumor dependency on OXPHOS (Nouri *et al*, 2020; Mirali & Schimmer, 2020). In fact, ClpP is overexpressed in several malignancies, both solid (including breast, lung, liver, ovary, bladder, prostate, uterus, stomach, prostate, testis, thyroid, and non-small cell lung cancer) and hematologic, in particular leukemia. Experimental data exist for some of these cancers on ClpP essentiality and on the effects of its manipulation, mainly focusing on deregulation of OXPHOS and subsequent increased ROS production and decreased respiration (Seo *et al*, 2016; Cormio *et al*, 2017; Luo *et al*, 2020; Cole *et al*, 2015). The most extensive work on ClpP as a therapeutic target has been performed in acute leukemia by Cole *et al*, who demonstrated that ClpP knockdown reduced growth and viability of several leukemic cell lines *in vitro*, and hampered engraftment of leukemia progenitors in mouse models. In line with ClpP expected role, its knockdown caused accumulation of SDHA and of misfolded CII, reduced OXPHOS and increased ROS. Of note, they were able to demonstrate that ClpP inhibition with A2-32-01 (a β-lactone (3RS,4RS)-3-(non-8-en-1-yl)-4-(2-(pyridin-3-

ylethyl)oxetan-2-one) affected both leukemia cell lines and primary patient samples and was able to reduce engraftment of primary samples into mouse marrow with no evident toxicities (Cole *et al*, 2015). While these compounds are highly unstable and only partially selective for hClpP and therefore not suitable for clinical development, these data confirm the existence of a therapeutic window for ClpP inhibition in cancer. This conclusion is also supported by the mild phenotype of ClpP mutations in humans (Perrault syndrome) and in mice, as previously mentioned (Jenkinson *et al*, 2013; Gispert *et al*, 2013).

A different strategy to target ClpP has also been proposed. Different classes of small molecules that hyperactivate ClpP exist, leading to uncontrolled but selective degradation of ClpP substrates. They do not bind directly ClpP but rather ClpX, and allow for opening of the pore and increased proteolytic activity. Decreased respiratory chain proteins, impaired respiratory chain complex activity and increased ROS production are the toxic consequences leading to cancer cell death in context of high ClpP expression (Nouri *et al*, 2020; Ishizawa *et al*, 2019). The first example of ClpP activators came from studies in bacteria and identified antibiotics acyldepsipeptides (ADEPs) as potent interactors of ClpP (Brötz-Oesterhelt *et al*, 2005). An ADEP analog, ADEP-41, is effective against mitochondrial ClpP and causes death of malignant cells (Wong *et al*, 2018). More recently, the imipridones have been identified as ClpP activators and the firs-in-class compound ONC201 is already in clinical trials for multiple cancers (Ishizawa *et al*, 2019).

Mitochondria in Multiple Myeloma

MM is commonly considered glycolytic, as evident by its increased FDG-PET avidity, that also correlates with prognosis (Bartel *et al*, 2009). Indeed, inhibition of glucose uptake is toxic for MM cells (McBrayer *et al*, 2012). However, several lines of research have been demonstrating that MM cells rely on mitochondria for survival and resistance to therapy. Recently, genomic analysis revealed that during evolution from precursor MGUS to MM malignant plasma cells acquire increased mitochondrial mass, and that this is likely sustained by increased expression of key regulators of mitochondrial biogenesis (Ruiz-Heredia *et al*, 2021). Similarly, gene signatures of OXPHOS were found to be overexpressed in MM vs normal plasma cells and inhibition of master transcription

factor responsible for mitochondrial biogenesis PGC1a proved highly effective in inhibiting MM cells growth (Xiang *et al*, 2020). Moreover, experiments with inhibitors of mitochondrial translation (chloramphenicol or tigecylcine) showed high efficacy in MM cell lines (Ortiz-Ruiz *et al*, 2021; Tian *et al*, 2016). Clues of a relevant role for mitochondria also came from our proteomic and electron microscopy studies documenting abundant and constantly turned-over mitochondria in human primary myeloma cells and MM cell lines (Oliva *et al*, 2017). A role for mitochondria in MM biology is supported also by the existence of an active transfer of mitochondria from stromal cells to malignant plasma cells mediated by CD38 (Marlein *et al*, 2019). Moreover, several paper have identified increased mitochondrial activity as a mechanism of resistance to therapy, in particular proteasome inhibitors but also targeted therapies (Besse *et al*, 2018, 2019; Waldschmidt *et al*, 2021). Finally, in conditions of metabolic or bioenergetics stress, mitochondria were proven to be essential and their plastic adaptation necessary for survival (Dalva-Aydemir *et al*, 2015).

Among the first evidence of the precise role of mitochondria in MM, a very strong dependency of MM on glutamine metabolism was discovered. This need for high amounts of glutamine in MM is largely attributable to the high rate of glutaminolysis to generate glutamate which, through transaminases or Glu dehydrogenase, provides the anaplerotic Krebs cycle intermediate 2-oxoglutarate (Bolzoni *et al*, 2016). These studies, however, did not explore if the need for 2-oxoglutarate came from its extramitochondrial functions or from its role as TCA-cycle intermediate for generation of NADH for the electron transport chain. In fact, formal investigation of OXPHOS status in MM cells revealed high heterogeneity among cell lines, ranging from high to low oxygen consumption (Bajpai *et al*, 2020). It has to be noted that in this context MM cell lines recapitulate very poorly the biology of the disease, being able to abnormally proliferate outside the bone marrow. This is likely to cause metabolic rewiring to support adaptation to different oxygen tensions, and might generate severe bias in interpretation of MM bioenergetics. Indeed, experimental evidence exist suggesting that growth of MM cells within the bone marrow could favor an OXPHOS shift (Marlein *et al*, 2019) and experiments with inhibitors of electron transport chain showed only partial toxicity in MM cell lines (Bajpai *et al*, 2020).

Overall, there is growing evidence that, although glycolytic, MM cells depend on mitochondria for survival, especially in conditions of stress. However, we have very limited understanding of what are the mitochondrial functions essential for MM and of the impact of mitochondrial perturbation as a tool to target this disease.

Aim of the work

In this work, we hypothesize that myeloma cells require a strict control of mitochondrial homeostasis to guarantee their survival. Since MM cells have specific biological reasons to be exposed to high burdens of mitochondrial stress and damage, namely the continued production of huge amounts of immunoglobulins leading to high energy expenditure and ROS accumulation, we reasoned that exploring adaptive responses to mitochondrial stress could unveil novel therapeutic targets in this disease.

Building on the growing body of knowledge supporting the role of UPR^{mt} responses and of mechanisms of mitochondrial homeostasis in supporting tumorigenesis and proliferation of malignant cells, we aimed at:

- Evaluating the relevance of UPR^{mt} in MM cells and testing its manipulation as an anti-myeloma tool;
- Identifying UPR^{mt} players that maintain mitochondrial homeostasis and explore their inhibition as therapeutic strategy against MM;
- Characterizing the mitochondrial and cellular consequences of manipulation of mitochondrial homeostasis.

Results

UPR mt in multiple myeloma

To test if mitochondria in MM are exposed to mitochondrial stress we analyzed the expression of crucial UPR^{mt} players in a unpublished RNA-sequencing (RNA-seq) cohort (360 newly diagnosed patients versus 16 healthy donors, IFM 2009 trial (Attal *et al*, 2017)). We found that mRNAs of mitochondrial chaperones HSPD1 and HSPE1, and proteases CLPP and LONP1 are all significantly higher in malignant PCs (**Fig.10**).

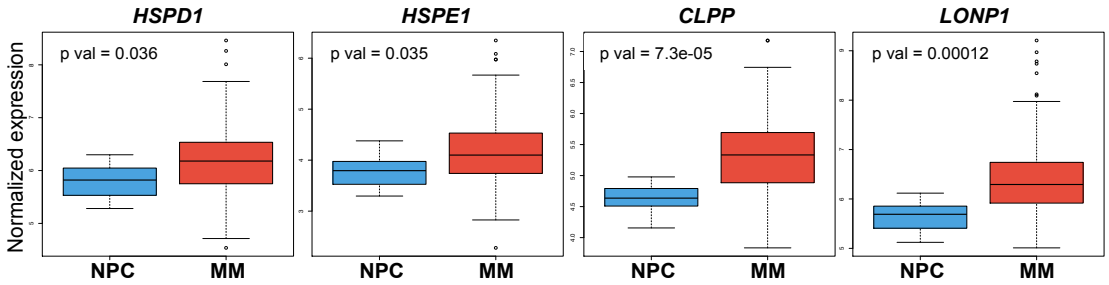

Figure 10. Expression of UPR^{mt} genes in MM. *Boxplots showing normalized expression (transcripts per million) of 4 core UPR^{mt} genes detected by RNA-seq of CD138+ cells isolated from 360 MM patients (MM) and 16 healthy donor (normal plasma cells, NPC). The center line represents the median, the box limits upper and lower quartiles, and the whiskers 1.5x the interquartile range. T-test with Benjamini-Hochberg correction for multiple testing was was used for statistical analysis.*

A precise definition of the transcriptional program controlled by UPR^{mt} is still missing and is likely to be cell and context dependent. To explore more broadly the UPR^{mt} status in MM cells, we selected 30 genes annotated as UPR^{mt} related and analyzed the correlation of their expression in MM patients (Cole *et al*, 2015). We identified a subset of 14 genes showing strong correlation with one another and with canonical UPR^{mt} genes (SCG5, IMMT, HSPD1, HSPE1, SCAP, CLPP, PFDN6, RUVBL2, SIL1, SAMM50, NDUFAF1, MKKS, PPIA, TRAP1), (**Fig.11A**). RNA-seq data confirmed that expression of this group of genes (putative MM-specific "UPRmt signature") is significantly higher in MM vs normal PCs, although its expression does not carry a prognostic value (**Fig.11B-C**). Of note, we also used publicly available RNA-seq data (Cancer Cell Line Encyclopedia, CCLE) (Barretina *et al*, 2012) to evaluate the expression of mitochondrial

chaperones and proteases in MM cell lines and found these UPR^{mt} core genes concertedly upregulated, but independent from other stress pathways (**Fig.11E**).

Altogether these data demonstrate that MM cells show a concerted and specific upregulation of UPR^{mt} targets, suggesting that an adaptive response to mitochondrial stress is already active in basal conditions in these cells.

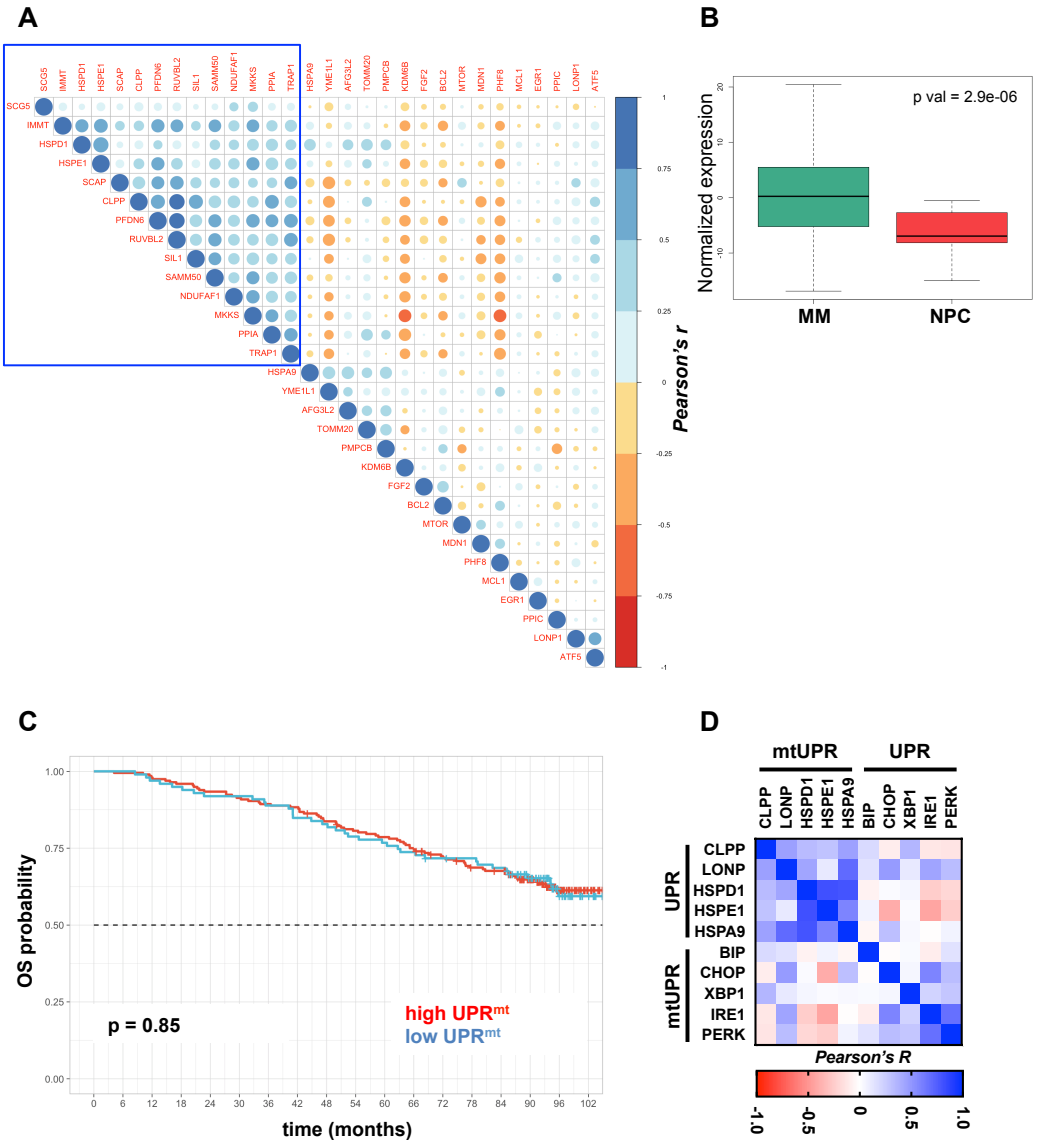

Figure 11. UPR^{mt} in multiple myeloma. *A) Correlation coefficient (Pearson's r) of expression levels of a curated list of UPR^{mt} related genes in CD138+ cells isolated from 360 MM as determined by RNA-seq. Blue square highlights highly correlated genes used for suggesting a MM specific UPR^{mt} signature. B) Boxplots showing normalized expression of UPR^{mt} signature in MM vs NPC. The center line represents the median, the box limits upper and lower quartiles, and the whiskers 1.5x the interquartile range. C) Kaplan-Meier curves showing overall survival (OS) of high vs low UPR^{mt} patients, identified as higher or lower than median. D) Correlation coefficient (Pearson's r) of expression levels of core UPR^{mt} and UPR genes in MM cell lines based on Cancer Cell Line Encyclopedia RNA-seq data.*

ATF5 dependent UPRmt

To weigh the relevance of UPR^{mt} in MM, we selected to impair this transcriptional response by depleting ATF5, the master transcription factor suggested to regulate UPR^{mt} activation in eukaryotes. We adopted a lentiviral platform that allows simultaneous shRNA mediated knockdown of ATF5 (ATF5^{kd}) and expression of surface markers for analysis or selection (low affinity nerve growth factor, LNGFR) (**Fig.12A**). We tested three different constructs (sh70 against 3' UTR region, sh39 and shF1 against the coding sequence) in four different MM cell lines selected for high or low ATF5 mRNA expression levels based on public RNA-seq databases (Barretina *et al*, 2012) (**Fig.12B**).

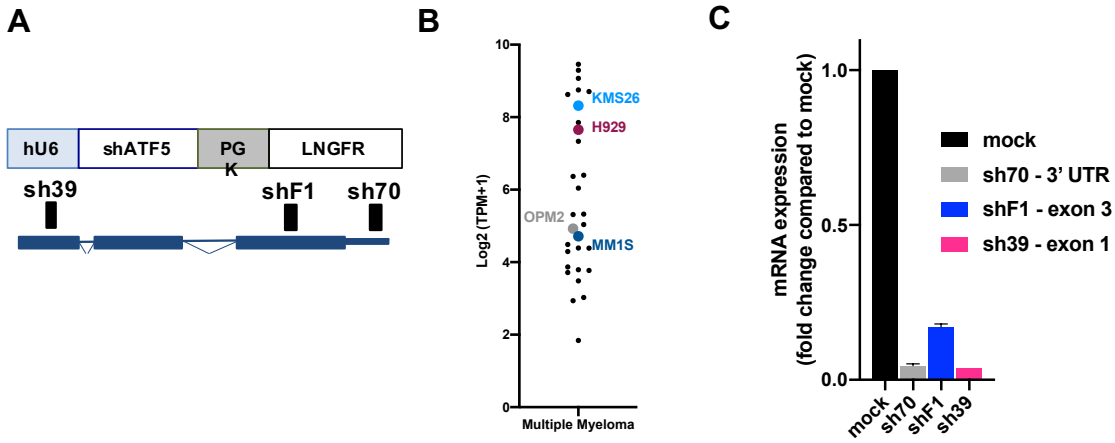

Figure 12. ATF5 knockdown in MM cells. *A) Schematic representation of constructs used for ATF5 knockdown showing their target region on ATF5 gene. B) Dot plot showing ATF5 expression in MM cell lines based on Cancer Cell Line Encyclopedia RNA-seq data. C) Barplot showing fold changes in ATF5 expression in NCI-H929 cell line after infection with either mock or anti-ATF5 shRNA expressing lentiviral vectors. Mean of 3 experiments ± SD.*

After confirmation of ATF5 silencing by qPCR (**Fig.12C**), we monitored the kinetics of disappearance or persistence of LNGFR^{+} cells by flow cytometry and checked for expression of canonical UPR^{mt} targets (*HSPA9, HSPD1*, *HSPE1*, *CLPP*, *LONP1*) in the four different cell lines and with the three different constructs (**Fig.13**). We observed inconsistent and discordant effects of ATF5^{kd}, both in terms of cellular toxicity and impairment of UPR^{mt}. In fact, while it was possible to identify a threshold of 70% downregulation of ATF5 mRNA correlated with appearance of cellular toxicity, this was clearly independent from downregulation of the transcripts of HSPD1, HSPE1, HSPA9, CLPP and LONP1.

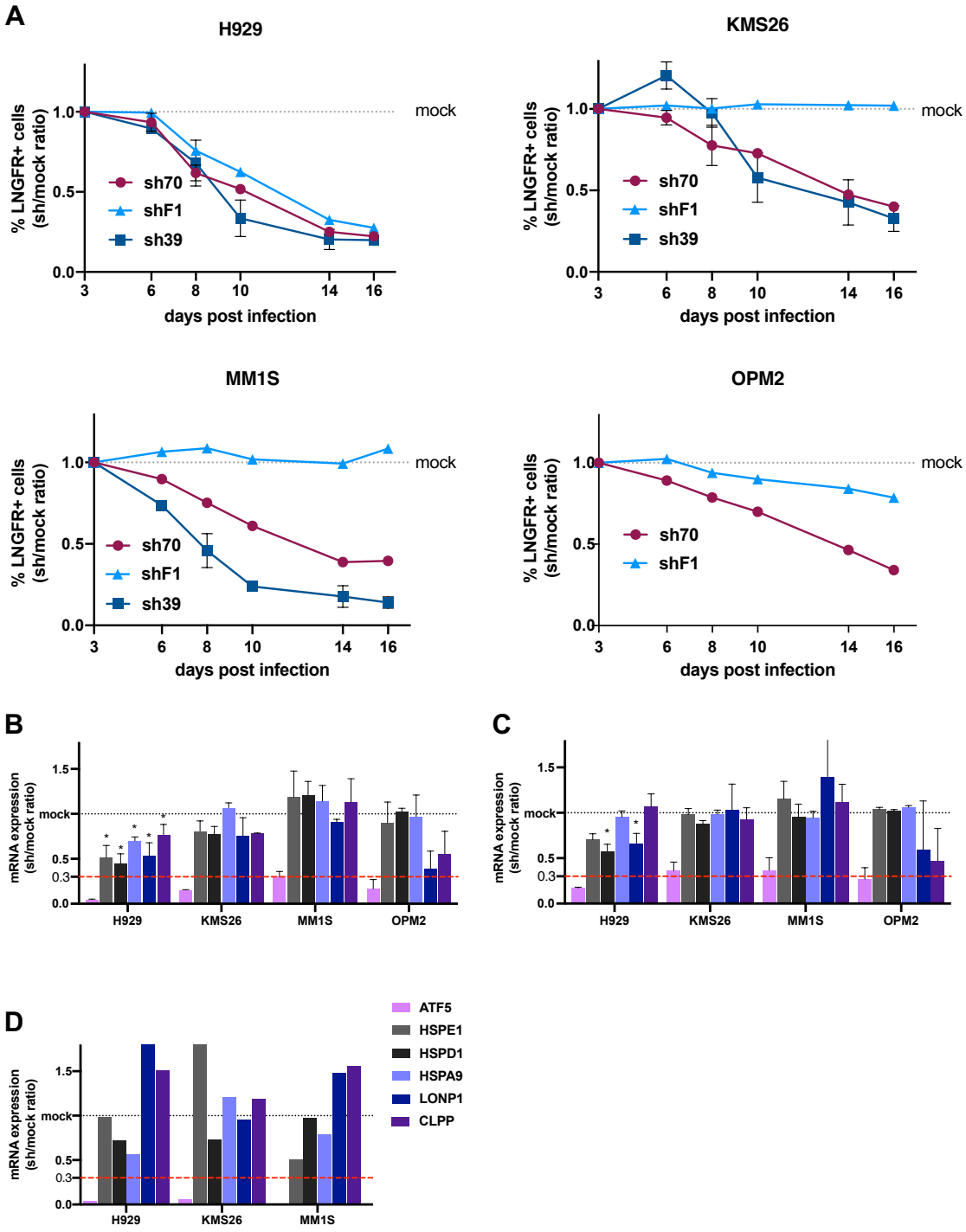
A
H929
KMS26
MM1S
OPM2
% LNGFR+ cells (sh/mock ratio)
days post infection
mock
sh70
shF1
sh39
B
C
mRNA expression (sh/mock ratio)
H929
KMS26
MM1S
OPM2
D
ATF5
HSPE1
HSPD1
HSPA9
LONP1
CLPP

Figure 13. Effects of ATF5 knockdown in MM cell lines. *A) Curves showing the fold change in LNGFR+ cells by flow cytometry at the indicated timepoints after infection of MM cell lines (KMS26, H929, OPM2, MM1S) with anti-ATF5 (sh70, shF1, sh39) or mock shRNA expressing lentiviral vectors. Results are normalized on mock infected cells, and graphs represent the mean ± SD of at least 2 independent experiments. In the bottom panels, bar plots showing fold changes of mRNA levels of UPR^{mt} genes in MM cell lines (KMS26, H929, OPM2, MM1S) 3 days after infection with mock or anti-ATF5 shRNA expressing lentiviral vectors, as determined by RT-qPCR. Values are normalized on mock infected cells, and results are shown for B) sh70 (mean of three independent experiments ± SD) C) shF1 (mean of three independent experiments ± SD) D) sh39 (one experiment). Two-way ANOVA with Sidak correction for multiple testing was used for statistical testing.*

Finally, to formally ask if ATF5 is mediating UPR^{mt} regulation in MM cells, we used pharmacological treatments to induce UPR^{mt} (paraquat and bortezomib) in parental and ATF5^{kd} MM cells and found a similar upregulation of UPR^{mt} targets in both conditions (**Fig.14**).

Altogether, these data suggest that ATF5 does not mediate, or is at least dispensable for, UPR^{mt} activity in MM cells and led us to explore different avenues to challenge mitochondrial proteostasis in MM.

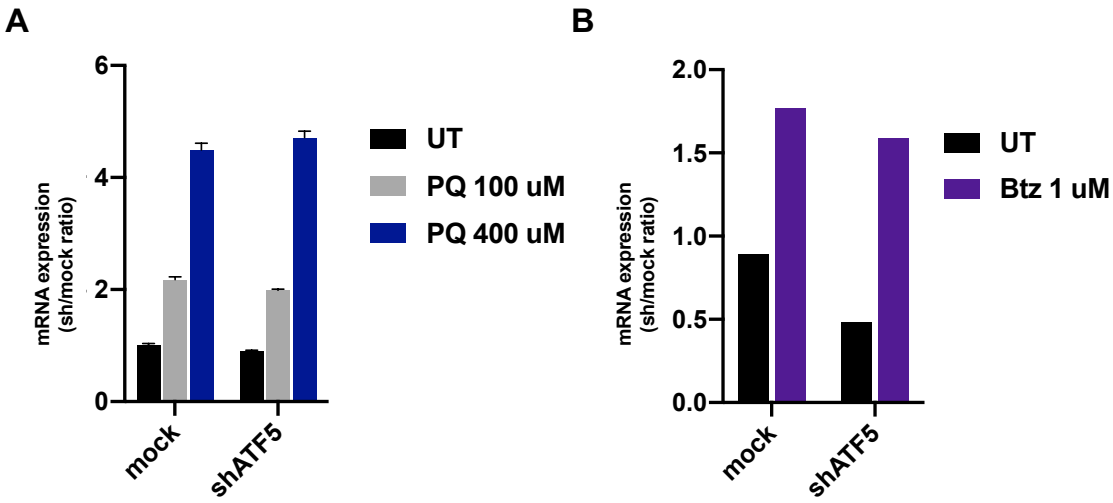

Figure 14. Effects of ATF5 knockdown on UPR^{mt} activation. *Bar plots showing fold changes of mRNA levels of HSPD1 in MM cell infected with mock or anti-ATF5 shRNA expressing lentiviral vectors, as determined by RT-qPCR. Cells were treated with A) paraquat (PQ) for 48h (mean of three independent experiments ± SD) or B) bortezomib (Btz) for 1h, at the indicated doses (one experiment).*

ClpP essentiality in MM

Having identified high expression of ClpP in primary samples of MM patients, and given the available data on ClpP manipulation in leukemia (Cole *et al*, 2015; Nouri *et al*, 2020) , we explored ClpP as a therapeutic target in MM.

First, immunohistochemistry analyses confirmed high expression in malignant plasma cells in trephine biopsies of myeloma patients (**Fig.15A**). We used our RNA-seq cohort to confirm high ClpP expression in all different cytogenetic subgroups of MM patients, with a slightly higher expression in the high-risk patients with chromosome 1q gain (**Fig.15B**).

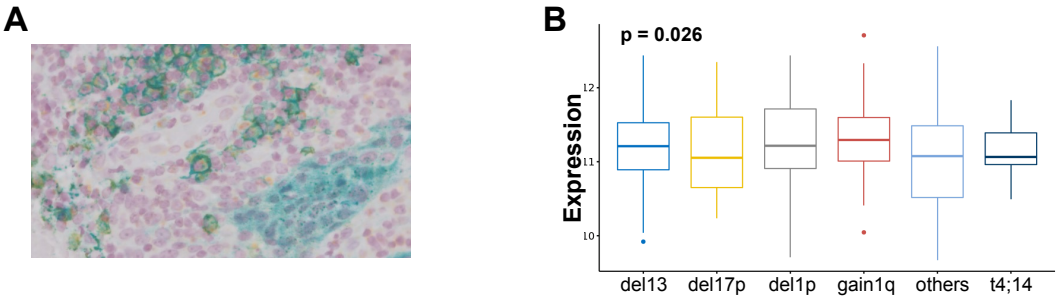

Figure 15. ClpP expression in MM. *A) Immunohistochemistry of bone marrow trephine biopsy of a newly diagnosed MM patient. In yellow ClpP, in blue CD138, in green double positive plasma cells. B) Boxplots showing normalized expression of ClpP across different genetic subgroups in RNA-seq data of newly diagnosed MM patients. The center line represents the median, the box limits upper and lower quartiles, and the whiskers 1.5x the interquartile range. Kruskal-wallis test was used for statistical testing.*

We then used public expression data in CCLE (Barretina *et al*, 2012) to assess ClpP levels in cancer cell lines and found that MM expresses the highest levels of ClpP, comparable to, or even higher than, paradigmatic ClpP-dependent leukemia (**Fig.16A**). Among MM cell lines, ClpP expression is variable and is not correlated with mitochondrial abundance measured by amount of structural membrane proteins or fluorescent staining with Mitotracker™ Green FM (**Fig.16B-C**).

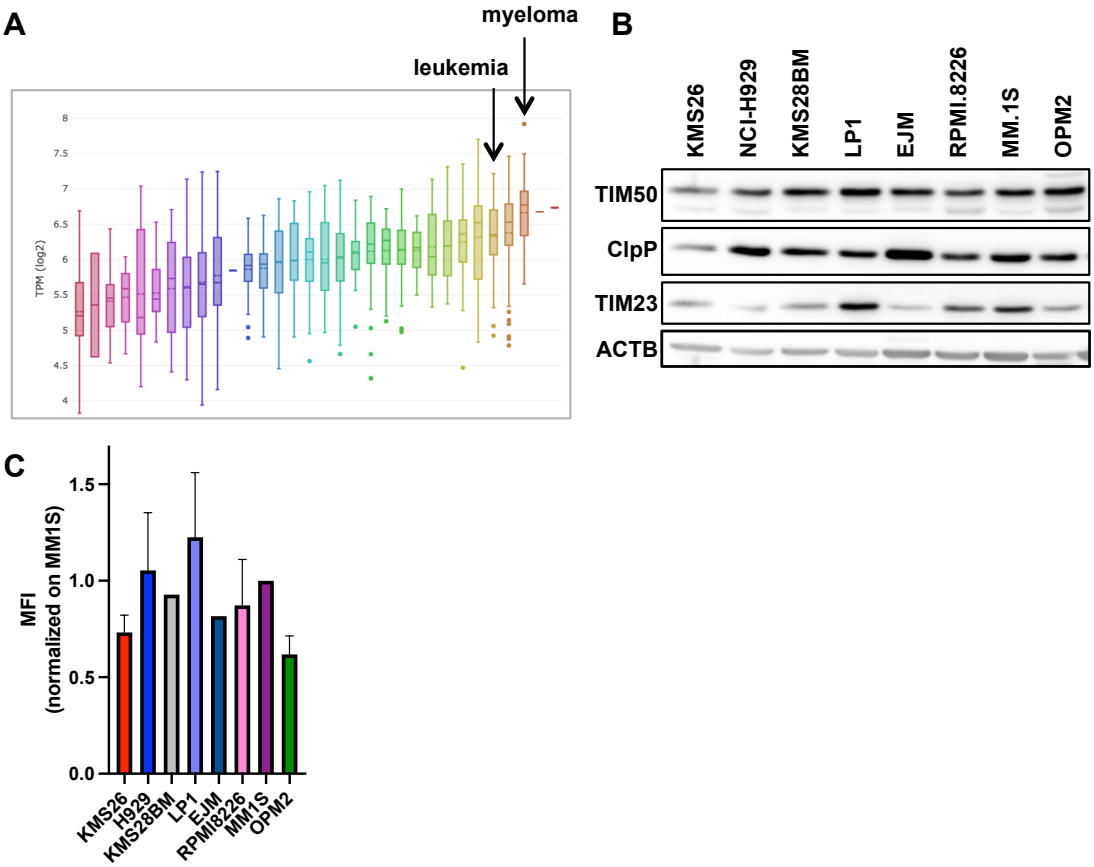

Figure 16. ClpP expression in MM cell lines. *A) Boxplots showing normalized expression of ClpP across tumors in public RNA-seq data (Cancer Cell Line Encyclopedia). The center line represents the median, the box limits upper and lower quartiles, and the whiskers 1.5x the interquartile range. B) Western blot analysis of ClpP, transporter of the inner mitochondrial membrane (TIM23) and outer mitochondrial membrane (TIM50) (1 representative experiment of 3 replicates is shown). Actin was used as loading control. C) Barplots showing flow cytometry quantification of mitochondrial mass by MitoTracker Green FM in a panel of MM cell lines. Mean fluorescence intensity (MFI) ± SD of 3 experiments.*

To challenge the relevance of these findings, we performed lentiviral mediated ClpP knockdown (ClpP^{kd}) with two different shRNAs in a broad panel of myeloma cell lines and in leukemia cells already shown to require ClpP for survival (**Fig.17A**). Flow cytometry monitoring of the ClpP^{kd} cells by LNGFR expression showed that both MM and leukemic cells were progressively outcompeted in culture, at similar rates (**Fig.17B-C**). To further confirm the dependence of MM on ClpP, we used a different genetic manipulation strategy based on a lentiviral vector for constitutive expression of Cas9 and a single guide-RNA (sgRNA) targeting *CLPP* to generate knockout (ClpP-KO) cells. Absence of ClpP caused a clear trend towards a reduction in proliferation rate (**Fig.17D**).

Altogether, these data suggest that manipulation of mitochondrial proteostasis is toxic for MM cells and that ClpP could offer a novel therapeutic target in this disease.

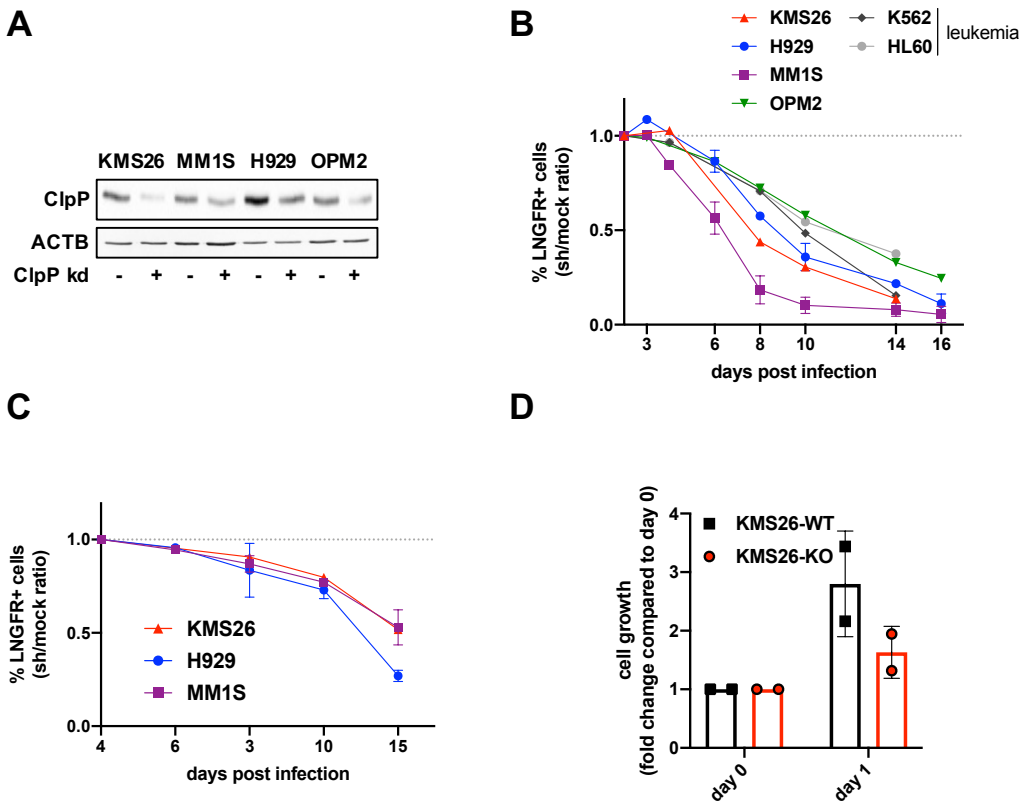

Figure 17. Toxicity of ClpP knockdown in MM cell lines*. A) Western blot analysis showing ClpP protein level in MM cell lines after infection with mock or antiClpP shRNA expressing lentiviral vectors. Actin (ACTB) was used as a loading control (1 representative experiment of 3 replicates is shown). B) Curves showing the fold change in LNGFR+ cells by flow cytometry at the indicated timepoints after infection of MM (KMS26, H929, OPM2, MM1S) and leukemic (K562, HL-60) cell lines with anti-CLPP (construct #73) or mock shRNA expressing lentiviral vectors. Results are normalized on mock infected cells, and graphs represent the mean ± SD of 3 independent experiments. C) Curves showing the fold change in LNGFR+ cells by flow cytometry at the indicated timepoints after infection of MM (KMS26, H929, MM1S) cell lines with anti-CLPP (construct #61) or mock shRNA expressing lentiviral vectors. Results are normalized on mock infected cells, and graphs represent the mean ± SD of 3 independent experiments. D) Barplot showing fold change of cell proloiferation in wild type (KMS26-WT) or knockout (KMS26-KO) cells compared to day 0, as measured by Cyquant Direct Proliferation assay (mean ± SD of 2 independent experiments).*

Associations of ClpP dependencies in cancer cell lines

To investigate the possible role of ClpP in cancer we analyzed the data publicly available in the Cancer Cell Lines Encyclopedia project (Barretina *et al*, 2012). In particular, we focused on expression data obtained by RNA-seq experiments and dependency scores derived by clustered regularly interspaced short palindromic repeats (CRISPR)-screening experiments. We first explored the correlation of ClpP dependency and ClpP expression across all the cancer cell lines characterized in the project, and we did not observe any significant correlation between the two measures (**Fig.18A**). This suggests that lineage or cell specific features rather than ClpP abundance are what defines the relevance of this protease in different cancers. We also looked for dependencies highly correlated with ClpP dependency. The top co-dependency we identified is with the ATPase ClpX, essential partner of ClpP for its activity (**Fig.18B**). This expected co-dependency validates the approach and excludes a non-proteolytic role for ClpP.

Other identified correlated dependencies include other mitochondrial proteases (PITRM1, MIPEP), mitochondrial ribosomes subunits (MRPL44, MRPL4), proteins involved in redox homeostasis (SOD2) and a chaperone of mitochondrial RNA (LRPPRC) (**Fig.19C**). Interestingly, no components of respiratory complexes were identified as dependencies associated with ClpP.

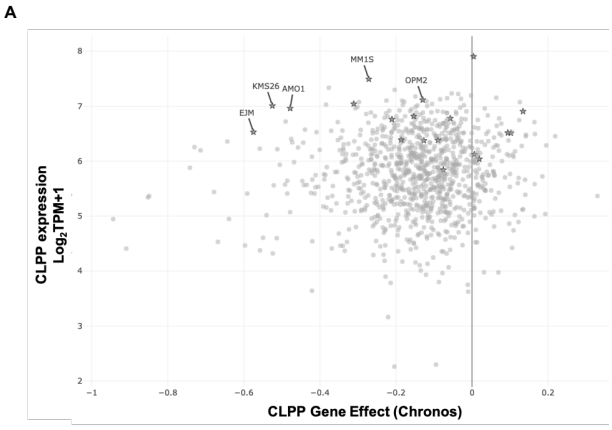

C

Gene	Correlation (Pearson's)	p value
CLPX	0,485	5,40448E-32
MPV17L2	0,357	5,00018E-05
SOD2	0,343	1,50581E-25
C1QBP	0,303	4,25626E-15
MIPEP	0,285	3,98277E-05
LRPPRC	0,278	2,31538E-07
MRPL44	0,273	4,2551E-19
PITRM1	0,27	1,88685E-08
RPUSD4	0,267	2,32482E-16
GADD45GIP1	0,266	6,93889E-18
SLC30A9	0,264	0,000421335
MRPL4	0,261	1,60981E-10
MRPL38	0,256	4,57475E-05
NDUFB10	0,254	2,63525E-10
GRSF1	0,253	2,27839E-12
MRPL41	0,25	0,163121662

Figure 18. Codependencies of ClpP in cancer cell lines. *A) Dot plot showing the relationship between ClpP expression by RNA seq and dependency on ClpP in 1074 cancer cell lines. Dependency score is derived by CRISPR knockout screens analyzed by Chronos algorithm. Each dot represents a cell line, stars represent MM cell lines. B) Dot plot showing the correlation of dependency scores for ClpP and ClpX in 1074 cancer cell lines, derived by CRISPR knockout screens analyzed by Chronos algorithm. Each dot represents a cell line, stars represent MM cell lines with high dependency scores for ClpP (KMS26, AMO1, EJM). C) List of dependencies highly correlated with ClpP in CRISPR knockout studies of 1074 cancer cell lines, analyzed by Chronos algorithm. Pearson's r and p value of each correlation are shown. All data in this figure are publicly available in the DepMap project.*

We then focused on MM cell lines and explored the features of ClpP dependency in these cells. We identified a subgroup of MM cell lines highly dependent on ClpP (KMS26, EJM, AMO1), while the majority of MM cell lines showed a dependency score around 0. To identify differences correlated with this differential sensitivity, we compared RNA-seq and CRISPR screen data of the group of MM cell lines highly dependent on ClpP and of a group of 11 cell lines with very low dependency scores (**Fig. 19A**). *CCL5*, encoding C-C Motif Chemokine Ligand 5, is the only gene identified as a possible exclusive dependency in the group of highly ClpP dependent cell lines. In RNA-seq data, few genes resulted differently expressed between the two groups with a relevant fold change (**Fig.19B**). In particular, translation factor EIF2D appears less expressed in ClpP dependent cell lines, while the list of genes higher in this group includes DOK4, RGCC, SERPINF1, ADAM19 and SPSB1 (**Fig.19C**). Of note, none of these genes has a clear relationship with ClpP, or with mitochondria in general.

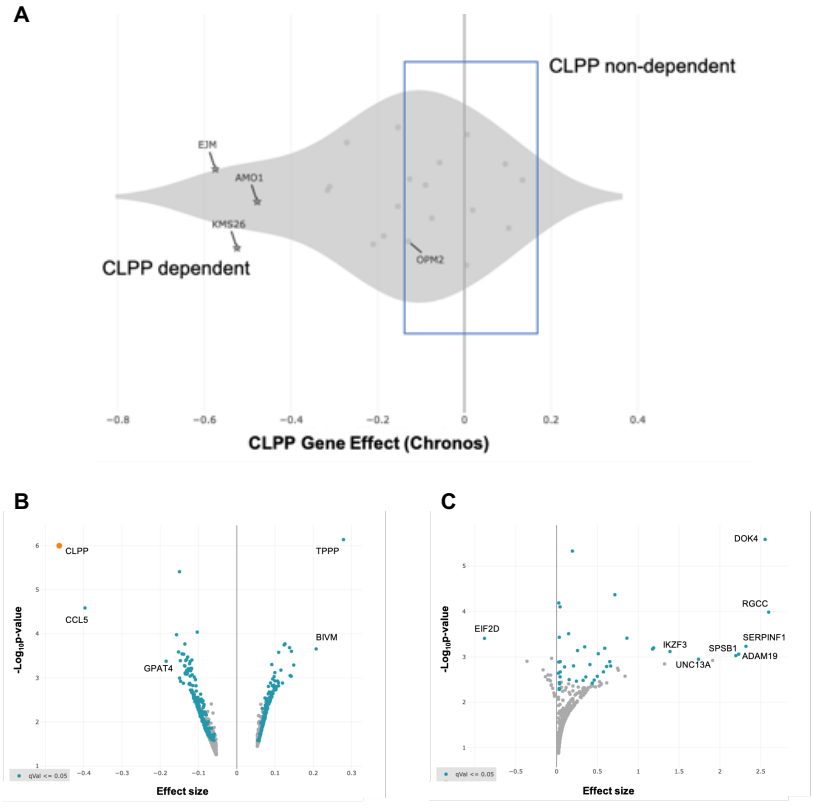

Figure 19. Associations of ClpP dependency in MM cell lines. *A) Dot plot showing ClpP dependency scores in MM cell lines, calculated by analyzing CRISPR knockout screens data with Chronos algorithm. Stars indicate the MM cell lines with the highest dependency on ClpP (gene effect score approximately -0.5). Blue square identifies cell lines selected as "ClpP non-dependent" subgroup for further analysis. B) Volcano plot showing dependencies identified as differently enriched in the "ClpP dependent" versus "ClpP non-dependent" MM cell lines. Blue dots identify genes with FDR q-value < 0,05. C) Volcano plot showing genes differentially expressed in the "ClpP dependent" versus "ClpP non-dependent" MM cell lines. Blue dots identify genes with FDR q-value < 0,05.*

Effects of ClpP knockdown in MM cells

ClpP exact role in mammalian cells is still debated and is likely to be cell and context dependent. As previously mentioned, it is suggested that ClpP is essential to maintain efficiency of OXPHOS, either by direct degradation of components of respiratory complexes or by regulation of mitochondrial translation machinery (Cole *et al*, 2015; Szczepanowska *et al*, 2016; Mirali & Schimmer, 2020; Szczepanowska *et al*, 2020; Szczepanowska & Trifunovic, 2021a). This led us to hypothesize that the toxicity of $ClpP^{kd}$ in MM cell must be due to impairment of mitochondrial respiration, whose exact contribution to bioenergetic balance in MM cells is largely unknown (Xiang *et al*, 2020; Dalva-Aydemir *et al*, 2015; Marlein *et al*, 2019).

To test this hypothesis, we first performed Seahorse Glycolytic Rate Assay (GRA) in a panel of MM cell lines to assess proton efflux specific to glycolysis and therefore derive the amount of medium acidification attributable to glycolysis versus OXPHOS. We characterized a broad panel of MM with GRA, and found that only KMS26 and H929 ($OXPHOS^{+}$) show relevant OXPHOS contribution to proton efflux, while the majority of cell lines range from mostly to exclusively glycolytic (OPM2, $OXPHOS^{-}$) (**Fig.20A**). Accordingly, ATP synthase (Complex V) inhibition with oligomycine caused significant reduction of total cellular ATP only in $OXPHOS^{+}$ cell lines (**Fig.20B**). Similarly, $ClpP^{kd}$ caused significant ATP depletion only in cells with high OXPHOS (KMS26) (**Fig.20C**).

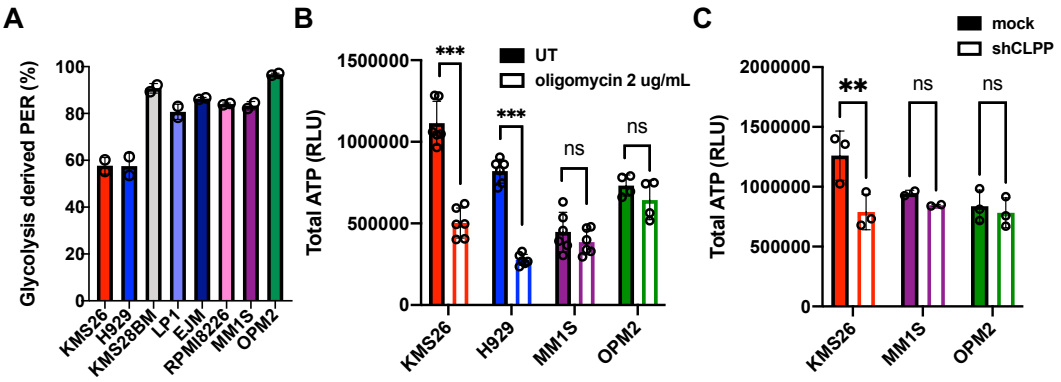

Figure 20. Bioenergetic balance in MM. *A) Barplots showing % of proton efflux rate (PER) coming from glycolysis in 8 MM cell lines (KMS26, H929, KMS28BM, LP1, EJM, RPMI8226; MM1S, OPM2), measured by Seahorse Glycolytic Rate Assay (mean ± SD of 2 independent experiments). B) Barplots showing intracellular ATP quantification by Cell Titer Glo after treatment of MM cell lines (KMS26, H929, MM1S, OPM2) with oligomycin for 1h (mean ± SD of at least 4 independent experiments). Raw values of relative luminescence units are shown (RLU). Paired t-tests with Holm-Sidak correction for multiple comparisons were used for statistical analysis. C) Barplots showing intracellular ATP quantification by Cell Titer Glo 3 days after infection of MM cell lines (KMS26, MM1S, OPM2) with anti-CLPP (construct #73) or mock shRNA expressing lentiviral vectors (mean ± SD of 3 independent experiments). Values of relative luminescence units are shown (RLU). Paired t-tests with Holm-Sidak correction for multiple comparisons were used for statistical analysis.*

To formally test the impact of ClpP^{kd} on OXPHOS in MM cells, we measured oxygen consumption rate (OCR) with Mitostress Seahorse Assay after ClpP^{kd} in LNGFR-sorted MM cells. This experiment confirmed that, as suggested by the GRA, basal OXPHOS activity is strikingly different in KMS26 and OPM2 cells. Surprisingly, ClpP^{kd} only minimally and inconsistently affected OXPHOS activity in both cases, as revealed by measurements of basal OCR, maximal respiration and ATP coupled respiration (**Fig.21**).

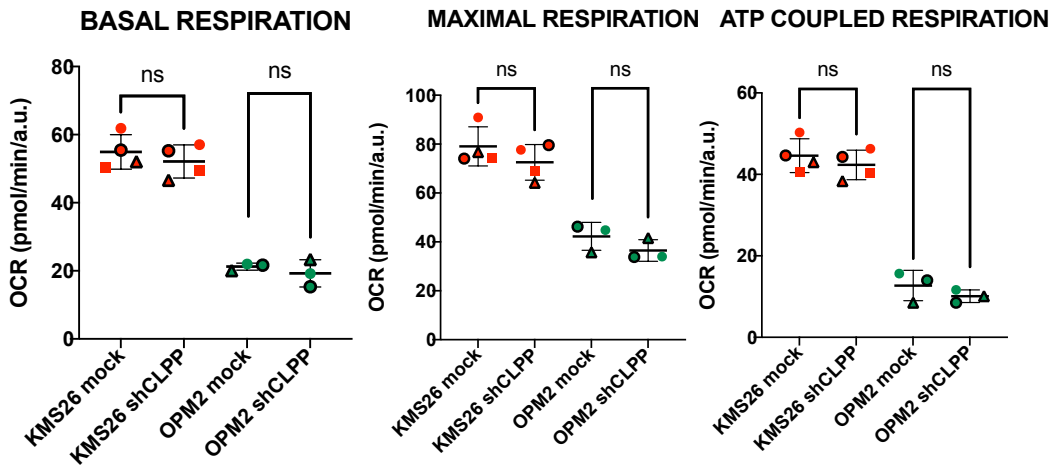

Figure 21. Oxygen consumption rate after ClpP knockdown*. Dot plots showing oxygen consumption rates (OCR) of MM cell lines (KMS26, red and OPM2, green) 3 days after infection with anti-CLPP (construct #73) or mock shRNA expressing lentiviral vectors, measured by Seahorse Mitostress test. Basal, maximal and ATP coupled OCR are shown (mean ± SD of at least 3 independent experiments). Paired t-tests with Holm-Sidak correction for multiple comparisons were used for statistical analysis*

Further supporting this observation of no effect on OXPHOS by ClpP^{kd}, our experiments failed to demonstrate any of the expected sequelae of damage on the electron transport chain, such as loss of mitochondrial membrane potential or accumulation of reactive oxygen species (**Fig.22A-B**).

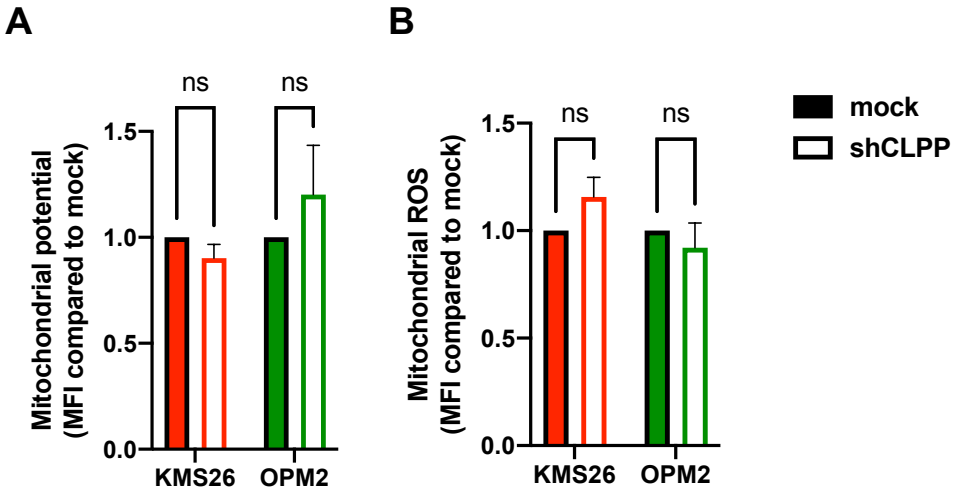

Figure 22. Mitochondrial activity after ClpP knockdown. *A) Barplots showing flow cytometry determination of mitochondrial transmembrane potential with MitoRed CMXRos in MM cell lines (KMS26, OPM2) 3 days after infection with anti-CLPP (construct #73) or mock shRNA expressing lentiviral vectors. Fold change compared to MFI of mock transduced cells is shown (mean ± SD of 3 independent experiments). Paired t-tests with Holm-Sidak correction for multiple comparisons were used for statistical analysis. B) Barplots showing flow cytometry determination of mitochondrial transmembrane potential with MitoSOX in MM cell lines (KMS26, OPM2) 3 days after infection with anti-CLPP (construct #73) or mock shRNA expressing lentiviral vectors. Fold change compared to MFI of mock transduced cells is shown (mean ± SD of 3 independent experiments). Paired t-tests with Holm-Sidak correction for multiple comparisons were used for statistical analysis.*

These data suggest that an OXPHOS independent mechanism of toxicity exists for ClpP^{kd} in MM cells. Indeed, our previous experiments had shown ClpP^{kd} toxicity extending to exclusively glycolytic cell line OPM2 (**Fig.17B**). Moreover, analysis of purified LNGFR^{+} cells after ClpP^{kd} confirmed a profound effect on cell proliferation in glycolytic cell line OPM2, and significant apoptosis induction both in cells with high (KMS26) and minimal OXPHOS (MM1S) (**Fig.23A-C**).

Altogether, these data strongly support the hypothesis that the toxicity observed in MM cells after ClpP^{kd} is not, or at least not appreciably, explained but its expected impact on integrity of the electron transport chain.

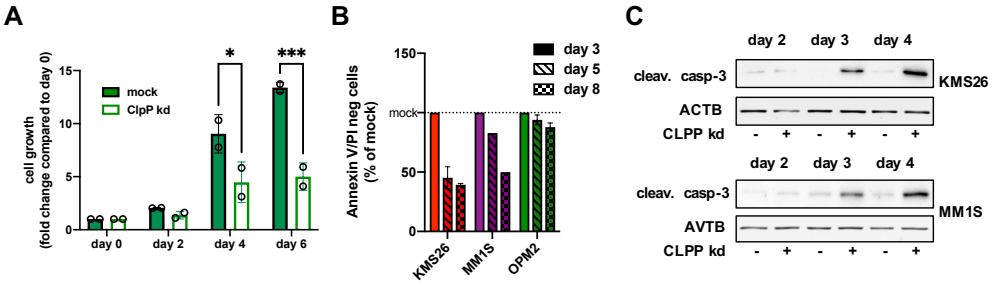

Figure 23. Effects of ClpP knockdown in glycolytic cell lines. *A) Barplots showing fold change of cell proliferation in KMS26 cells infected with anti-CLPP (construct #73) or mock shRNA expressing lentiviral vectors, as measured by Cyquant Direct Proliferation assay. Fold change compared to day 0 (first day of observation, 3 days after infection) is shown (mean ± SD of 2 independent experiments). ANOVA with Sidak correction for multiple comparisons was performed for statistical testing. B) Barplots showing flow cytometry assessment of annexin V/PI staining in MM cell lines (KMS26, MM1S, OPM2) infected with anti-CLPP (construct #73) or mock shRNA expressing lentiviral vectors. The percentage of annexin V/PI negative cells in knockdown samples compared to mock treated cells is shown, normalized on day 3 after infection (first day of observation) (mean ± SD of 3 independent experiments for KMS26 and OPM2, 1 preliminary experiment for MM1S). C) Western blot analysis of caspase-3 cleavage in MM cell lines (KMS26, MM1S) 3 days infection with anti-CLPP (construct #73) or mock shRNA expressing lentiviral vectors. Actin was used as loading control (1 representative experiment of 2 biological replicates is shown).*

To further confirm this hypothesis and to understand the bases of ClpP dependence in MM cells we decided to deploy a threefold orthogonal approach aimed at deciphering the proteomic, transcriptomic and metabolomic sequelae of ClpP ablation in both high and low OXPHOS MM cells, namely KMS26 and OPM2. To avoid confounding effects due to activation of apoptotic pathways, we isolated LNGFR^{+} cells 48 hours after lentiviral infection by flow-cytometry assisted cell sorting, plated them in complete growth medium and processed samples the day after (**Fig.24**). This early timepoint of analysis corresponds to a significant decrease in ClpP mRNA and protein abundance (approximately 50%), but precedes the appearance of significant cell death (**Fig.17A, 23B**). In a parallel but independent approach, we planned to identify MM specific ClpP substrates.

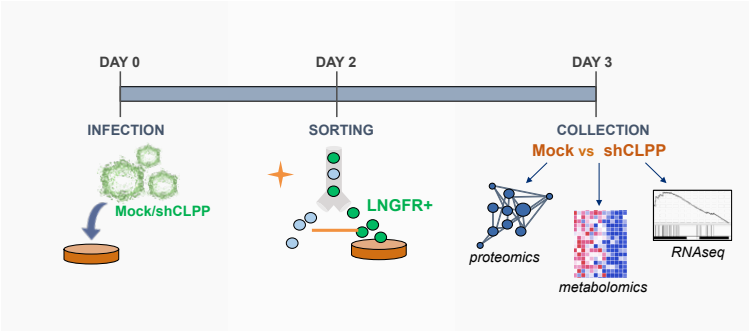

Figure 24. Experimental workflow of –omic analysis. *MM cells (KMS26, OPM2) were transduced with either mock or anti-ClpP shRNA expressing lentiviral vectors. LNGFR^{+} cells were isolated by flow-cytometry assisted cell sorting 48h after infecton, plated in complete growth medium for 24h and then processed for analysis.*

Effects of ClpP knockdown on proteome

First, we performed proteomics by label-free liquid chromatoghraphy-tandem mass spectrometry (LC-MS/MS) of both OXPHOS^{+} (KMS26) and OXPHOS^{-} (OPM2) cells after shRNA mediated ClpP^{kd}. To maximize the significance of our findings, we performed each analysis in biological duplicate and excluded proteins whose accumulation or depletion was not consistent between the two replicates. We were able to identify 1756 proteins in KMS26 and 1852 proteins in OPM2, with 1225 proteins identified in both cell lines, attesting to the solidity of our technique. We hypothesized that proteome changes identified in both cell lines would inform on common OXPHOS independent mechanisms of toxicity. We identified 342 and 185 proteins deregulated by more than 30% in both replicates in KMS26 and OPM2 respectively, but only 21 were shared (18 up, 3 down) (**Fig.25**). Of these 21 proteins, only acyl-CoA thioesterase 7 (ACOT7) is annotated as mitochondrial. It catalyzes the hydrolysis of acyl-CoAs to the free fatty acid and coenzyme A (CoASH), providing the potential to regulate intracellular levels of acyl-CoAs, free fatty acids and CoASH. ACOT7 preferentially hydrolyzes palmitoyl-CoA, but has a broad specificity acting on other fatty acyl-CoAs with chain-lengths of C8-C18 (Yamada *et al*, 1999; Ellis *et al*, 2013), suggesting a possible impact of ClpP manipulation on lipid metabolism in MM cells.

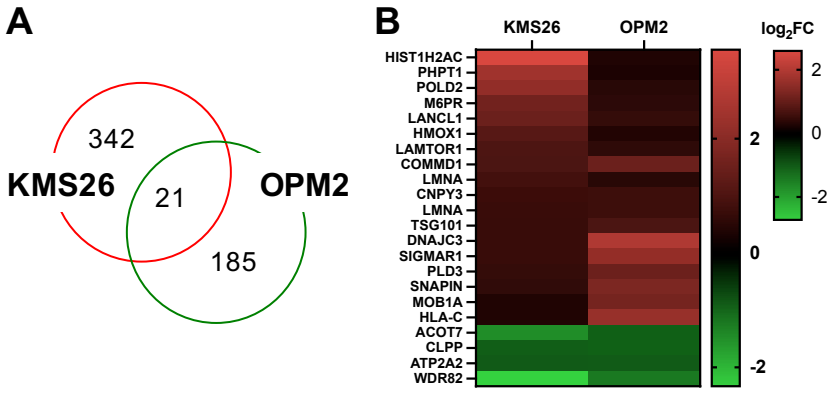

Figure 25. Changes in total proteome after ClpP knockdown. *A) Venn-diagram showing overlap of proteins with a change in abundance (positive or negative) of at least 30% after ClpP knockdown in both biological replicates, in KMS26 and OPM2 cells. B) Heatmap showing log$_2$fold change of the 21 proteins deregulated in both cell lines.*

In view of the limited overlap in proteome changes between the two cell lines, we hypothesized that the biology of addiction to ClpP might be different. Indeed, unbiased Gene Set Enrichment Analysis (GSEA) identified significant effects of ClpP^{kd} only in KMS26 cells. Among depleted pathways, we found a very broad and highly significant depletion of proteins involved in RNA metabolism, ribosome assembly and translation. No pathway was significantly enriched with an FDR <0.25 after ClpP^{kd} but there was a trend for heightened interferon (IFN)-γ mediated response (**Fig.26**).

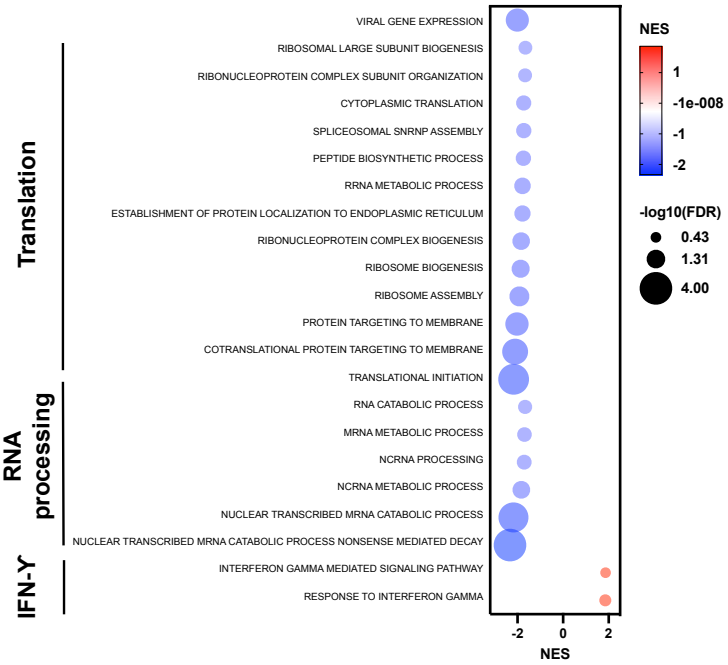

Figure 26. Enrichment analysis of proteome changes after ClpP knockdown. *Bubble chart showing the results of gene set enrichment analysis (GSEA) of proteomic changes in KMS26 cells after ClpP knockdown. Bubbles color indicates normalized enrichment score (NES), bubbles size represents negative log_{10}false discovery rate (FDR). Gene ontology terms of biological processes were used for analysis.*

Depletion of ribosomes was confirmed by polysome profiling (**Fig.25**), and is likely due the loss of ATP seen in KMS26 cells after ClpP manipulation (Iadevaia *et al*, 2014). On the opposite, unbiased analysis of OPM2 proteome with GSEA, ClueGO or STRING only revealed a significant depletion in proteins involved in G-to-M transition, in line with the cell proliferation arrest observed in these cells after ClpP^{kd} (**Fig.23A**). We also looked biasedly at the pathways more deeply affected in KMS26, but did not confirm similar changes in OPM2 suggesting a different impact of ClpP on cellular proteome.

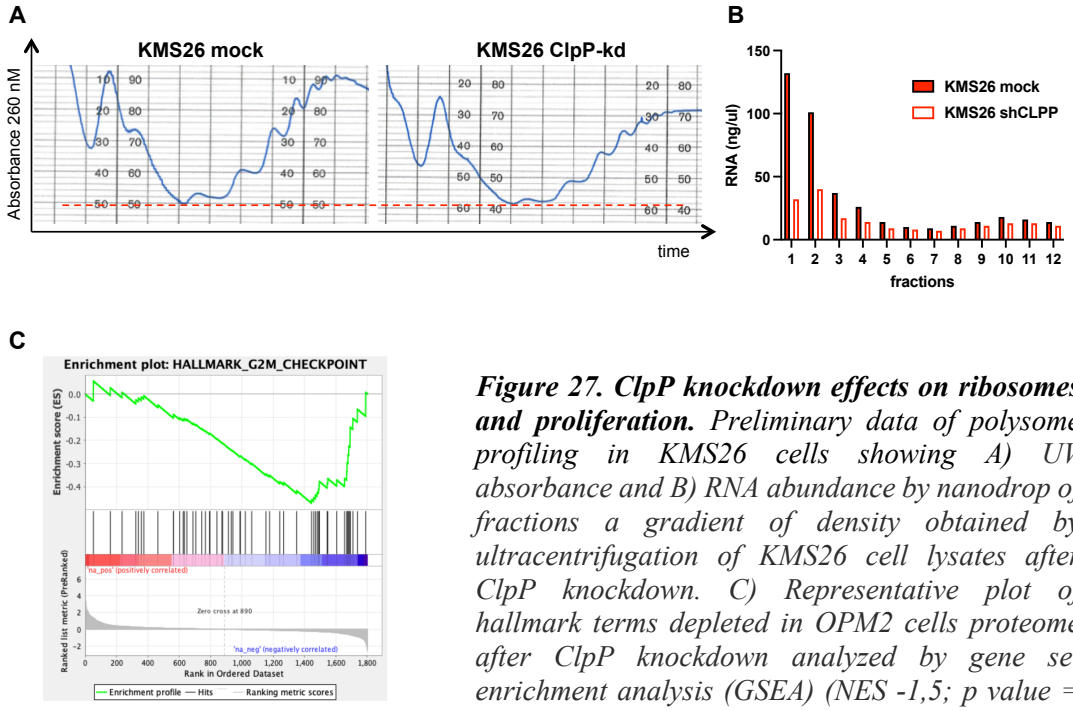

Figure 27. ClpP knockdown effects on ribosomes and proliferation. *Preliminary data of polysome profiling in KMS26 cells showing A) UV absorbance and B) RNA abundance by nanodrop of fractions a gradient of density obtained by ultracentrifugation of KMS26 cell lysates after ClpP knockdown. C) Representative plot of hallmark terms depleted in OPM2 cells proteome after ClpP knockdown analyzed by gene set enrichment analysis (GSEA) (NES -1,5; p value = 0,009; FDR = 0,19).*

Since ClpP^{kd} is likely to affect in first place mitochondrial proteins, we used a comprehensive annotation of mitochondrial proteins (Mitocarta 3.0 (Rath *et al*, 2021)) to specifically investigate mitochondrial changes. We were able to investigate 277 mitochondrial proteins in KMS26 and 287 in OPM2, of which 202 were identified by mass spectrometry in both cell lines. When looking at mitochondrial changes in the two cell lines separately, we did not identify enrichment or depletion of specific mitochondrial compartments or pathways following ClpP^{kd} (**Fig.28A-B**). Indeed, changes in mitochondrial proteome were for the most part cell line specific, but we did identify few proteins modestly but commonly deregulated in both KMS26 and OPM2 (MRPL12, AK2, SFXN23 upregulated; ACOT7, HTRA2, ALDH4A1 downregulated) (**Fig.28C**). These proteins belong to different mitochondrial pathways and functions, do not seem related one with the other and have not been previously connected to ClpP.

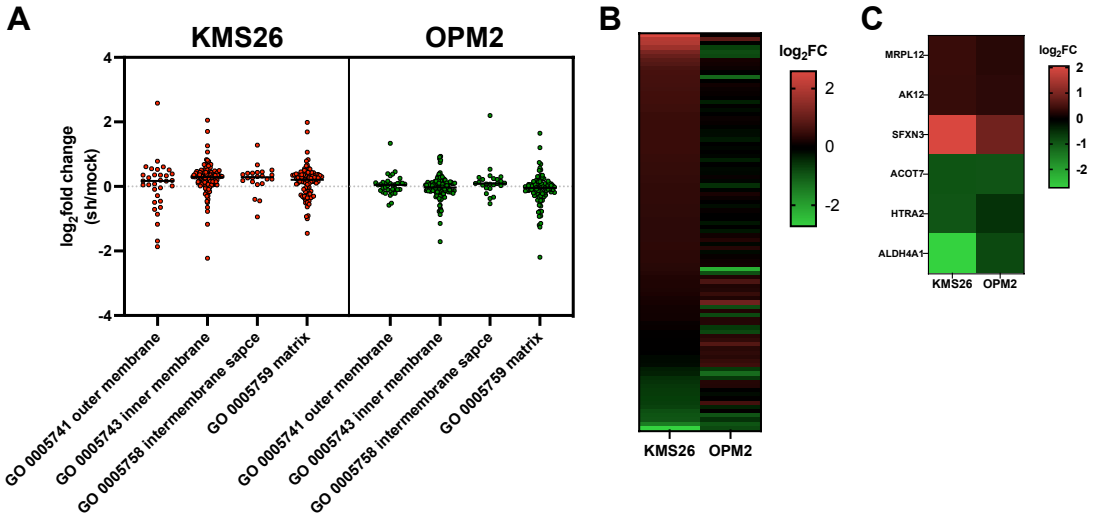

Figure 28. Effects of ClpP knockdown on mitochondrial proteome. *A) Dot plot showing log$_2$fold change of mitochondrial proteins identified by mass spectrometry in total cell lysate after ClpP knockdown in KMS26 and OPM2 cell lines, divided by mitochondrial compartments. B) Heatmap showing log$_2$fold change of mitochondrial proteins identified by mass spectrometry in total cell lysate after ClpP knockdown in both KMS26 and OPM2 with a log$_2$fold change of at least 0,3 in one cell line. C) Heatmap showing log$_2$fold change of mitochondrial proteins identified by mass spectrometry in total cell lysate after ClpP knockdown enriched or depleted in both KMS26 and OPM2.*

To gain a deeper insight in mitochondrial changes caused by ClpP^{kd} we performed LC-MS/MS after cell fractioning, in order to obtain an enrichment for mitochondria and identification of a higher number of mitochondrial proteins. We focused on OXPHOS^{+} KMS26 cells and optimized a commercially available kit to separate cytosolic (F1) and organellar fractions (F2 – enriched in mitochondria) (**Fig.29A**). We analyzed two ClpP^{kd} biological replicates and found 445 mitochondrial proteins consistently identified in F2 (covering over one third of the organellar proteome), attesting to a good performance of our separation and mass spectrometry approaches. On the opposite, we did not detect any significant amount of mitochondrial proteins in F1 (94 proteins identified) (**Fig.29B**).

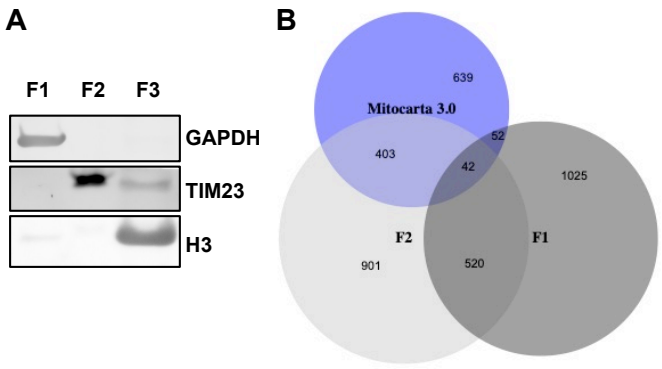

Figure 29. Cellular fractionation for mitochondrial enrichment. *A) Western blot analysis showing enrichment of cytosolic (GAPDH), mitochondrial (TIM23) and nuclear (H3) proteins in the different cellular fractions of KMS26 cells (1 representative experiment of 3 replicates is shown). B) Venn diagram showing the overlap between mitochondrial proteins listed in Mitocarta 3.0 and proteins identified by mass spectrometry in cytosolic (F1) and organellar (F2) cellular fractions in KMS26 cells.*

GSEA revealed that the mitochondrial proteins identified are depleted of various constituents of mitochondrial membrane, ribosomal components and enzymes responsible for mitochondrial tRNAs synthesis (FDR<0.25, p value < 0.01) (**Fig.30A**). ClueGO analysis of mitochondrial proteins with at least a 30% reduction or 50% increase confirmed depletion of mitochondrial translational apparatus and enrichment for enzymes involved in transmembrane transporter activity and fatty-acyl-CoA synthesis (**Fig.30B**).

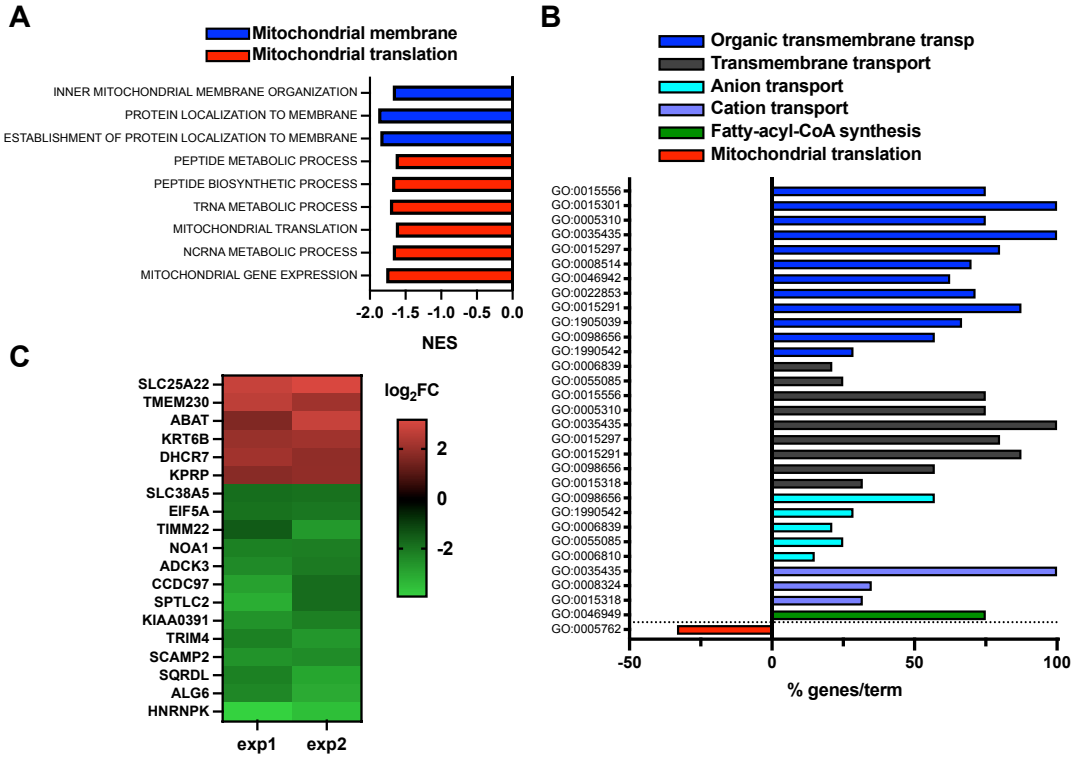

Figure 30. Effects of ClpP knockdown on isolated mitochondrial proteome*. A) Bar chart showing normalized enrichment score (NES) of depleted gene ontology (GO) terms identified by gene set enrichment analysis (GSEA) of proteomic changes in mitochondria enriched fractions of KMS26 cells after ClpP knockdown (p value < 0,05; FDR < 0,2). B) Bar chart showing enriched or depleted GO terms identified by ClueGO analysis of proteins with at least a 30% reduction or 50% increase in mitochondria enriched fractions of KMS26 cells after ClpP knockdown. C) Heatmap showing log_2fold change of the mitochondrial proteins accumulated or depleted with a log_2fold change of at least 0,5 in mitochondria enriched fractions of KMS26 cells after ClpP knockdown.*

Of note, while among deregulated proteins we confirmed those previously identified in our whole cell proteomics, this targeted approach allowed us to unveil a subset of highly impacted mitochondrial proteins, enriched in the mitochondrial fraction, amenable to further investigations as direct effectors of $ClpP^{kd}$ toxicity (e.g. EIF5A, SCAMP2, SLC25A22) (**Fig.30C**). Altogether, this proteomic approach data suggests that silencing of ClpP causes a strongly significant depletion of proteins involved in both cytosolic and mitochondrial translation, possibly perturbs fatty acid metabolism and mitochondrial transmembrane transporters, and identifies a subset of proteins to be further studied as possible mediators of $ClpP^{kd}$ toxicity in MM cells.

Identification of ClpP substrates

Substrates of ClpXP proteolytic activity have been characterized with different approaches and very divergent results according to the technique and cell type (Mabanglo *et al*, 2022). To deepen our understanding of ClpP biology in MM cells, we first performed co-immunoprecipitation (IP) of an overexpressed FLAG-tagged ClpP ($ClpP^{WT\text{-}FLAG}$) followed by LC-MS/MS to identify potential substrates, in two biological replicates of KMS26 cells. To distinguish the privileged substrates of ClpP in MM, we then exploited the ability of inactivated ClpP to accept and retain proteins translocated into its chamber. Active-site mutation in Escherichia coli, Staphylococcus aureus, Caulobacter crescentus and mouse have already been used as substrate trap (Flynn *et al*, 2003; Bhat *et al*, 2013; Feng *et al*, 2013; Szczepanowska *et al*, 2016). We modified our FLAG-tagged ClpP expressing system by replacing the conserved Ser-149 residue in the consensus active site with an alanine (S149A, $ClpP^{MUT\text{-}FLAG}$). Mutant ClpP is expected to assemble with endogenous ClpP and cause a reduction of catalytic activity and allow identification of entrapped substrates by LC-MS/MS of FLAG-IPed lysates ($ClpP^{MUT\text{-}FLAG}$) (**Fig.31A-B**).

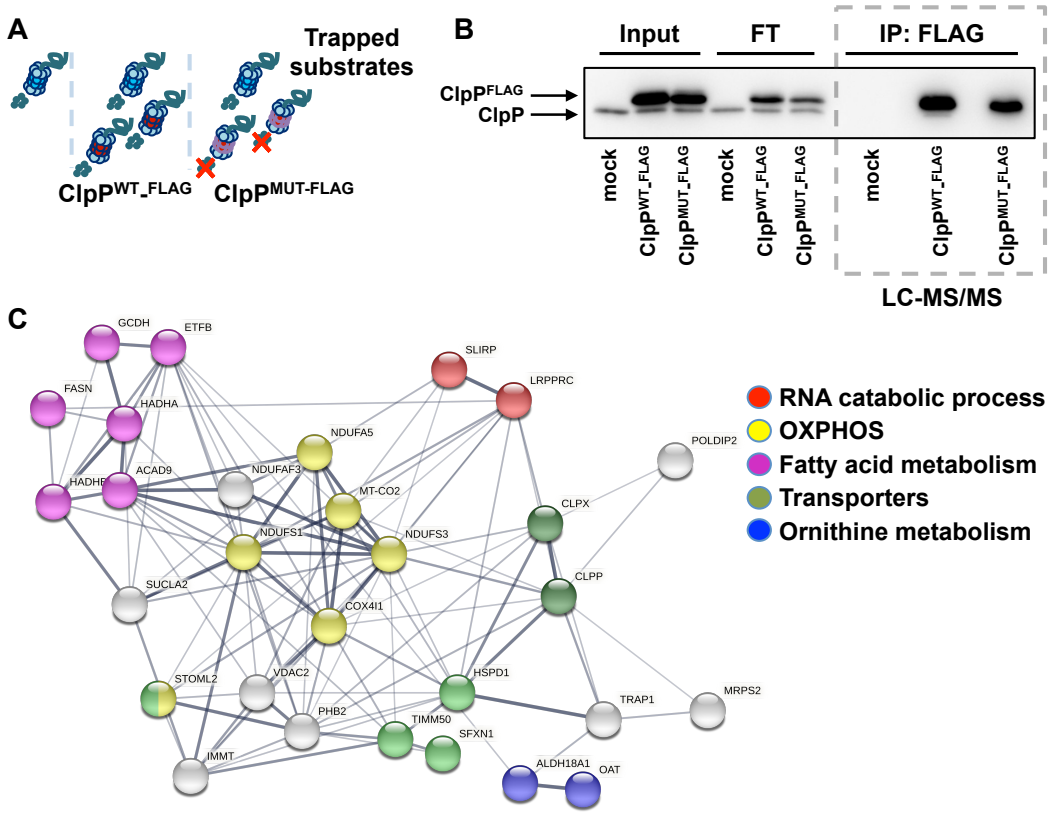

Figure 31. Identification of ClpP substrates*. A) Schematic depiction of the experimental setting. FLAG-tagged ClpP, either wild type (WT-FLAG) or mutated (MUT-FLAG) in the catalytic site, was overexpressed in KMS26 cells. B) Western blot analysis showing endogenous and FLAG-tagged ClpP in total cell lysate (input), and in flow-through (FT) or immunoprecipitated (IP) lysates after immunoprecipitation with anti-FLAG antibody, in KMS26 cells. C) Putative ClpP substrates identified by co-immunoprecipitation of FLAG-tagged ClpP (WT-FLAG or MUT-FLAG) ClpP followed by mass spectrometry. Proteins were selected on the basis of specific presence in IP of WT-FLAG ClpP compared to mock IP, and further enrichment in IP of MUT-FLAG ClpP compared to WT-FLAG ClpP. Proteins were then analyzed with STRING for their interactions and functional annotation.*

We first identified 46 mitochondrial proteins specifically enriched in IP of ClpP$^{WT-FLAG}$ over mock cells. Confirming the validity of this approach in our cell system, we identified ClpXP ATPase subunit ClpX and 18 other proteins that were already described as ClpP substrates in humans and/or mouse with different approaches. To prioritize the most relevant substrates in MM cells, we focused on proteins that were enriched at least two folds in ClpP$^{MUT-FLAG}$ over ClpP$^{WT-FLAG}$ pulldown in both biological replicates. We thus generated a list of 29 bona fide ClpP substrates in MM cells, of which 19 had never been identified before as ClpP substrates in humans (**Table 1, Fig.31C**).

Protein	WT/MOCK (intensity ratio)	MUT/WT (intensity ratio)	KMS26 ClpP^{kd}	OPM2 ClpP^{kd}	KMS26 ClpP^{kd} F2
CLPX	#DIV/0!	16,1417	#N/A	#N/A	-0,0740
CLPP	1263,6442	1,0000	-0,9087	-0,9280	-1,2055
ALDH18A1	#DIV/0!	14,8507	-0,0878	-0,1212	#N/A
ACAD9	#DIV/0!	10,9717	0,2044	-0,2275	0,2196
NDUFAF3	#DIV/0!	7,3700	0,4681	-0,1012	#N/A
LRPPRC	38,7818	3,8272	-0,0244	-0,0304	-0,0137
SLIRP	18,5755	2,3295	0,2938	#N/A	-0,3536
MRPS2	#DIV/0!	4,5712	#N/A	#N/A	0,1323
NDUFS3	2,2291	2,3007	-0,0594	-0,1519	0,3313
NDUFA5	#DIV/0!	2,2904	-0,1549	0,0258	#N/A
POLDIP2	#DIV/0!	3,4887	0,4510	-0,0894	-0,3118
OAT	5,4347	3,4030	-0,0388	#N/A	-0,8853
FASN	#DIV/0!	3,0384	-0,4223	-0,4792	1,6611
SUCLA2	#DIV/0!	2,8207	0,3398	-0,1557	0,5532
HADHB	#DIV/0!	1,0228	0,3575	-0,0457	0,4060
LAP3	#DIV/0!	0,6507	#N/A	-0,0259	#N/A
TIMM50	53,9695	1,1992	0,1313	-0,0712	-0,2336
TRAP1	34,6913	1,4539	0,2656	-0,2223	-0,2350
HADHA	14,8732	0,7843	0,3024	#N/A	0,1203
ETFB	8,9362	1,9125	0,3619	-2,1951	#N/A
STOML2	6,9189	2,1999	0,1461	0,1024	-0,1476
SFXN1	4,6447	1,4614	0,2927	-0,2028	#N/A
SDHA	3,7676	1,9245	#N/A	-0,1596	#N/A
NDUFS1	3,4714	2,8849	0,5058	#N/A	0,0776
GCDH	3,2756	1,7877	0,3556	-0,2367	-0,2716
IMMT	3,2461	1,4499	0,0579	0,0440	0,1732
VDAC2	3,0983	1,5621	-0,0889	0,0268	0,1130
COX4I1	3,0095	2,6571	0,2031	0,0924	-0,0199
HSPD1	2,8217	1,3629	0,1838	0,0602	-0,4445
PHB2	2,7397	1,6396	0,3536	-0,0966	0,3603
MT-CO2	2,2354	1,4032	0,1357	0,0814	0,4076

Table 1. List of putative ClpP substrates*. Proteins were selected as putative substrates on the basis of specific presence in IP of WT-FLAG ClpP compared to mock IP, and further enrichment in IP of MUT-FLAG ClpP compared to WT-FLAG ClpP. Log_2fold change after ClpP knockdown in KMS26 cells, OPM2 cells and F2 of KMS26 cells is shown. In italic previously described ClpP substrates. Proteins with a mutant/wild type ratio >2 in both replicates are highlighted.*

Of particular interest, substrates highly enriched in the catalytically inactive ClpP$^{MUT\text{-}FLAG}$ include components of CI, enzymes involved in ornithine (OAT, ALDH18A1) metabolism and LRPPRC and its protein partner SLIRP, a complex suggested to act as a mitochondrial RNA chaperone that stabilizes RNA structures to expose the required sites for translation (Siira *et al*, 2017). We analyzed accumulation of these proteins in our previous proteomic data of total lysates and mitochondria enriched F2, but we did not significant enrichments. This is compatible with an accumulation of specifically misfolded substrates and not a change in their total abundance.

Altogether these data support the hypothesis that ClpP exerts specific functions in MM cells via degradation of specific substrates and that its manipulation generates a widespread perturbation of mitochondrial translational apparatus.

Transcriptomic effects of ClpP knockdown

Mitochondria are known signaling and transcriptional modulators. We hypothesized that perturbation of mitochondrial homeostasis by $ClpP^{kd}$ might generate activation of transcriptional responses. We therefore used the already established experimental approach of $ClpP^{kd}$ in $OXPHOS^{+}$ and $OXPHOS^{-}$ cell lines KMS26 and OPM2 to perform bulk RNA-sequencing (RNA-seq). Each cell line provided three replicates of both mock and knockdown cells.

One sample of OPM2 $ClpP^{kd}$ was excluded from the analysis because a huge percentage of reads were dropped during the trimming process (possibly due to poor sample quality or contamination). From the principal component analysis (PCA) we observed that $OPM2^{kd}$ samples separate well from the others so we proceeded with the preliminary analysis while waiting to repeat the sequencing.

We performed unsupervised clustering analysis and principal component analysis (PCA) considering the expression values of the top 500 most variable genes, in order to focus on the main sources of variability in the dataset (**Fig.32A-B**). Similarly to proteomics data, we confirmed that the strongest separation between samples is driven by the cell line (PC1 explaining the 88.9% of the total variance) and subsequently by the treatment ($ClpP^{kd}$ vs. $ClpP^{mock}$) on the second component (7.9% of total variance) (**Fig.32C-D**). Within each cell line, samples are segregated according to their treatment. This phenomenon is more evident in OPM2 samples on PC1/PC2, but it is visible also in KMS26 cells.

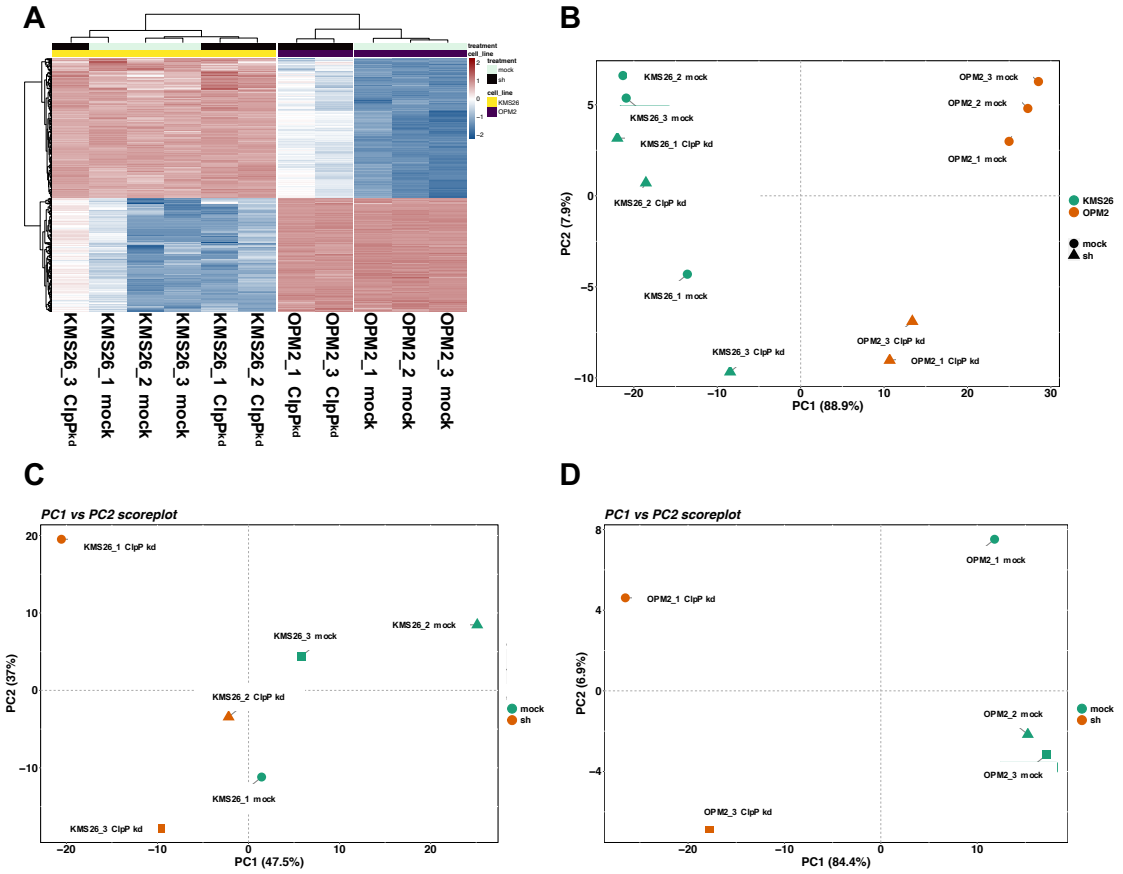

Figure 32. RNA-sequencing of MM cell lines after ClpP knockdown*. A) Heatmap showing unsupervised clustering of RNA-seq samples of KMS26 and OPM2 cells after infection with mock or antiClpP shRNA expressing lentiviral vectors, based on the 500 most variable mRNAs. B) Principal component analysis (PCA) of RNA-seq samples of KMS26 and OPM2 cells after infection with mock or antiClpP shRNA expressing lentiviral vectors, based on the 500 most variable mRNAs Paired samples are identified by shapes. Principal component analysis (PCA) of RNA-seq samples after infection with mock or antiClpP shRNA expressing lentiviral vectors, based on the 500 most variable mRNAs, in C) KMS26 and D) OPM2 cell lines.*

We first performed unbiased GSEA of KMS26 and OPM2 cells separately. By using a highly stringent cut-off (nominal p value< 0.01, FDR <0.05 and NES >1.8) we were still able to identify several pathways affected by $ClpP^{kd}$ in the two cell lines. In particular, $OXPHOS^{+}$ KMS26 confirmed most of the changes suggested by our proteomic analysis, showing depletion of mRNAs encoding proteins involved in cytosolic RNA metabolism and translation, mitochondrial translation and mitochondrial structure and transport (**Fig.33A**). $OXPHOS^{-}$ OPM2 cells showed depletion of cytoskeleton and actin related mRNAs, and enrichment for pathways related to cell growth, regulation of immunological responses and responses to IFN-γ (**Fig.33B**).

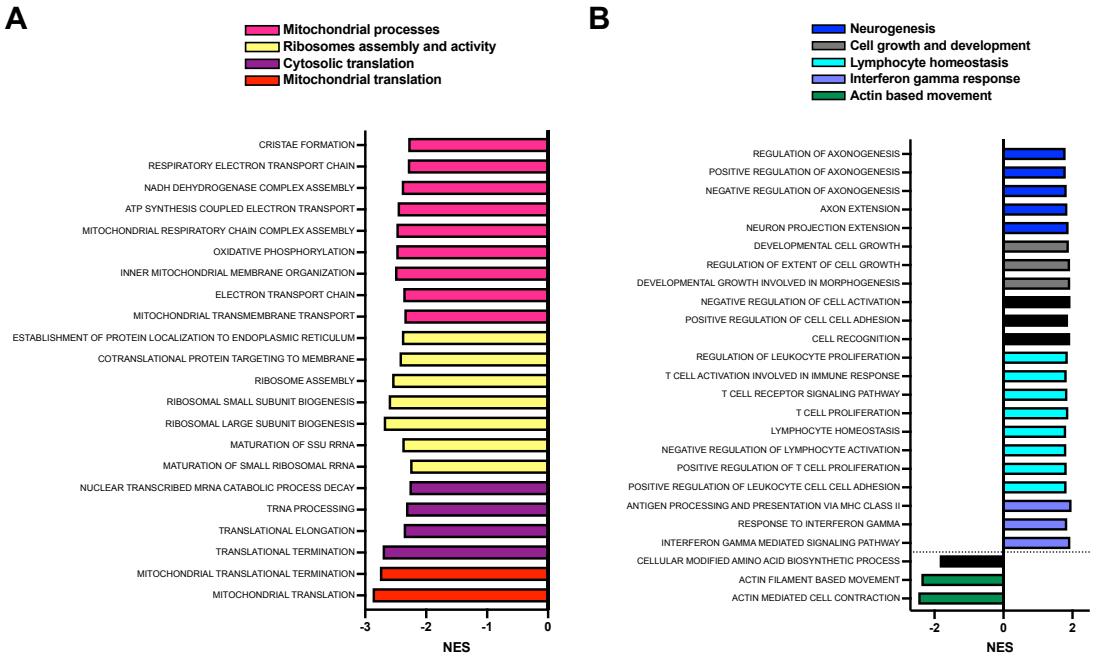

Figure 33. Gene-set enrichment analysis of RNA-seq of ClpP^{kd} cells. *A) Bar chart showing normalized enrichment score (NES) of depleted gene ontology (GO) terms identified by gene set enrichment analysis (GSEA) of RNA-seq of KMS26 cells after ClpP knockdown with very high confidence (p value < 0,01, FDR < 0,01). B) Bar chart showing normalized enrichment score (NES) of depleted gene ontology (GO) terms identified by gene set enrichment analysis (GSEA) of RNA-seq of OPM2 cells after ClpP knockdown with very high confidence (p value < 0,01, FDR < 0,01)*

We then analyzed the most affected single genes in the two cell lines. Very few genes were affected commonly among the two cell lines with high fold changes and low p values (150 genes with $\log_2$fold change>0.5 and p value < 0.05), and enrichment analysis did not detect any specific gene ontology term up- or downregulated. Only 12 genes encoding for mitochondrial proteins were affected. Of note, when we compared all the significant pathways identified by GSEA in the two cell lines (FDR <0.25) we identified 9 biological processes affected in both cell lines (GO:BP terms). They are mainly related to modulation of immune responses and IFN-γ response (**Fig.34A-B**).

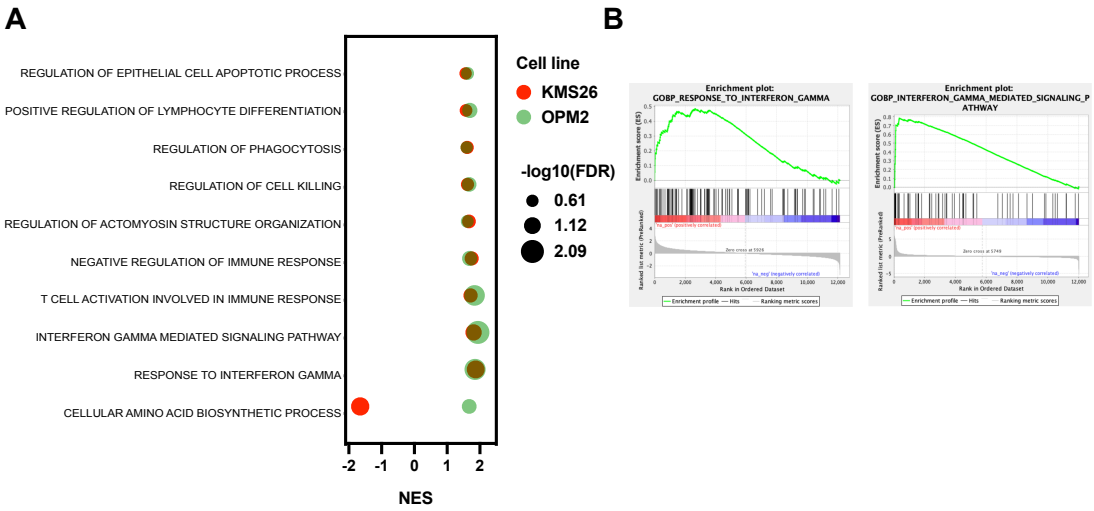

Figure 34. Deregulated processes common to both KMS26 and OPM2 after ClpP knockdown. *A) Bubble chart showing enriched and depleted gene ontology terms identified by gene set enrichment analysis (GSEA) of RNA-seq of KMS26 and OPM2 cells after ClpP knockdown (FDR< 0,25) after ClpP knockdown. B) Plots of IFN-γ related gene ontology terms enriched in RNA-seq of KMS26 cells after ClpP knockdown analyzed by gene set enrichment analysis (GSEA) (NES >1,5; FDR < 0,1; p value < 0,001).*

Altogether, our RNA-seq data suggest that ClpP^{kd} generates both cell line specific responses and a common activation of transcriptional programs while no common effect on mitochondrial proteome is evident.

Metabolic effects of ClpP knockdown

Since mitochondria host major metabolic reactions in cells, we performed metabolomics by ultra-high-performance liquid chromatography (UHPLC) – mass spectrometry, to identify the effects of ClpP^{kd} on mitochondrial functions that might prove crucial for MM. Using the previously described experimental approach, we performed untargeted metabolomics of both OXPHOS^{+} KMS26 and OXPHOS^{-} OMP2 cells after ClpP^{kd}.

PCA analysis showed that KMS26 and OPM2 are well separated, confirming that, as previously noted, they are intrinsically different (**Fig.35A**). ClpP^{kd} generates a clearly separated cluster in KMS26 cells, while the effects on OPM2 cells look less consistent. Of note, changes in ATP abundance reflect our previous experiment, confirming that OPM2 cells do not suffer significant depletion upon ClpP^{kd}. Interestingly, KMS26 cells

show accumulation of glucose and depletion of lactate upon ClpP^{kd}, suggesting that at least part of the ATP drop can be explained by non-mitochondrial effects of ClpP^{kd} on basal glycolysis (**Fig.35B**).

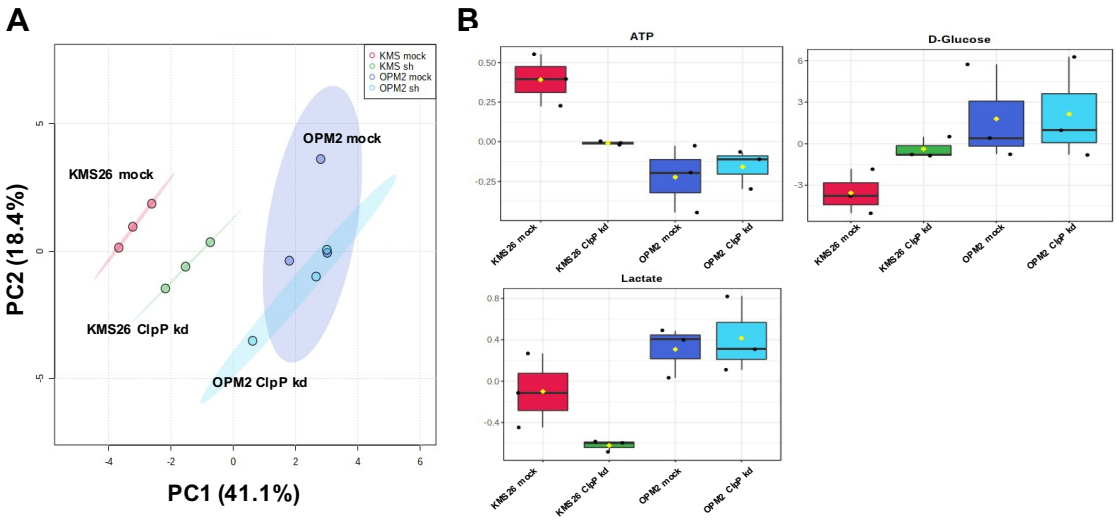

Figure 35. Metabolomics of MM cells after ClpP knockdown*. A) Principal component analysis (PCA) of metabolomics data of KMS26 and OPM2 cells after infection with mock or antiClpP shRNA expressing lentiviral vectors. B) Whisker plot showing relative the relative abundance of ATP, glucose and lactate quantified by mass spectrometry in KMS26 and OPM2 cells after infection with mock or antiClpP shRNA expressing lentiviral vectors. The center line represents the median, the box limits upper and lower quartiles, and the whiskers 1.5x the interquartile range. Black dots represent single samples, the yellow dot represent the mean.*

To identify highly significant changes caused by ClpP^{kd} we first analyzed KMS26 cells and identified statistically significant accumulation of poly-unsaturated fatty acids (PUFA), in particular eicosapentaenoic acid and eicosatetraenoic acid, and depletion of polyamines (putrescine, spermidine) and glutathione and cystathionine (**Fig.36A**). Given the higher experimental variability, analysis of OPM2 suffered limited statistical power, but still showed a trend for similar changes in accumulation of PUFA and depletion of polyamines. Moreover, when we focused on metabolites affected in similar ways in both cell line, we also found a concerted accumulation of several species of acyl-carnitines (**Fig.36B**).

Altogether, while further biological replicates are required to reach definitive confirmation and understanding of the affected metabolites, our preliminary data suggest that ClpP^{kd} blocks lipid catabolism and perturbs the polyamines pathway.

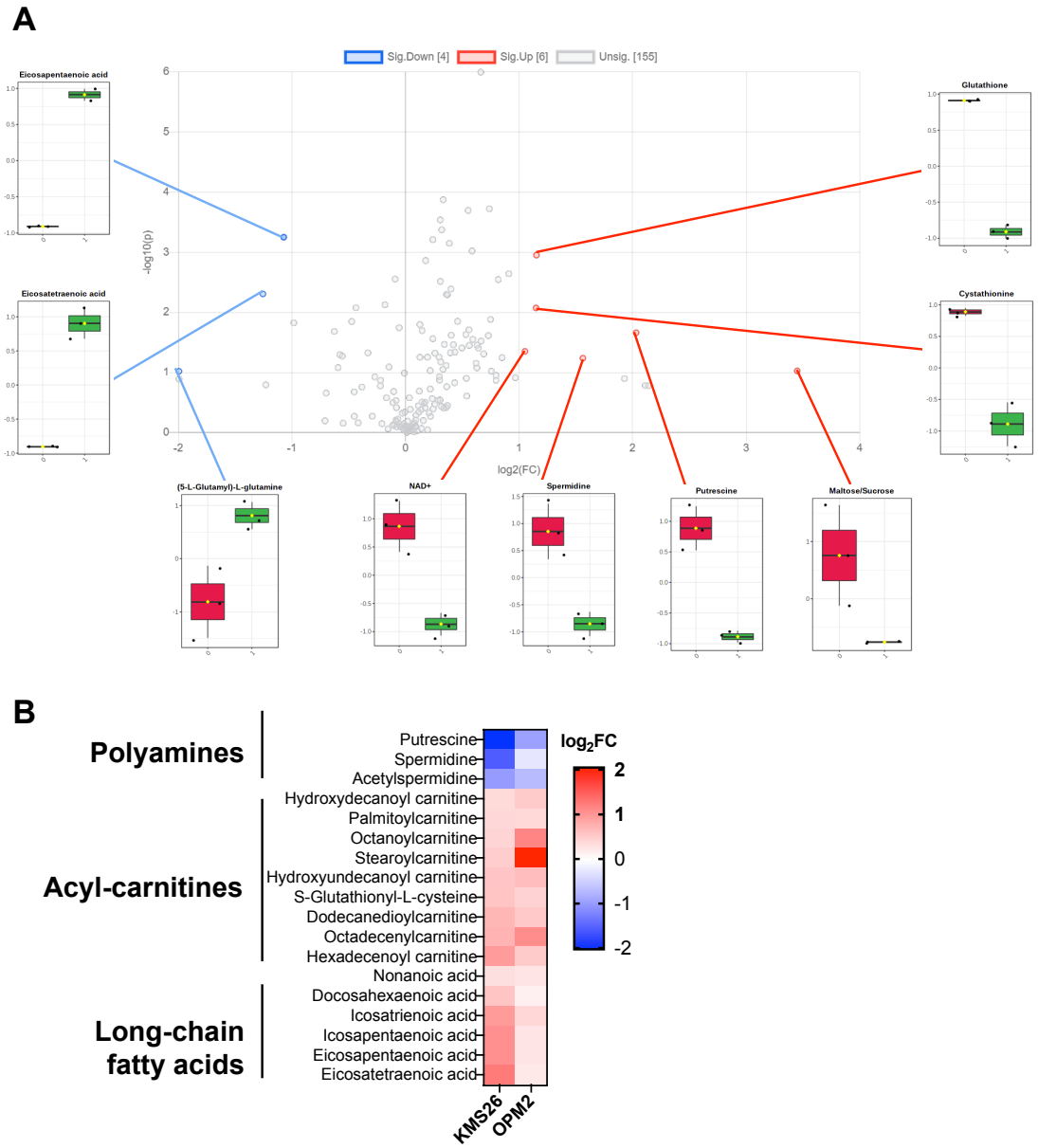

Figure 36. Significant metabolic changes after ClpP knockdown in MM cells. *A) Volcano plot showing log_2fold change and -log_{10}p value of changes in metabolites after ClpP knockdown in KMS26 cells. Whisker plots of significantly affected metabolites (log_2fold change >/<1, -log_{10}p value >1) are shown. ANOVA with post hoc Tukey's test was used for statistical analysis. Plots of significant metabolites are shown. The center line represents the median, the box limits upper and lower quartiles, and the whiskers 1.5x the interquartile range. Black dots represent single samples, the yellow dot represent the mean. B) Heatmap showing log_2fold change of changes in metabolites accumulated or depleted in both KMS26 and OPM2 cell lines after ClpP knockdown.*

Integrated interpretation of proteomics, transcriptomics and metabolomics

The aim of our unbiased proteomic, transcriptomic and metabolomic characterization was to elucidate the role of ClpP in maintaining MM cells viability and to identify ClpP-dependent features amenable to therapeutic targeting. We therefore integrated our findings to generate and test several hypotheses.

ClpP is a major protease of mitochondrial matrix. While its role in activating UPR^{mt} signaling in mammals is debated, we hypothesized that its knockdown could generate perturbation of mitochondrial proteostasis and lead to compensatory strategies. We therefore checked the mRNA and protein levels of the key UPR^{mt} elements previously identified as upregulated in MM cells (HSPD1, HSPE1, HSPA9, LONP1). We found that in KMS26 cells mRNAs UPR^{mt} chaperones HSPD1, HSPE1 and HSPA9 were modestly but significantly reduced, while protein levels were not significantly affected. Surprisingly, we found that these proteins were instead significantly accumulated in the F1 (non-mitochondrial) fraction (**Fig.35A**). Similar changes were not confirmed in OPM2 cells, but prompted us to look at other mitochondrial proteins accumulated in F1 after $ClpP^{kd}$. In fact, we identified approximately 20 proteins of mitochondrial matrix whose mRNA is unaffected or slightly reduced, but are significantly accumulated outside of mitochondria. We hypothesize this might be due to a defect in mitochondrial import machinery, but further exploration of these defects is needed (**Fig.37A**).

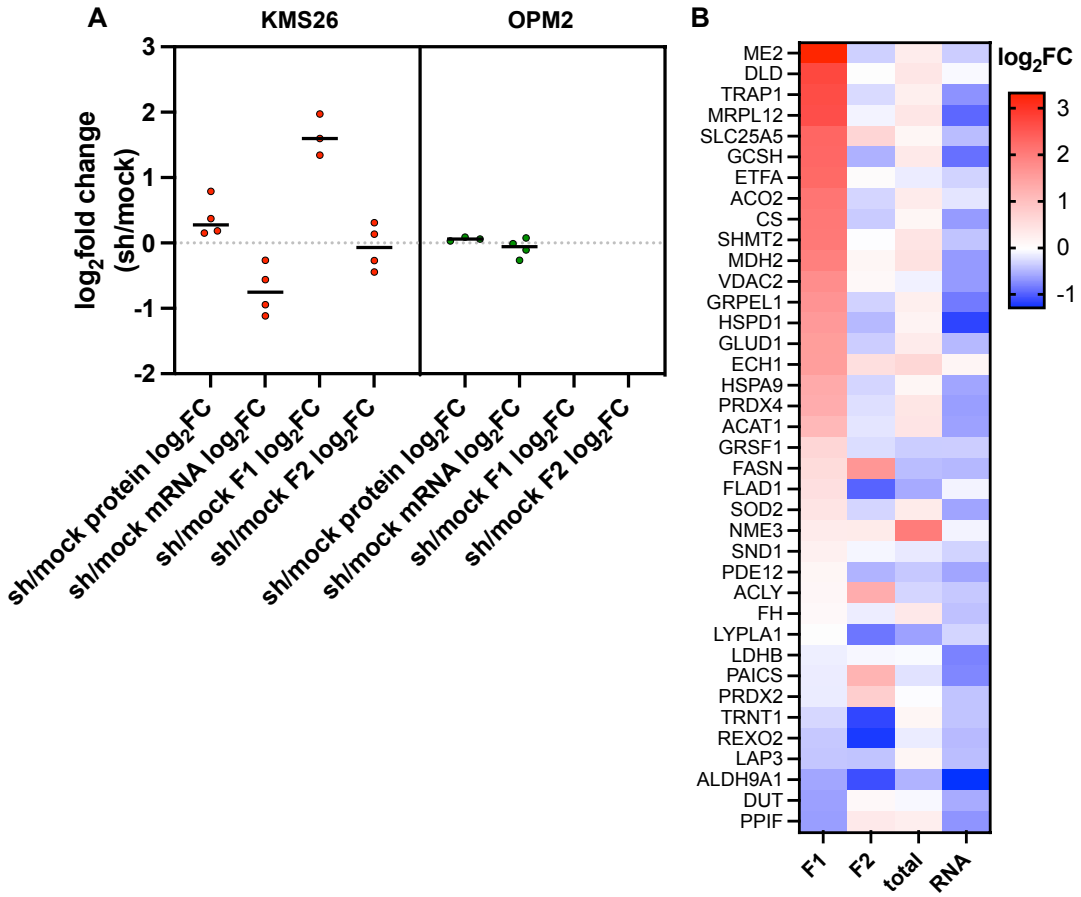

Figure 37. Possible defective import of mitochondrial proteins*. A) Dot plot showing log₂fold change of protein and mRNA changes of UPR^{mt} effectors (HSPD1, HSPE1, LONP1, ClpP) in total cell lysate of KMS26 and OPM2 cells, in RNA-seq and in cytosolic or mitochondrial fractions of KMS26 cells after ClpP knockdown. B) Heatmap showing log₂fold change of selected proteins in cytosolic fraction, mitochondria enriched fraction, total cell lysate and of mRNAs in RNA-seq of KMS26 cells after ClpP knockdown. Only proteins annotated as mitochondria but consistently identified by mass spectrometry in the cytosolic fraction of KMS26 cells are shown.*

To analyze metabolomics data, we focused on the two major pathways affected by ClpP manipulation in both KMS26 and OPM2, namely polyamines and fatty acids. We found decreased amounts of putrescine and spermidine in both cell lines, while other metabolites of the pathway (arginine, ornithine, spermine) were differentially affected in the two cell lines. We used RNA-seq and proteomics data to look for changes in the enzymes involved in polyamines metabolism. We identified downregulation of the whole pathway in KMS26 at a transcriptional level, but also a significant decrease in mRNA and protein levels of spermidine synthase (SRM) in both cell lines (**Fig.38A-B**). Of note, among high confidence putative substrates of ClpP proteolytic activity, we had identified

the enzymes Aldehyde Dehydrogenase 18 Family Member A1 (ALDH18A1) and ornithine aminotransferase (OAT), that might play a role in regulating ornithine availability for this pathway.

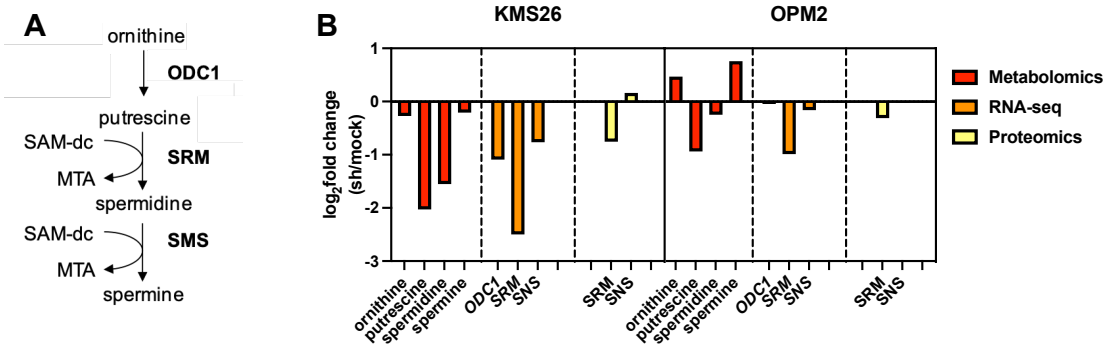

Figure 36. Effects of ClpP knockdown on the polyamines pathway*. A) Schematic description of the polyamines pathway. ODC1: ornithine decarboxylase; SRM: spermidine synthase; SMS: spermine synthase; SAM-dc: S-Adenosyl-L-Methionine Decarboxylase; MTA: 5'-methylthioadenosine. B) Bar plot showing log₂fold change of mRNAs, proteins and metabolites involved in the polyamines pathway in KMS26 and OPM2 cell lines after ClpP knocdown. Blank columns represent non-detected items with the applied technique.*

While arginine tracing experiments are ongoing to confirm the impact of ClpP^{kd} on this pathway, these data strongly suggest that mitochondrial damage leads to a decrease in polyamines via a transcriptional downregulation of at least some of the enzymes responsible for their synthesis. Preliminary experiments show that supplementation of spermidine might be able to rescue the proliferation defect caused by ClpP^{kd} (**Fig.39A**). Polyamines are known to maintain mitochondrial homeostasis in B cells via hypusination of eIF5A, increased translation of TFEB and induction of autophagy (Puleston *et al*, 2019). While TFEB target genes previously identified as downstream of spermidine/eIF5A axis were not depleted in our RNA-seq data (**Fig.39B**), preliminary data suggest that ClpP^{kd} causes an impairment of autophagy in MM cells. Indeed, initial experiments in KMS26 cells showed reduced LC3-II flux, coupled with a decrease in the soluble form of prototypical cargo receptor p62, suggestive of its aggregation due to non-degradation (**Fig.39C-D**). Proteomics data also showed a trend for accumulation of several resident proteins of the endoplasmic reticulum, previously identified as substrate of autophagy in MM cells (Milan *et al*, 2015), at least in KMS26 cells (**Fig.37E**). Given

the dependence of MM cells on autophagy, it is tempting to speculate that polyamine depletion would be toxic due to impairment of the high autophagic flux in these cells.

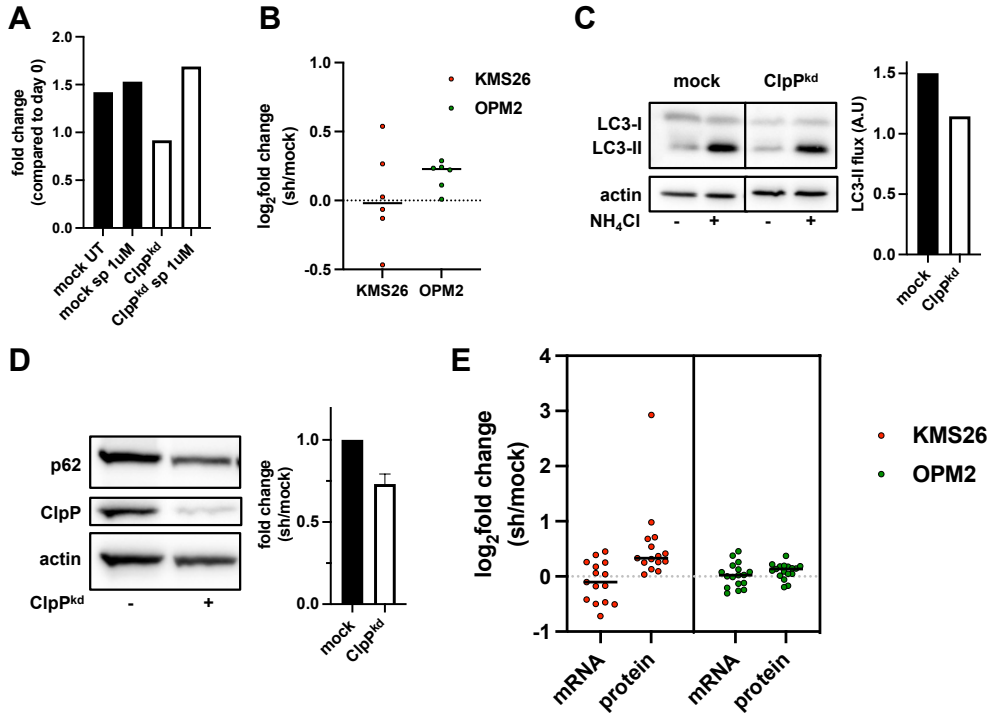

Figure 39. Autophagic defects after ClpP knockdown. *A) Bar plot showing proliferation of OPM2 cells 3 days after infection with mock or anti-ClpP shRNA expressing vectors and treatment with 1uM spermidine for 24h. Proliferation was defined as fold change in cell number compared to day 0, measured by Cyquant Proliferation assay (1 preliminary experiment). B) Dot plot showing log$_2$fold changes in mRNA levels of TFEB canonical target genes by RNA-seq after ClpP knockdown in both KMS26 and OPM2 cell lines; C) western blot analysis of LC3-II accumulation upon treatment with ammonium chloride (NH_4Cl) for 2h in KMS26 cells 3 days after infection with mock or anti-ClpP shRNA expressing vectors (1 preliminary experiment). D) western blot analysis of soluble p62 accumulation in KMS26 cells 3 days after infection with mock or anti-ClpP shRNA expressing vectors (1 preliminary experiment). E) Dot plot showing log$_2$fold change of mRNAs and proteins abundance detected by RNA-seq and proteomics in KMS26 and OPM2 cell lines after infection with mock or anti-ClpP shRNA expressing vectors. Resident proteins of the ER detected are shown.*

Another class of metabolites widely affected by ClpP^{kd} was that of poly-unsaturated-fatty-acids (PUFA). In particular, we identified increased levels of both omega-6 (icosatrienoic acid or dihomo-gamma-linolenic acid, eicosatetraenoic acid or arachidonic acid) and omega-3 (eicosapentaenoic acid or EPA and docosohexaenoic acid or DHA) PUFA (**Fig.36**). We therefore analyzed the expression of enzymes involved in PUFA metabolism in our RNA-seq data, but identified only few significantly affected genes.

Moreover, the results were discordant among the two cell lines, making further interpretation of these findings challenging (**Fig.40**).

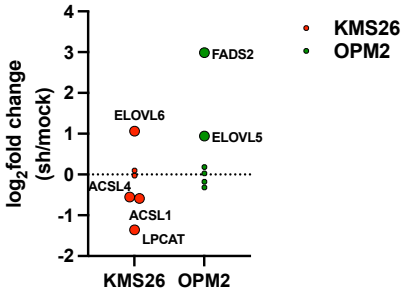

Figure 40. Expression levels of enzymes involved in PUFA metabolism. *Dot plot showing log_2fold change of mRNAs abundance of genes encoding for enzymes involved in poly-unsaturated fatty acids, as detected by RNA-seq of KMS26 and OPM2 cell lines after infection with mock or anti-ClpP shRNA expressing vectors.*

While we did not detect evident changes in abundance of saturated fatty acids, we detected an accumulation of carnitine-conjugated fatty acids with chain lengths higher than C_8. Interestingly, our proteomic analysis had identified several suggestions of perturbation of fatty acid metabolism after $ClpP^{kd}$. First, ACOT7, consistently downregulated in both KMS26 and OPM2 (**Fig.25B, 28C**), is an acyl-CoA thioesterase that preferentially hydrolyzes palmitoyl-CoA, but has a broad specificity acting on other fatty acyl-CoAs with chain-lengths of C8-C18. Moreover, it has been proposed that ACOT7 may play a role in processing of arachidonoyl-CoA to arachidonic acid. Perturbation of ACOT7 would therefore be compatible with a block in the necessary processing of medium and long chain acyl-CoA as substrates for β-oxidation. Of note, our screening of ClpP substrates had identified at least three enzymes involved in β-oxidation: acyl-CoA dehydrogenase 9 (ACAD9), that catalyzes the first step of β-oxidation and has high affinity for long chain fatty acids (e.g. palmitic acid or longer), HADHA and HADHB, which are the two subunits of trifunctional protein hydroxyacyl-CoA dehydrogenase/3-ketoacyl-CoA thiolase/enoyl-CoA hydratase, which catalyzes the last three steps of β-oxidation (**Fig.31C**). While we did not detect a differential abundance of these proteins in our proteomic approach, it is tempting to speculate that their dysregulation due to $ClpP^{kd}$ would lead to perturbation of β-oxidation process.

Since GSEA of RNA-sequencing showed a shared upregulation of IFN-γ mediated responses in both KMS26 and OPM2, we used our proteomic data to check for their abundance after $ClpP^{kd}$. Of the proteins detected by mass spectrometry, all resulted

upregulated, in particular in KMS26 (**Fig.41A**). We then looked at the genes driving the enrichment of these pathways and found that they include CIITA and MHC class II molecules, but also genes that mostly respond to type-I IFN (STAT1, HLA-G). It has recently been proposed that mitochondrial damage and ClpP loss specifically are able to induce activation of cGAS-STING pathway and IFN type-I responses (Torres-Odio *et al*, 2021). We analyzed the impact of $ClpP^{kd}$ on mRNA and protein abundance of a panel of interferon-stimulated genes recently identified as induced in ClpP-knockout mice. Interestingly, all those identified by our RNA-seq and proteomic data resulted upregulated, with many reaching relevant fold changes and statistical significance, in particular in KMS26 (IFIT3, LGALS9, DDX58 (RIG-I), IFIT5, ZBP1, CXCL10; $log_2FC > 1.5$; p-value < 0.05) (**Fig.41B**). Of note, as recently described, activation of interferon signaling was associated with a highly significant increased expression of CD38 in our RNA-seq data (log_2 fold change = 1,13; p value $9{,}2^{-09}$). These data suggest that mitochondrial damage induced by $ClpP^{kd}$ might generate both type I and type II interferon responses, with increased immunogenicity of MM cells. While these findings are unlikely to explain the cell intrinsic toxicities observed in our cell lines, their potential therapeutic relevance is evident and will justify further studies.

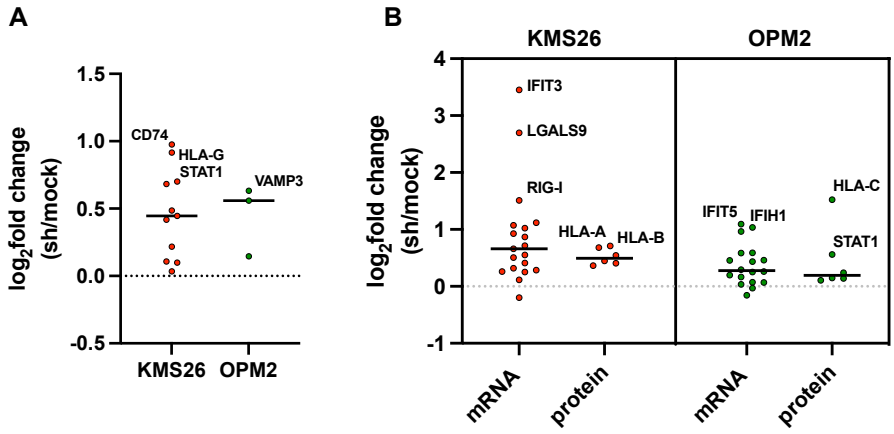

Figure 41. Effects of ClpP knockdown on interferon mediated responses. *A) Dot plot showing log_2fold change in abundance of proteins involved in interferon-γ response, as measured by mass spectrometry in KMS26 and OPM2 cell lines after infection with mock or anti-ClpP shRNA expressing vectors. B) Dot plot showing log_2fold change of mRNAs and protein levels of genes involved in type-I interferon responses in KMS26 and OPM2 cell lines after infection with mock or anti-ClpP shRNA expressing vectors.*

Discussion

Our work started from the observation that MM cells show high expression of crucial effectors of the adaptive UPR^{mt} transcriptional axis. This is in line with the hypothesis that increased mitochondria observed in MM cells are in fact essential, and that maintenance of their homeostasis in the stressful environment of malignant plasma cells requires specific measures. Indeed, a recent work presented at the ASH 2021 Meeting (Trudel S *et al*, oral communication, December 13th, 2021, Atlanta, USA) reached our same conclusions and identified a signature of heightened UPR^{mt} in MM patients. While the adaptive potential of this transcriptional pathway in responding to mitochondrial stress is well established both in mammals and lower organisms, its role in cancer is largely unexplored and might unveil novel vulnerabilities. Moreover, activation of UPR^{mt} has a potential *mitohormetic* effect: mild mitochondrial stresses can generate a transcriptional response that modifies the whole cell and not only resolves the original mitochondrial damage, but renders the whole system more efficient (Yun & Finkel, 2014; Ristow & Zarse, 2010; Birsoy *et al*, 2014). Interestingly, it has recently been proposed that *mitohormesis* could also be beneficial for cancer cells, that would exploit persistent activation of this pathway to gain metastatic advantage (Kenny *et al*, 2019). While we do not have any demonstration that this is the case in MM, it is tempting to speculate that the continued and stressful synthesis of immunoglobulins in MM sustains a chronic, beneficial activation of UPR^{mt}.

We used a knockdown strategy to challenge the role of ATF5 in mediating basal or stress-induced UPR^{mt} and found that this transcription factor could be dispensable in MM. Seminal works exist suggesting the that ATF5 is the mammalian homologue of the master UPR^{mt} transcription factor ATFS-1 identified in *C.elegans* and that it might play a role in stressed cancer cells. (Fiorese *et al*, 2016; Deng & Haynes, 2017). However, its function is intrinsically intertwined with the activity of CHOP and ATF4, and disentangling ATF5 role from the broader activation of the ISR is becoming more and more difficult (Anderson & Haynes, 2020). Moreover, other axes of UPR^{mt} signaling are being discovered, including via estrogen receptor or sirtuins (Kenny & Germain, 2017). In this context, we could hypothesize that ATF5 is not responsible for UPR^{mt} activity in MM, or could be substituted for by others transcription factors when not available. We

must also note that our knockdown strategies strongly diminished, but did not completely abrogate, ATF5 protein. Since ATF5 is continuously synthetized and degraded, with rapid shuttling towards nucleus upon mitochondrial impairment, it is possible that a small residual amount of ATF5 is sufficient to activate transcription of target genes. Formal proof of ATF5 non-essentiality in MM cells will come from ongoing CRISPR-KO experiments. Nonetheless, whenever we reached profound knockdown efficiency, we did detect cell cycle arrest, suggesting a UPR^{mt} independent mechanism of toxicity. Actually, a relevant paper has suggested that ATF5 is required in the correct interaction of centrioles and pericentriolar material (PCM) during mitosis (Madarampalli *et al*, 2015), raising the hypothesis that $ATF5^{kd}$ effects seen in MM cells are dependent on its structural, non-transcriptional role.

Mitochondria are only recently being explored as therapeutic target in MM and very few potential therapeutic targets have been identified. We explored the importance of ClpP in MM and confirmed that its genetic downregulation leads to proliferation arrest or even cell death. While further experiments with isopropil-β-D-1-tiogalattopiranoside (IPTG)-inducible knockdown systems in mouse models are ongoing and will confirm the relevance of ClpP as therapeutic target, these preliminary data confirm its potential value in hematological cancers. Many questions remain still open and will require further elucidation prior to reasonable clinical translation of these findings. First, the transcriptional and/or epigenetic mechanisms that regulate ClpP expression and upregulation in cancer are not understood. In a similar way, the relative contribution of ClpP activity to cancer initiation rather than dissemination and progression needs to be elucidated. Finally, and even more importantly, considering the high expression of ClpP in some healthy tissues (e.g. endocrine organs and gastrointestinal tissues) and the mild phenotype of ClpP loss in both humans and mice, the question of why ClpP manipulation is toxic to malignant but not benign cells calls for further investigations (Nouri *et al*, 2020).

In the perspective of clinical translatability, it is important to notice that pharmacological inhibition of ClpP has been proposed, but is limited by the high homology of human and bacterial ClpP. Initially, trans-b-lactones were identified as inhibitors of bacterial ClpP and indeed show antibacterial activity both *in vitro* and *in*

vivo (Böttcher & Sieber, 2008). One of these synthetic β-lactones, A2-32-01, has been used by Cole *et al.* to inhibit ClpP in leukemia cells thanks to its cross-reactivity with hClpP. However, its toxicity on bacteria and its extreme instability (up to 90% of the compound is degraded after 1 hour in cell culture) make it very unsuitable for clinical development (Cole *et al*, 2015). Two different classes of molecules are being developed as inhibitors of human ClpP. First, derivatives of phenyl esters compounds (that are active against bacterial ClpP) have been synthetized with potent and selective activity against hClpP. In particular TG42 and TG53 seem able to kill liver cancer cells, although more data are needed to prove that they act via ClpP (Gronauer *et al*, 2018). In a parallel effort a new class of boron-based peptidomimetics with high specificity for the human form of ClpP has been developed and holds promise for future development of this therapeutic strategy (Tan *et al*, 2019). Our future experiments include the crystallization of inhibitor-bound ClpP to determine the physical structure and mechanism of inhibition of these compounds and help pharmacological optimization. Finally, it is interesting to mention that while few efforts have been done to inhibit ClpX, the ATPase offers a good therapeutic potential that could be explored in the future.

While MM has usually been considered a glycolytic cancer, recent works highlighted the importance of OXPHOS also in myeloma (Marlein *et al*, 2019; Dalva-Aydemir *et al*, 2015; Xiang *et al*, 2020). Our work confirmed high glycolysis in all MM cell lines, with contribution of OXHPOS ranging from partial to negligible. Previous data on the mechanisms of toxicity of ClpP inhibition in leukemic cells pointed at reduced degradation of mainly CI and CII components and impaired OXPHOS (Cole *et al*, 2015). Having demonstrated that all MM cell lines are addicted to mitochondrial protease ClpP, we therefore hypothesized an OXPHOS independent, ClpP sustained, essential mitochondrial function in MM. Indeed our data prove that $ClpP^{kd}$ does not impair oxygen consumption in both $OXPHOS^{+}$ and $OXPHOS^{-}$ cell lines. Moreover, metabolomics analysis excluded significant changes in TCA cycle and in glutamine metabolism, a previously identified source of TCA cycle intermediates in MM cells (Bolzoni *et al*, 2016). Further supporting the hypothesis of an OXPHOS-independent role of ClpP, we did not detect the expected changes in mitochondrial membrane potential and production of reactive oxygen species. In conclusion, it is likely that in MM ClpP activity extends

well beyond degradation of few components of the electron transport chain and that its substrates and functions are, to a certain extent, MM-specific (Mabanglo *et al*, 2022; Nouri *et al*, 2020). These results are in partial contrast with the hypothesis by Cole *et al.* of an OXPHOS dependent mechanism of toxicity of ClpP inhibition in leukemia. However we have to notice the demonstration of high OXPHOS in leukemic stem cells is way more solid and convincing than in MM cells (Lagadinou *et al*, 2013; Škrtić *et al*, 2011). Moreover, while their work convincingly demonstrated the impact of ClpP on CII activity and oxygen consumption, no formal demonstration that this was the cause of cellular toxicity was achieved. So it is possible that by using a cellular model less depending on OXPHOS, we are unveiling different mitochondrial functions regulated by ClpP and nonetheless essential for cancer.

We performed unbiased proteomics, RNA-seq and metabolomics to dissect the sequelae of $ClpP^{kd}$, together with a co-immunoprecipitation approach to identify specific substrates in multiple myeloma and we integrated the findings of these orthogonal studies to identify the cellular responses to $ClpP^{kd}$. All our data strongly and concordantly identified a profound difference between the two cell lines before manipulation, that translated in a limited overlap of the changes generated by $ClpP^{kd}$. While this is somehow expected in light of the large genomic heterogeneity of human MM cell lines and makes results difficult to generalize (Sarin *et al*, 2020), it also ensures that what is consistently identified in different cell lines has solid and general value. Among the KMS26 specific changes, we identified a very strong transcriptional and proteomic depletion of ribosomal proteins. Since ribosome assembly is a huge and demanding anabolic process (Iadevaia *et al*, 2014), its slowdown is in line with the observed ATP depletion in this cell line and confirms the reliability of our approach. Interestingly, we identified a very significant reduction also of mitochondrial translational machinery, both in terms of mRNAs and proteins. Previous works in ClpP-KO mice have identified a defect in mitochondrial ribosomes following the accumulation of ClpP susbtrate ERAL1, a 12S chaperone needed for the formation of functional small ribosomal subunits (Szczepanowska *et al*, 2016). While we did observe a similar accumulation of MRPL12, we did not identify accumulation of ERAL1 or of components of the small ribosomal subunits. Rather, we detected a general loss of not only ribosomal proteins, but also of enzymes responsible

for mitochondrial tRNAs synthesis. Since the downregulation seems to stem from reduced transcription, we hypothesize that a similar mechanism to cytosolic ribosomal biogenesis might regulate synthesis and assembly of mitoribosomes. Since this phenotype is limited to one of two cell lines we tested, we do not believe it is a plausible explanation for the common toxicity we observed.

Very few works had explored ClpP substrates in mammals, and the only two performed in humans were based on leukemia cells and on proximity ligation. We selected to analyze both the interactome of the wild-type protein and of an inactive mutant by co-immunoprecipitation followed by mass spectrometry to achieve stringent results. Indeed, we did identify many already described ClpP substrates, but also novel unprecedented candidates. Among them, the complex formed by SLIRP and LRPPRC caught our attention because it implies ClpP in mitochondrial translation in a different way from the previously described regulation of mitoribosomes assembly. Indeed, LRPPRC forms a complex with SLIRP and binds mitochondrial RNA and acts as an RNA chaperon, helping its translation, stabilization and polyadenylation (Siira *et al*, 2017). Of note, it was recently demonstrated that Drosophila leucine-rich pentatricopeptide repeat domain-containing protein 1 (DmLRPPRC1) is a specific substrate of ClpXP (Matsushima *et al*). Of note, in proteomic studies of CLpP^{kd} cells we did not identify accumulation of putative ClpP substrates. This is only partly surprising, since previous studies in leukemia have already demonstrated how knockdown of ClpP leads to specific accumulation of misfolded substrates, and not to a change in the overall protein abundance (Cole *et al*, 2015).

Focusing on consistent effects in the two cell lines, metabolomics yielded precious hypothesis to inform further evaluation of proteomics and RNA-seq data. We identified an unprecedented effect of ClpP^{kd} on abundance of polyamines, likely dependent of transcriptional downregulaton of key enzymes of this biosynthetic pathway. Notably, virtually nothing is known on spermidine in myeloma, apart from pioneering reports of circulating spermidine as a potential marker for disease activity and response to therapy (Durie *et al*, 1977; Van Dobbenburgh *et al*, 1983). Among its pleiotropic effects, spermidine sustains autophagy via hypusination of eIF5A and has been shown to have protective effects against aging and age-related diseases (Madeo *et al*, 2018), including

age-associated decline of Ab responses sustained by plasma cells (Zhang & Simon, 2020). Moreover, polyamines may exert widespread and cell type-specific effects on gene expression, protein translation and cell metabolism. While their specific roles in MM need further elucidation, our findings have strong translational potential in light of the current availability of inhibitors of spermidine synthesis and of eIF5A hypusination in early clinical development stage.

Metabolomics also identified an extensive dysregulation of fatty acid metabolism, specifically an accumulation of long-chain acyl-carnitines. Long chain fatty acid are important substrates of beta oxidation. We found an accumulation of their carnitine-bound species, that are produced for mitochondrial import through the CPT1/CTP2 transporters: their increase could derive from a defect of import across mitochondrial membranes or from decreased processing in beta oxidation processes. We hypothesize that these changes might be explained by $ClpP^{kd}$ induced decreased ACOT7 or dysregulated degradation of ClpP substrates ACAD9, HADHA and HADHB, key enzymes of fatty acid oxidation. Defective beta-oxidation has recently been identified in ClpP-KO mice, and mainly attributed to accumulation of very long-chain acyl-CoAs dehydrogenase (VLCAD), previously identified in the same model as a putative ClpP substrate (Becker *et al*, 2018). However, the sequalae of defective fatty acid oxidation are not straightforward, since we did not detect any change in the downstream citric acid cycle and we had already excluded an impact of $ClpP^{kd}$ on OXPHOS. It is therefore possible that defective β-oxidation is toxic to MM cells for non-energetic reasons, for example reduction in the production of acetyl-CoA, that serves as substrates for acetylation of proteins (mainly histones) and regulation of gene activation. On the other hand, we observed increased concentration of PUFA, mainly arachidonic acid. These fatty acids are not a usually used for β-oxidation, but rather are precursors of a variety of pro- and anti- inflammatory mediators (prostaglandins, leucotrienes, tromboxanes) and are essential components of cell membranes. The effects of their imbalance in MM cells is therefore potentially very broad.

Finally, our integrated analysis of RNA-seq and proteomics identified a possible effect of ClpP on the expression of interferon stimulated genes (ISG), both at transcriptional and proteomic levels. Recently, loss of ClpP in mouse and human fibroblasts has been

shown to activate type I interferon responses through mitochondrial stress-driven activation of cGAS-STING, via nucleoid disruption and mtDNA stress (Torres-Odio *et al*, 2021). Offering a mechanistic link between a nuclear ISG response and ClpP, our newly identified ClpP substrates include the nucleoid protein components POLDIP2 and HSPD1/HSP60 (Fig.2), the latter known to be required for nucleoid division (Kucej & Butow, 2007). Unprecedented ClpP substrates in our data also include both members of the LRPPRC-SLIRP RNA chaperone complex, known to stabilize mtRNA to orchestrate translation (Siira *et al*; Aibara *et al*, 2020), hinting at mtRNA, in addition to mtDNA, instability as an additional source of mitochondrial stress capable of activating type I IFN responses independent of cGAS-STING, as recently suggested (Tigano *et al*, 2021; Dhir *et al*, 2018). These data acquire translational relevance in light of the demonstrations that dysfunction of innate and adaptive immunity within the myeloma BM microenvironment is a major obstacle in myeloma therapy (Nakamura *et al*, 2020). Notably, a promising strategy to enhance anti-tumor immunity is exactly activating the cGAS-STING (cyclic GMP-AMP synthase-stimulator of IFN genes) pathway (Ou *et al*, 2021; Pyeon *et al*, 2020). Recently, the first-in-class proteasome inhibitor, bortezomib has been shown to induce immunogenic cell death and to stimulate anti-myeloma immunity via activation of type I IFN signaling via the cGAS-STING axis (Gulla *et al*, 2021). Moreover, relevant to MM immunotherapies, since the cGAS-STING axis has been shown to induce CD38, overcoming IL-6 and stroma-dependent suppression (Xing *et al*, 2021), we found CD38 expression also induced in ClpP kd MM cells. Altogether, the data urge us to dissect the circuit linking ClpP-dependent mitochondrial stress and ISG responses and to appraise its pathophysiological relevance in vivo.

Altogether, our work identifies ClpP as a valuable therapeutic target in MM and supports further studies aimed at validating its targetability and at developing pharmacological inhibitors. Moreover, by studying the mechanisms that lead to MM cell suffering after ClpP manipulation, we generated preliminary data to devise possible synergistic approaches and to identify other mitochondria related, ClpP-independent, vulnerabilities of MM.

Materials and methods

[Parts of the following methods were previously described and published in works of which I am co-author (Milan *et al*, 2015; Li *et al*, 2019; Xu *et al*, 2020; Szalat *et al*, 2018; Fucci *et al*, 2020)*]*

Myeloma patients RNA-seq analysis

Primary malignant and benign plasma cells were purified from MM patients and healthy donors after informed consent was provided, in accordance with the Declaration of Helsinki and under the auspices of a Dana-Farber Cancer Institute Institutional Review Board approved protocol. CD138+ plasma cells were purified from bone marrow aspirates using anti-CD138 microbeads (Miltenyi Biotech, Auburn, CA, USA). Newly diagnosed MM patients were enrolled in the DFCI 2009 trial (ClinicalTrials.gov number, NCT01191060) and primary results of the trail have been published (Attal *et al*, 2017) .

RNA-sequencing was performed as per standard methods. Briefly, total RNA was put through quality control by Bioanalyzer using the RNA Pico Kit (Agilent, Santa Clara, CA). Following library preparation with NEBNext Ultra RNA Library Prep Kit for Illumina (New England BioLabs, Ipswich, MA), DNA libraries were expanded with the Universal Library Quantification Kit for Illumina (Kapa Biosystems, Wilmington, MA) and run on the 7900HT Fast quantitative PCR machine (ABI, Grand Island, NY). RNA-seq reads were mapped to the human genome (build hg19) using TopHat 2.0.10 and a gene annotation corresponding to Ensembl GRCh37. Gene abundance was quantified from mapped reads and gene-level counts were transformed to reads per million (RPM) for normalization. For comparison of groups of genes, all genes were scaled to the same range (z-score, -2 to +2), and a sum of z-scores obtained for each patient.

Cell cultures and treatment

Human MM cell lines KMS26, NCI-H929, MM.1S, OPM2, RPMI-8226, LP1, KMS28BM and EJM were kindly provided by Dr. Nikhil Munshi, Dana-Farber Cancer Institute (Boston, MA, USA), after identity confirmation by STR sequencing. MM cells

were cultured in RPMI media (GIBCO-Life Technologies, Cat# 61870) supplemented with 10% fetal bovine serum (Euroclone, Cat# ECS0180L), L-glutamine (2 mM; GIBCO-Life Technologies, Cat# 25030-024), penicillin (100 U/ml; GIBCO-Life Technologies, Cat# 15140-122), streptomycin (100 µg/ml; Lonza) and sodium pyruvate (1 mM; GIBCO-Life Technologies, Cat# 11360-039). HEK293T were cultured in Dulbecco's modified Eagle's medium (DMEM, GIBCO-Life Technologies, Cat# 41965039) supplemented as described above for RPMI media. All lines were periodically tested for mycoplasma negativity. Cells were treated with bortezomib (Cell Signaling Technologies, Cat# 2204), paraquat (Sigma-Aldrich, Cat# 36451) and ammonium chloride (Sigma-Aldrich, Cat# 254134), at the doses indicated in the figures.

Genetic manipulation

Lentiviral viruses to stably express anti-*CLPP* (Sh73: TRCN0000291173; Sh61: TRCN0000046861), anti-*ATF5* (Sh39: TRCN0000017639; Sh70: TRCN0000430270), and control shRNAs (SHC202 Non-Mammalian) were generated starting from Mission shRNAs (Sigma-Aldrich). Puromycin resistance gene was substituted with the truncated human CD271 (LNGFR). Lentiviruses to stably express anti-*CLPP* and control sgRNAs were generated starting from Addgene #52961plasmid (kind gift of Simone Cardaci); puromycin resistance gene was substituted with BFP. Human C-ter wild-type *FLAG-CLPP* (OHu27691D ORF Clone (GenScript) was cloned in a plasmid with a bidirectional human PGK-miniCMV promoter co-expressing the protein of interest and truncated human CD271. The human S152A mutant form of CLPP, equivalent to the murine S149A, was subsequently generated by site specific mutagenesis with the In-Fusion HD Cloning kit (Takara, Diatech, Cat# 638920).

SgRNAs were designed as per standard protocols adapted to the Zhang Lentiviral CRISPR toolbox strategy (Sanjana *et al*, 2014).

Lentiviral vectors were packaged with the vector of interest (shRNAs, sgRNA or FLAG-protein cDNAs) plus, pMD2-VSV-G, pMDLg/pRRE and pCMV-Rev plasmids in HEK293T cells for 14 h, then medium was replaced. 30 h after medium change, cell supernatants were collected, ultra-centrifuged, filtered and added to MM cells for 16 h.

Transduced cells were grown for 48 h and infection efficiency was determined analyzing BFP positivity or checking LNGFR expression with flow cytometry.

Flow cytometry analysis and sorting

For mitochondrial mass determination, mitochondrial ROS production and mitochondrial transmembrane potential cells were collected and stained with MitoTracker Green FM, MitoSOX, MitoTracker Red CMXROS, respectively (Life Technologies, Cat# M7514, M36008, M7512) according to manufacturer's instructions. For apoptosis detection, cells were stained with APC-conjugated AnnexinV and propidium iodide following the manufacturer's instructions (BD PharmMingen, Cat #556547). Cells were analyzed with Accuri C6 Flow Cytometer and FCS Express 7 Flow Research Edition (De Novo Softwares).

Sorting of transduced MM cells was performed after staining with FITC-conjugated anti-LNGFR (Biolegened, Cat# 345104) or based on BFP expression with BD FACSAria Fusion instrument (BD Biosciences).

qRT-PCR

RNA was extracted with TriFAST (Euroclone, Cat# EMR507100), 1000 ng RNA retro-transcribed with ImProm-II Reverse Transcriptase System (Promega, Cat# A3800), and cDNA corresponding to 5 ng of original RNA used as template in qPCR reactions. qPCRs were performed using SYBR green I master mix (Roche, Cat# 04887352001) on Roche LightCycler 480. Data were analyzed on Roche LC480 software with Advance Relative Quantification using human H3 expression as normalizer.

Primers used are:

H3:	FW GTGAAGAAACCTCATCGTTACAGGCCTGGT
	REV CTGCAAAGCACCGATAGCTGCGCTCTGGAA
ATF5:	FW GCTGGGATGGCTCGTAGACT
	REV TCGCTCAGTCATCCAGTCAGA
CLPP:	FW GCCAAGCACACCAAACAGAG
	REV AGGGTGGACCAGAACCTTGT
HSPD1:	FW TGCTCACCGTAAGCCTTTGG
	REV AAACCCTGGAGCCTTGACTG
HSPE1:	FW CGGAGGGAGTAATGGCAGGA

REV ACTGGTTGAATCTCTCCACCCT
HSPA9: FW ACTCCTGCGTGGCAGTTATG
REV CGGCATTCCAACAAGTCGCT
LONP1: FW CTGCTGGACAACCACTCCTC
REV CCTCCATGCCGTAGTGGTCT

Cell proliferation assay

Cell proliferation was measured with CyQUANT Direct Cell Proliferation Assay Kit (Invitrogen, Cat# 35011). Briefly, 10000 cells were plated in flat bottom clear, black polystyrene, 96 wells plates (Merck, Cat# CLS3614) and fluorescence was analyzed with a Victor plate reader (Perkin-Elmer, Waltham MA).

Intracellular ATP quantification

ATP was quantified with the luminescent CellTiter-Glo assay following the manufacturer's instructions (Promega, G7570). Briefly, for each condition 80000 MM cells were plated in quadruplicates on white 96-well multi-well plates and were analyzed with a Victor plate reader (Perkin-Elmer, Waltham MA).

Seahorse assays

We measured OCR and ECAR by SeaHorse XFe96 Analyzer (Agilent Technologies) using SeaHorse XF Cell Mito Stress Test and Glycolytic Rate Assay kits, following the manufacturer's instructions. The day of the assay cells were counted and attached to 96-well Seahorse cell culture microplates, pre-coated with Corning™ Cell-Tak (Life Sciences, Cat# DLW354242) according to manufacturer's instructions, at a density of 80,000 cells per well, in XF RPMI Medium pH 7.4 with 1 mM HEPES (Agilent Technologies) supplemented with 10 mM glucose, 1 mM sodium pyruvate, and 2 mM L-glutamine. The plate was incubated at 37 °C for 1 h in a non-CO_2 incubator. For the Mito Stress Test assay after OCR baseline measurements, oligomycin A, FCCP, and rotenone/antimycin A (R/AA) were added sequentially to each well to reach the final concentrations of 2 μM, 0.5 μM, and 0.5 μM, respectively. For the Glycolytic Rata assay after ECAR baseline measurements, R/AA and 2-deoxy-glucose (2-DG) were added

sequentially to each well to reach the final concentrations of 0.5 μM, and 50 mM, respectively. Results were analyzed using Seahorse Wave Desktop Software Version 2.6 (Agilent Technologies), normalized by cell number using CyQUANT Direct Cell Proliferation Assay (Invitrogen, Cat# 35011). OCR data are expressed as pmol of oxygen per minute per arbitrary units (pmol/min/a.u.), ECAR data as mpH per minute per arbitrary units (mpH/min/a.u.). Data from Wave Desktop 2.6 software were exported also into the XF Report Generators for calculation of the parameters from Mito Stress Test and Glycolytic Rate Assays. In the Mito Stress Test assay, basal respiration was calculated by subtracting the minimum OCR measurement after R/AA injection from the last OCR measurement before oligomycin injection; ATP coupled respiration by subtracting the minimum OCR measurement after oligomycin A injection from the last OCR measurement before oligomycin A injection; maximal respiration by subtracting the minimum OCR measurement after R/AA injection from the maximal OCR measurement after FCCP injection. In the glycolytic rate assay, initial OCR and ECAR measurements were used to determine the total proton efflux rate (PER); sequential addition of R/AA and 2-DG were used to determine the mitoPER (PER from mitochondrial respiration) and compensatory glycoPER (PER from glycolysis) respectively.

Immunoblot analyses

Total cellular extracts were obtained by lysis in 150 mM NaCl, 10 mM Tris-HCl (pH 7.5), protease inhibitor cocktail (Roche, 05056489001), PhosSTOP phosphatase inhibitor (Sigma-Aldrich, 4906845001) and 1% SDS (Sigma-Aldrich, 05030). Genomic DNA was mechanically removed using 0,5ml Insumed syringes (PIC solution). For soluble fractions, cells were collected and lysed in 150 mM NaCl, 10 mM TrisHCl (pH 7.5) and Igepal CA-630 1% (Sigma-Aldrich, I3021) supplemented with protease inhibitors, for 15 min on ice. Insoluble material was pelleted at 13000 g for 15 minutes and solubilized in 1% SDS lysis buffer. Cellular fractionations were performed with Qproteome cell compartment kit (QIAGEN, Cat# 37502) following manufacturer's instructions. Protein amounts were quantified by DC protein assay (Bio-Rad, 5000116) as described by manufacturer. 15-45 mg of protein lysate were resolved in 8%, 12 or 15% SDS-PAGE

gels and blotted on nitrocellulose membrane (Mini-PROTEAN Tetra Cell, BioRad, Hercules CA). Membranes were blocked in 5% milk in 0.1% TBS-Tween, incubated with primary and secondary antibodies, thoroughly washed with 0.1% TBS-Tween. Images were obtained using ChemiDoc-it (UVP) for HRP-conjugated secondary Ab or FLA9000 (FujiFilm) for Alexa Fluor conjugated secondary antibodies. Densitometric analysis was performed using ImageJ software (https://imagej.nih.gov/ij/). Antibodies used are: rabbit anti-p62/SQSTM1 (Sigma-Aldrich, Cat# P0067); rabbit anti-LC3A (Novus Biological Cat# NB100-2331); mouse anti-β-actin (Sigma-Aldrich, Cat# A5441); mouse anti-FLAG M2 (Sigma-Aldrich, Cat# F1804); rabbit anti-CLPP (Abcam, Cat# ab124822); rabbit anti-GAPDH (Santa Cruz Biotechnologies, Cat# sc-25778); rabbit anti-H3 (Abcam Cat# ab1791); rabbit anti-cleaved caspase 3 (Cell Signaling Thecnologies; cat #9661), rabbit anti-TIM23 (Abclonal, cat# A8688); mouse anti-TIM50 (Santa Cruz Biotechnologies, Cat# sc-393678).

Immunoprecipitation

Cells were lysed in 150 mM NaCl, 10 mM Tris-HCl (pH 7.5) and 1% Igepal CA-630 (Sigma-Aldrich, I3021), supplemented with protease inhibitors as described above, incubated for 15 min on ice. Nuclei and insoluble materials were pelleted at 1000 g for 15 min. For immunoprecipitation of FLAG-tagged ClpP proteins, lysates were incubated for 16h with 30 µl of protein G Agarose beads (Millipore, Cat# 16-266) pre-conjugated with 5 µg of mouse monoclonal FLAG M2 antibody (Sigma-Aldrich, Cat# F1804). Beads were washed 4 times in 150 mM NaCl, 10 mM Tris-HCl (pH 7.5), and resuspended in Laemmli Buffer for SDS-PAGE resolution and subsequent processing for western blotting as previously described or mass spectrometry (see below).

Polysome profiling

Polysome profiling and RNA extraction from fractions were performed following the protocols previously described (Pringle *et al*, 2019). Briefly, mock and shCLPP KMS26 cells were counted and the same amount of cells was treated with 100 µg/ml cycloheximide (Sigma-Aldrich, Cat# C7698) for 3 min. Cells were lysed in 300 mM NaCl, 20 mM Tris-HCl (pH 7.5), 10 mM MgCl2, 100 µg/ml cycloheximide, RNase

Inhibitor (Promega, Cat# N251B) and 1% Igepal CA-630 (Sigma-Aldrich, Cat# I3021), supplemented with protease and phosphatase inhibitors as described above, incubated for 15 min on ice. Nuclei and insoluble materials were pelleted at 13000 g for 15 min. Lysates were loaded on top of a 7%–47% sucrose linear gradient containing 100 µg/ml cycloheximide and centrifuged at 39,000 rpm on a SW 41 rotor (Beckman Coulter) for 90 min. UV absorbance was measured with Bio-Rad Automated Econo System (Bio-Rad), 1ml fractions were collected and RNA re-quantified with NanoDrop 8000 (Thermo Scientific).

Proteomics

Soluble fractions mitochondrial fractions or immunoprecipitated proteins were processed for mass spectrometry, depending on the experimental setting. Immunoprecipitated proteins or 60µg of total protein lysate were loaded in a 4%–20% gradient SDS-PAGE and stained with Coomassie Brilliant Blue (Sigma-Aldrich, Cat# B7920). Gel slices sampling the entire length of the lanes were excised and processed. After reduction with 10mM DTT (Sigma-Aldrich, Cat# D9779), alkylation with 55 mM iodoacetamide (Sigma-Aldrich, Cat# I1149) and overnight digestion with trypsin 10ng/µl (Roche, Cat# 11418475001), tryptic peptides were desalted and concentrated on C18 Stage Tips (Proxeon Biosystems, Cat# SP301) following the manufacturer's instructions, and analyzed by LC-MS/MS with a Q-Exactive mass Spectrometer (Thermo Fisher Scientific). Raw data were processed with MaxQuant and peptides identified from MS/MS spectra against the Human Uniprot Complete Proteome Set database using the Andromeda search engine. Cysteine carbamidomethylation was used as fixed modification, methionine oxidation and protein N-terminal acetylation as variable modifications. Mass deviation for MS/MS peaks was set at 0.5 m/z units and the peptides and protein false discovery rates (FDR) were set to 0.01.

Metabolomics

Approximately $1x10^6$ cells were extracted in 1000 µL of ice cold extraction solution (methanol:acetonitrile:water 5:3:2 *v/v/v*). Suspensions were vortexed continuously for 30 min at 4°C. Insoluble material was removed by centrifugation at 18,000 g for 10 min at

4°C and supernatants were isolated for metabolomics analysis by ultra-high-performance liquid chromatography (UHPLC)-MS. Analyses were performed using a Vanquish UHPLC coupled online to a Q Exactive mass spectrometer (Thermo Fisher, Bremen, Germany). Ten microliters of sample extracts were loaded onto a Kinetex XB-C18 column (150x2.1 mm i.d., 1.7µm – Phenomenex). Samples were analyzed using a 3 minute isocratic condition or a 5, 9, and 17 min gradient, as described in state-of-the-art papers (Nemkov *et al*, 2017). Metabolite assignments were performed using MAVEN (Clasquin *et al*, 2012). Graphs and statistical analyses were prepared with and MetaboAnalyst 4.0 (Chong *et al*, 2018).

RNA-sequencing of MM cell lines

500 thousand cells were collected and lysed on ice in 500 microliters of TRiFast (Euroclone, Cat#MR517100). All subsequent purification steps were performed with RNeasy Micro Kit, following manufacturer's instruction (Qiagen, Cat #74004).
Libraries were prepared using Illumina TruSeq Stranded kit, according to the manufacturer's instructions. Sequencing was performed on a Illumina NovaSeq 6000 machine (Illumina, San Diego, CA) obtaining an average of 30 millions of single-end reads per sample. The raw reads produced from sequencing were trimmed using Trimmomatic, version 0.32, to remove adapters and to exclude low-quality reads from the analysis. The remaining reads were then aligned to the human genome hg38 using STAR, version 2.5.3a. Reads were eventually assigned to the corresponding genomic features using featureCounts, according to the Gencode basic annotations (Gencode version 31). Quality of sequencing and alignment was assessed using FastQC, RseQC and MultiQC tools. Expressed genes were defined as those genes showing at least 1 Count Per Million reads (CPM) on at least a selected number of samples, depending on the size of the compared groups (Chen *et al*, 2016). Low-expressed genes that did not match this criteria were excluded from the corresponding dataset. Gene expression read counts were exported and analyzed in R environment (v. 4.0.3) to identify differentially expressed genes (DEGs), using the DESeq2 Bioconductor library (v. 1.30.1, https://doi.org/10.1186/s13059-014-0550-8). *P*-values were adjusted using a threshold

for false discovery rate (FDR) < 0.05. Significant genes were identified as those genes showing FDR < 0.05.

Data analysis

Proteomics and RNA-sequencing data were analyzed with Pre-ranked Gene Set Enrichment Analysis (GSEA) (Subramanian *et al*, 2005), ClueGO (Bindea *et al*, 2009) or STRING (Szklarczyk *et al*, 2019), as indicated in figure legends. The gene-sets included in the GSEA analyses were obtained from Hallmark and the Gene Ontology collections as they are reported in the MSigDB database. Venn diagrams were obtained with BioVenn (Hulsen *et al*, 2008). Graphs and data analysis were obtained using Prism v6.0 software (GraphPad). Statistical significance was tested as indicated in the figure legends. Asterisks indicate the following *p* values: $^{*}p < 0.05$; $^{**}p < 0.01$; $^{***}p < 0.001$; $^{****}p < 0.0001$.

References

Affer M, Chesi M, Chen WD, Keats JJ, Demchenko YN, Tamizhmani K, Garbitt VM, Riggs DL, Brents LA, Roschke A V., *et al* (2014) Promiscuous MYC locus rearrangements hijack enhancers but mostly super-enhancers to dysregulate MYC expression in multiple myeloma. *Leukemia* 28: 1725–1735

Aibara S, Singh V, Modelska A & Amunts A (2020) Structural basis of mitochondrial translation. *Elife* 9: 1–17

Anand R, Langer T & Baker MJ (2013) Proteolytic control of mitochondrial function and morphogenesis. *Biochim Biophys Acta* 1833: 195–204

Anderson NS & Haynes CM (2020) Folding the Mitochondrial UPR into the Integrated Stress Response. *Trends Cell Biol* 30: 428–439

Angelastro JM, Canoll PD, Kuo J, Weicker M, Costa A, Bruce JN & Greene LA (2006) Selective destruction of glioblastoma cells by interference with the activity or expression of ATF5. *Oncogene* 25: 907–916

Attal M, Lauwers-Cances V, Hulin C, Leleu X, Caillot D, Escoffre M, Arnulf B, Macro M, Belhadj K, Garderet L, *et al* (2017) Lenalidomide, Bortezomib, and Dexamethasone with Transplantation for Myeloma. *N Engl J Med* 376: 1311–1320

Avet-Loiseau H, Gerson F, Magrangeas F, Minvielle S, Harousseau JL & Bataille R (2001) Rearrangements of the c-myc oncogene are present in 15% of primary human multiple myeloma tumors. *Blood* 98: 3082–3086

Bajpai R, Sharma A, Achreja A, Edgar CL, Wei C, Siddiqa AA, Gupta VA, Matulis SM, McBrayer SK, Mittal A, *et al* (2020) Electron transport chain activity is a predictor and target for venetoclax sensitivity in multiple myeloma. *Nat Commun* 11: 1228

Barretina J, Caponigro G, Stransky N, Venkatesan K, Margolin AA, Kim S, Wilson CJ, Lehár J, Kryukov G V., Sonkin D, *et al* (2012) The Cancer Cell Line Encyclopedia enables predictive modelling of anticancer drug sensitivity. *Nature* 483: 603–607

Bartel TB, Haessler J, Brown TLY, Shaughnessy JD, Van Rhee F, Anaissie E, Alpe T, Angtuaco E, Walker R, Epstein J, *et al* (2009) F18-fluorodeoxyglucose positron emission tomography in the context of other imaging techniques and prognostic factors in multiple myeloma. *Blood* 114: 2068–2076

Becker C, Kukat A, Szczepanowska K, Hermans S, Senft K, Brandscheid CP, Maiti P & Trifunovic A (2018) CLPP deficiency protects against metabolic syndrome but hinders adaptive thermogenesis. *EMBO Rep* 19: e45126

Bergsagel PL & Kuehl WM (2005) Molecular pathogenesis and a consequent classification of multiple myeloma. *J Clin Oncol* 23: 6333–6338

Bergsagel PL, Kuehl WM, Zhan F, Sawyer J, Barlogie B & Shaughnessy J (2005) Cyclin D dysregulation: an early and unifying pathogenic event in multiple myeloma. *Blood* 106: 296–303

Besse A, Stolze SC, Rasche L, Weinhold N, Morgan GJ, Kraus M, Bader J, Overkleeft HS, Besse L & Driessen C (2018) Carfilzomib resistance due to ABCB1/MDR1 overexpression is overcome by nelfinavir and lopinavir in multiple myeloma. *Leukemia* 32: 391–401

Besse L, Besse A, Mendez-Lopez M, Vasickova K, Sedlackova M, Vanhara P, Kraus M, Bader J, Ferreira RB, Castellano RK, *et al* (2019) A metabolic switch in proteasome inhibitor-resistant multiple myeloma ensures higher mitochondrial metabolism, protein folding and sphingomyelin synthesis. *Haematologica* 104: E415–E419

Bhat NH, Vass RH, Stoddard PR, Shin DK & Chien P (2013) Identification of ClpP

substrates in Caulobacter crescentus reveals a role for regulated proteolysis in bacterial development. *Mol Microbiol* 88: 1083–1092

Bianchi G & Ghobrial IM (2013) Molecular mechanisms of effectiveness of novel therapies in multiple myeloma. *Leuk Lymphoma* 54: 229–241

Bindea G, Mlecnik B, Hackl H, Charoentong P, Tosolini M, Kirilovsky A, Fridman WH, Pagès F, Trajanoski Z & Galon J (2009) ClueGO: a Cytoscape plug-in to decipher functionally grouped gene ontology and pathway annotation networks. *Bioinformatics* 25: 1091–1093

Birsoy K, Possemato R, Lorbeer FK, Bayraktar EC, Thiru P, Yucel B, Wang T, Chen WW, Clish CB & Sabatini DM (2014) Metabolic determinants of cancer cell sensitivity to glucose limitation and biguanides. *Nature* 508: 108–112

Bisikirska B, Bansal M, Shen Y, Teruya-Feldstein J, Chaganti R & Califano A (2016) Elucidation and Pharmacological Targeting of Novel Molecular Drivers of Follicular Lymphoma Progression. *Cancer Res* 76: 664–674

Bobrovnikova-Marjon E, Grigoriadou C, Pytel D, Zhang F, Ye J, Koumenis C, Cavener D & Diehl JA (2010) PERK promotes cancer cell proliferation and tumor growth by limiting oxidative DNA damage. *Oncogene* 29: 3881–3895

Boise LH, Kaufman JL, Bahlis NJ, Lonial S & Lee KP (2014) The Tao of myeloma. *Blood* 124: 1873–1879 doi:10.1182/blood-2014-05-578732 [PREPRINT]

Bolzoni M, Chiu M, Accardi F, Vescovini R, Airoldi I, Storti P, Todoerti K, Agnelli L, Missale G, Andreoli R, *et al* (2016) Dependence on glutamine uptake and glutamine addiction characterize myeloma cells: A new attractive target. *Blood* 128: 667–679

Böttcher T & Sieber SA (2008) Beta-lactones as specific inhibitors of ClpP attenuate the production of extracellular virulence factors of Staphylococcus aureus. *J Am Chem Soc* 130: 14400–14401

Brötz-Oesterhelt H, Beyer D, Kroll HP, Endermann R, Ladel C, Schroeder W, Hinzen B, Raddatz S, Paulsen H, Henninger K, *et al* (2005) Dysregulation of bacterial proteolytic machinery by a new class of antibiotics. *Nat Med* 11: 1082–1087

Carey BW, Finley LWS, Cross JR, Allis CD & Thompson CB (2014) Intracellular α-ketoglutarate maintains the pluripotency of embryonic stem cells. *Nat 2014 5187539* 518: 413–416

Castilla C, Congregado B, Conde JM, Medina R, Torrubia FJ, Japón MA & Sáez C (2010) Immunohistochemical Expression of Hsp60 Correlates With Tumor Progression and Hormone Resistance in Prostate Cancer. *Urology* 76: 1017.e1-1017.e6

Chandel NS, McClintock DS, Feliciano CE, Wood TM, Melendez JA, Rodriguez AM & Schumacker PT (2000) Reactive oxygen species generated at mitochondrial complex III stabilize hypoxia-inducible factor-1alpha during hypoxia: a mechanism of O2 sensing. *J Biol Chem* 275: 25130–25138

Chen A, Qian D, Wang B, Hu M, Lu J, Qi Y & Liu DX (2012) ATF5 is overexpressed in epithelial ovarian carcinomas and interference with its function increases apoptosis through the downregulation of Bcl-2 in SKOV-3 Cells. *Int J Gynecol Pathol* 31: 532–537

Chen Y, Lun ATL & Smyth GK (2016) From reads to genes to pathways: Differential expression analysis of RNA-Seq experiments using Rsubread and the edgeR quasi-likelihood pipeline. *F1000Research* 5

Chong J, Soufan O, Li C, Caraus I, Li S, Bourque G, Wishart DS & Xia J (2018) MetaboAnalyst 4.0: Towards more transparent and integrative metabolomics analysis. *Nucleic Acids Res* 46: W486–W494

Clasquin MF, Melamud E & Rabinowitz JD (2012) LC-MS data processing with MAVEN: A metabolomic analysis and visualization engine. *Curr Protoc Bioinforma* Chapter 14

Cole A, Wang Z, Coyaud E, Voisin V, Gronda M, Jitkova Y, Mattson R, Hurren R, Babovic S, Maclean N, *et al* (2015) Inhibition of the Mitochondrial Protease ClpP as a Therapeutic Strategy for Human Acute Myeloid Leukemia. *Cancer Cell* 27: 864–876

Cormio A, Musicco C, Gasparre G, Cormio G, Pesce V, Sardanelli AM & Gadaleta MN (2017) Increase in proteins involved in mitochondrial fission, mitophagy, proteolysis and antioxidant response in type I endometrial cancer as an adaptive response to respiratory complex I deficiency. *Biochem Biophys Res Commun* 491: 85–90

Dalva-Aydemir S, Bajpai R, Martinez M, Adekola KU, Kandela I, Wei C, Singhal S, Koblinski JE, Raje NS, Rosen ST, *et al* (2015) Targeting the metabolic plasticity of multiple myeloma with FDA-approved ritonavir and metformin. *Clin Cancer Res* 21: 1161–1171

Damerau K & St. John AC (1993) Role of Clp protease subunits in degradation of carbon starvation proteins in Escherichia coli. *J Bacteriol* 175: 53–63

Dang L, White DW, Gross S, Bennett BD, Bittinger MA, Driggers EM, Fantin VR, Jang HG, Jin S, Keenan MC, *et al* (2009) Cancer-associated IDH1 mutations produce 2-hydroxyglutarate. *Nature* 462: 739–744

Deng P & Haynes CM (2017) Mitochondrial dysfunction in cancer: Potential roles of ATF5 and the mitochondrial UPR. *Semin Cancer Biol* 47: 43–49

Dhir A, Dhir S, Borowski LS, Jimenez L, Teitell M, Rötig A, Crow YJ, Rice GI, Duffy D, Tamby C, *et al* (2018) Mitochondrial double-stranded RNA triggers antiviral signalling in humans. *Nature* 560: 238–242

Di K, Lomeli N, Wood SD, Vanderwal CD & Bota DA (2016) Mitochondrial Lon is over-expressed in high-grade gliomas, and mediates hypoxic adaptation: Potential role of Lon as a therapeutic target in glioma. *Oncotarget* 7: 77457–77467

Dluzen D, Li G, Tacelosky D, Moreau M & Liu DX (2011) BCL-2 is a downstream target of ATF5 that mediates the prosurvival function of ATF5 in a cell type-dependent manner. *J Biol Chem* 286: 7705–7713

Van Dobbenburgh OA, Houwen B, Jurjens H, Marrink J, Halie MR & Nieweg HO (1983) Plasma spermidine concentrations as early indication of response to therapy in human myeloma. *J Clin Pathol* 36: 804–807

Durie BGM, Salmon SE & Russell DH (1977) Polyamines as Markers of Response and Disease Activity in Cancer Chemotherapy. *Cancer Res* 37: 214–221

Ellis JM, Wong GW & Wolfgang MJ (2013) Acyl Coenzyme A Thioesterase 7 Regulates Neuronal Fatty Acid Metabolism To Prevent Neurotoxicity. 33: 1869–1882

Feng J, Michalik S, Varming AN, Andersen JH, Albrecht D, Jelsbak L, Krieger S, Ohlsen K, Hecker M, Gerth U, *et al* (2013) Trapping and proteomic identification of cellular substrates of the ClpP protease in staphylococcus aureus. *J Proteome Res* 12: 547–558

Fiorese CJ, Schulz AM, Lin YF, Rosin N, Pellegrino MW & Haynes CM (2016) The Transcription Factor ATF5 Mediates a Mammalian Mitochondrial UPR. *Curr Biol* 26: 2037–2043

Fischer F, Langer JD & Osiewacz HD (2015) Identification of potential mitochondrial CLPXP protease interactors and substrates suggests its central role in energy metabolism. *Sci Reports 2015 51* 5: 1–13

Fischer F, Weil A, Hamann A & Osiewacz HD (2013) Human CLPP reverts the longevity phenotype of a fungal ClpP deletion strain. *Nat Commun 2013 41* 4: 1–6

Fletcher MJ & Sanadi DR (1961) Turnover of rat-liver mitochondria. *Biochim Biophys Acta* 51: 356–360

Flynn JM, Neher SB, Kim YI, Sauer RT & Baker TA (2003) Proteomic discovery of cellular substrates of the ClpXP protease reveals five classes of ClpX-recognition signals. *Mol Cell* 11: 671–683

Fucci C, Resnati M, Riva E, Perini T, Ruggieri E, Orfanelli U, Paradiso F, Cremasco F, Raimondi A, Pasqualetto E, *et al* (2020) The Interaction of the Tumor Suppressor FAM46C with p62 and FNDC3 Proteins Integrates Protein and Secretory Homeostasis. *Cell Rep* 32: 108162

Gibellini L, Pinti M, Boraldi F, Giorgio V, Bernardi P, Bartolomeo R, Nasi M, De Biasi S, Missiroli S, Carnevale G, *et al* (2014) Silencing of mitochondrial Lon protease deeply impairs mitochondrial proteome and function in colon cancer cells. *FASEB J* 28: 5122–5135

Gispert S, Parganlija D, Klinkenberg M, Dröse S, Wittig I, Mittelbronn M, Grzmil P, Koob S, Hamann A, Walter M, *et al* (2013) Loss of mitochondrial peptidase Clpp leads to infertility, hearing loss plus growth retardation via accumulation of CLPX, mtDNA and inflammatory factors. *Hum Mol Genet* 22: 4871–4887

Greene LA, Lee HY & Angelastro JM (2009) The transcription factor ATF5: role in neurodevelopment and neural tumors. *J Neurochem* 108: 11–22

Gronauer TF, Mandl MM, Lakemeyer M, Hackl MW, Meßner M, Korotkov VS, Pachmayr J & Sieber SA (2018) Design and synthesis of tailored human caseinolytic protease P inhibitors. *Chem Commun (Camb)* 54: 9833–9836

Guha M, Fang JK, Monks R, Birnbaum MJ & Avadhani NG (2010) Activation of Akt is essential for the propagation of mitochondrial respiratory stress signaling and activation of the transcriptional coactivator heterogeneous ribonucleoprotein A2. *Mol Biol Cell* 21: 3578–3589

Guha M, Srinivasan S, Biswas G & Avadhani NG (2007) Activation of a novel calcineurin-mediated insulin-like growth factor-1 receptor pathway, altered metabolism, and tumor cell invasion in cells subjected to mitochondrial respiratory stress. *J Biol Chem* 282: 14536–14546

Gulla A & Anderson KC (2020) Multiple myeloma: the (r)evolution of current therapy and a glance into future. *Haematologica* 105: 2358–2367

Gulla A, Morelli E, Samur MK, Botta C, Hideshima T, Bianchi G, Fulciniti M, Malvestiti S, Prabhala RH, Talluri S, *et al* (2021) Bortezomib induces anti-multiple myeloma immune response mediated by cGAS/STING pathway activation. *Blood cancer Discov* 2: 468–483

Hamelin C, Cornut E, Poirier F, Pons S, Beaulieu C, Charrier JP, Haïdous H, Cotte E, Lambert C, Piard F, *et al* (2011) Identification and verification of heat shock protein 60 as a potential serum marker for colorectal cancer. *FEBS J* 278: 4845–4859

Hofsetz E, Demir F, Szczepanowska K, Kukat A, Kizhakkedathu JN, Trifunovic A & Huesgen PF (2020) The Mouse Heart Mitochondria N Terminome Provides Insights into ClpXP-Mediated Proteolysis. 19: 1330–1345

Horibe T & Hoogenraad NJ (2007) The Chop gene contains an element for the positive regulation of the mitochondrial unfolded protein response. *PLoS One* 2: e835

Hulsen T, de Vlieg J & Alkema W (2008) BioVenn - A web application for the comparison and visualization of biological lists using area-proportional Venn

diagrams. *BMC Genomics* 9: 1–6
Hurt EM, Wiestner A, Rosenwald A, Shaffer AL, Campo E, Grogan T, Bergsagel PL, Kuehl WM & Staudt LM (2004) Overexpression of c-maf is a frequent oncogenic event in multiple myeloma that promotes proliferation and pathological interactions with bone marrow stroma. *Cancer Cell* 5: 191–199
Iadevaia V, Liu R & Proud CG (2014) mTORC1 signaling controls multiple steps in ribosome biogenesis. *Semin Cell Dev Biol* 36: 113–120
Ishizawa J, Zarabi SF, Davis RE, Halgas O, Nii T, Jitkova Y, Zhao R, St-Germain J, Heese LE, Egan G, *et al* (2019) Mitochondrial ClpP-Mediated Proteolysis Induces Selective Cancer Cell Lethality. *Cancer Cell* 35: 721–737
Jenal U & Fuchs T (1998) An essential protease involved in bacterial cell-cycle control. *EMBO J* 17: 5658–5669
Jenkinson EM, Rehman AU, Walsh T, Clayton-Smith J, Lee K, Morell RJ, Drummond MC, Khan SN, Naeem MA, Rauf B, *et al* (2013) Perrault syndrome is caused by recessive mutations in CLPP, encoding a mitochondrial ATP-dependent chambered protease. *Am J Hum Genet* 92: 605–613
Kang SG, Dimitrova MN, Ortega J, Ginsburg A & Maurizi MR (2005) Human mitochondrial ClpP is a stable heptamer that assembles into a tetradecamer in the presence of ClpX. *J Biol Chem* 280: 35424–35432
Karpel-Massler G, Horst BA, Shu C, Chau L, Tsujiuchi T, Bruce JN, Canoll P, Greene LA, Angelastro JM & Siegelin MD (2016) A Synthetic Cell-Penetrating Dominant-Negative ATF5 Peptide Exerts Anticancer Activity against a Broad Spectrum of Treatment-Resistant Cancers. *Clin Cancer Res* 22: 4698–4711
Kenny TC, Craig AJ, Villanueva A & Germain D (2019) Mitohormesis Primes Tumor Invasion and Metastasis. *Cell Rep* 27: 2292–2303
Kenny TC & Germain D (2017) From discovery of the CHOP axis and targeting ClpP to the identification of additional axes of the UPRmt driven by the estrogen receptor and SIRT3. *J Bioenerg Biomembr* 49: 297–305
Kim SH, Forman AP, Mathews MB & Gunnery S (2000) Human breast cancer cells contain elevated levels and activity of the protein kinase, PKR. *Oncogene* 19: 3086–3094
Kim SH, Gunnery S, Choe JK & Mathews MB (2002) Neoplastic progression in melanoma and colon cancer is associated with increased expression and activity of the interferon-inducible protein kinase, PKR. *Oncogene* 21: 8741–8748
Koppen M & Langer T (2007) Protein degradation within mitochondria: versatile activities of AAA proteases and other peptidases. *Crit Rev Biochem Mol Biol* 42: 221–242
Kristinsson SY, Anderson WF & Landgren O (2014) Improved long-term survival in multiple myeloma up to the age of 80 years. *Leukemia* 28: 1346–1348
Kucej M & Butow RA (2007) Evolutionary tinkering with mitochondrial nucleoids. *Trends Cell Biol* 17: 586–592
Kumar SK, Dispenzieri A, Lacy MQ, Gertz MA, Buadi FK, Pandey S, Kapoor P, Dingli D, Hayman SR, Leung N, *et al* (2014) Continued improvement in survival in multiple myeloma: changes in early mortality and outcomes in older patients. *Leukemia* 28: 1122–1128
Kumar SK, Rajkumar V, Kyle RA, Van Duin M, Sonneveld P, Mateos MV, Gay F & Anderson KC (2017) Multiple myeloma. *Nat Rev Dis Prim* 3: 1–20
Lagadinou ED, Sach A, Callahan K, Rossi RM, Neering SJ, Minhajuddin M, Ashton JM,

Pei S, Grose V, O'Dwyer KM, *et al* (2013) BCL-2 Inhibition Targets Oxidative Phosphorylation and Selectively Eradicates Quiescent Human Leukemia Stem Cells. *Cell Stem Cell* 12: 329–341

Lee J V., Carrer A, Shah S, Snyder NW, Wei S, Venneti S, Worth AJ, Yuan ZF, Lim HW, Liu S, *et al* (2014) Akt-Dependent Metabolic Reprogramming Regulates Tumor Cell Histone Acetylation. *Cell Metab* 20: 306–319

Li G, Xu Y, Guan D, Liu Z & Liu DX (2011) HSP70 Protein Promotes Survival of C6 and U87 Glioma Cells by Inhibition of ATF5 Degradation. *J Biol Chem* 286: 20251–20259

Li N, Lopez MA, Linares M, Kumar S, Oliva S, Martinez-Lopez J, Xu L, Xu Y, Perini T, Senapedis W, *et al* (2019) Dual PAK4-NAMPT inhibition impacts growth and survival, and increases sensitivity to DNA-damaging agents in Waldenstrom macroglobulinemia. *Clin Cancer Res* 25: 369–377

Liu H, Colavitti R, Rovira II & Finkel T (2005) Redox-dependent transcriptional regulation. *Circ Res* 97: 967–974

Liu K, Ologbenla A & Houry WA (2014) Dynamics of the ClpP serine protease: a model for self-compartmentalized proteases. *Crit Rev Biochem Mol Biol* 49: 400–412

Lowth BR, Kirstein-Miles J, Saiyed T, Brötz-Oesterhelt H, Morimoto RI, Truscott KN & Dougan DA (2012) Substrate recognition and processing by a Walker B mutant of the human mitochondrial AAA+ protein CLPX. *J Struct Biol* 179: 193–201

Ludwig H, Novis Durie S, Meckl A, Hinke A & Durie B (2020) Multiple Myeloma Incidence and Mortality Around the Globe; Interrelations Between Health Access and Quality, Economic Resources, and Patient Empowerment. *Oncologist* 25: e1406–e1413

Luo J, Zeng B, Tao C, Lu M & Ren G (2020) ClpP regulates breast cancer cell proliferation, invasion and apoptosis by modulating the Src/PI3K/Akt signaling pathway. *PeerJ* 2020: e8754

Mabanglo MF, Bhandari V & Houry WA (2022) Substrates and interactors of the ClpP protease in the mitochondria. *Curr Opin Chem Biol* 66: 102078

Madarampalli B, Yuan Y, Liu D, Lengel K, Xu Y, Li G, Yang J, Liu X, Lu Z & Liu DX (2015) ATF5 Connects the Pericentriolar Materials to the Proximal End of the Mother Centriole. *Cell* 162: 580–592

Madeo F, Eisenberg T, Pietrocola F & Kroemer G (2018) Spermidine in health and disease. *Science* 359: 63–54

Marlein CR, Piddock RE, Mistry JJ, Zaitseva L, Hellmich C, Horton RH, Zhou Z, Auger MJ, Bowles KM & Rushworth SA (2019) CD38-Driven Mitochondrial Trafficking Promotes Bioenergetic Plasticity in Multiple Myeloma. *Cancer Res* 79: 2285–2297

Matsushima Y, Hirofuji Y, Aihara M, Yue S, Uchiumi T, Kaguni LS & Kang D (2017) Drosophila protease ClpXP specifically degrades DmLRPPRC1 controlling mitochondrial mRNA and translation. *Sci Rep* 7:8315

Maura F, Bolli N, Angelopoulos N, Dawson KJ, Leongamornlert D, Martincorena I, Mitchell TJ, Fullam A, Gonzalez S, Szalat R, *et al* (2019) Genomic landscape and chronological reconstruction of driver events in multiple myeloma. *Nat Commun* 10: 3835

McBrayer SK, Cheng JC, Singhal S, Krett NL, Rosen ST & Shanmugam M (2012) Multiple myeloma exhibits novel dependence on GLUT4, GLUT8, and GLUT11: implications for glucose transporter-directed therapy. *Blood* 119: 4686–4697

Milan E, Perini T, Resnati M, Orfanelli U, Oliva L, Raimondi A, Cascio P, Bachi A,

Marcatti M, Ciceri F, *et al* (2015b) A plastic SQSTM1/p62-dependent autophagic reserve maintains proteostasis and determines proteasome inhibitor susceptibility in multiple myeloma cells. *Autophagy* 11: 1161–1178

Mirali S & Schimmer AD (2020) The role of mitochondrial proteases in leukemic cells and leukemic stem cells. *Stem Cells Transl Med* 9: 1481–1487

Monaco SE, Angelastro JM, Szabolcs M & Greene LA (2007) The transcription factor ATF5 is widely expressed in carcinomas, and interference with its function selectively kills neoplastic, but not nontransformed, breast cell lines. *Int J Cancer* 120: 1883–1890

Morgan GJ, Walker BA & Davies FE (2012) The genetic architecture of multiple myeloma. *Nat Rev Cancer* 12: 335–348

Na Y, Kaul SC, Ryu J, Lee JS, Ahn HM, Kaul Z, Kalra RS, Li L, Widodo N, Yun CO, *et al* (2016) Stress Chaperone Mortalin Contributes to Epithelial-to-Mesenchymal Transition and Cancer Metastasis. *Cancer Res* 76: 2754–2765

Nakamura K, Smyth MJ & Martinet L (2020) Cancer immunoediting and immune dysregulation in multiple myeloma. *Blood* 136: 2731–2740

Nargund AM, Pellegrino MW FC et al (2012) Mitochondial Import Efficiency of ATFS-1 Regulates Mitochondrial UPR activation. *Science* 337: 587–590

Nargund AM, Fiorese CJ, Pellegrino MW, Deng P & Haynes CM (2015) Mitochondrial and Nuclear Accumulation of the Transcription Factor ATFS-1 Promotes OXPHOS Recovery during the UPRmt. *Mol Cell* 58: 123–133

Nemkov T, Hansen KC & D'Alessandro A (2017) A three-minute method for high-throughput quantitative metabolomics and quantitative tracing experiments of central carbon and nitrogen pathways. *Rapid Commun Mass Spectrom* 31: 663–673

Nouri K, Feng Y & Schimmer AD (2020) Mitochondrial ClpP serine protease-biological function and emerging target for cancer therapy. *Cell Death Dis* 11: 841

Nowicki S & Gottlieb E (2015) Oncometabolites: tailoring our genes. *FEBS J* 282: 2796–2805

Nukuda A, Endoh H, Yasuda M, Mizutani T, Kawabata K & Haga H (2016) Role of ATF5 in the invasive potential of diverse human cancer cell lines. *Biochem Biophys Res Commun* 474: 509–514

Nutt SL, Hodgkin PD, Tarlinton DM & Corcoran LM (2015) The generation of antibody-secreting plasma cells. *Nat Rev Immunol* 15: 160–171

Oliva L, Orfanelli U, Resnati M, Raimondi A, Orsi A, Milan E, Palladini G, Milani P, Cerruti F, Cascio P, *et al* (2017) The amyloidogenic light chain is a stressor that sensitizes plasma cells to proteasome inhibitor toxicity. *Blood* 129: 2132–2142

Ortiz-Ruiz A, Ruiz-Heredia Y, Morales ML, Aguilar-Garrido P, García-Ortiz A, Valeri A, Bárcena C, García-Martin RM, Garrido V, Moreno L, *et al* (2021) Myc-Related Mitochondrial Activity as a Novel Target for Multiple Myeloma. *Cancers (Basel)* 13: 1662

Ou L, Zhang A, Cheng Y & Chen Y (2021) The cGAS-STING Pathway: A Promising Immunotherapy Target. *Front Immunol* 12: 795048

Pellegrino MW, Nargund AM, Kirienko N V., Gillis R, Fiorese CJ & Haynes CM (2014) Mitochondrial UPR-regulated innate immunity provides resistance to pathogen infection. *Nat 2014 5167531* 516: 414–417

Pringle ES, McCormick C & Cheng Z (2019) Polysome Profiling Analysis of mRNA and Associated Proteins Engaged in Translation. *Curr Protoc Mol Biol* 125: e79

Puleston DJ, Buck MD, Klein Geltink RI, Kyle RL, Caputa G, O'Sullivan D, Cameron

AM, Castoldi A, Musa Y, Kabat AM, *et al* (2019) Polyamines and eIF5A Hypusination Modulate Mitochondrial Respiration and Macrophage Activation. *Cell Metab* 30: 352–363

Pyeon D, Vu L, Giacobbi NS & Westrich JA (2020) The antiviral immune forces awaken in the cancer wars. *PLoS Pathog* 16: e1008814

Quirós PM, Langer T & López-Otín C (2015) New roles for mitochondrial proteases in health, ageing and disease. *Nat Rev Mol Cell Biol* 16: 345–359

Rabinowitz M (1973) Protein synthesis and turnover in normal and hypertrophied heart. *Am J Cardiol* 31: 202–210

Rajkumar SV, Dimopoulos MA, Palumbo A, Blade J, Merlini G, Mateos M-V, Kumar S, Hillengass J, Kastritis E, Richardson P, *et al* (2014) International Myeloma Working Group updated criteria for the diagnosis of multiple myeloma. *Lancet Oncol* 15: e538–e548

Rath S, Sharma R, Gupta R, Ast T, Chan C, Durham TJ, Goodman RP, Grabarek Z, Haas ME, Hung WHWW, *et al* (2021) MitoCarta3.0: an updated mitochondrial proteome now with sub-organelle localization and pathway annotations. *Nucleic Acids Res* 49: D1541–D1547

Ristow M & Zarse K (2010) How increased oxidative stress promotes longevity and metabolic health: The concept of mitochondrial hormesis (mitohormesis). *Exp Gerontol* 45: 410–418

Ruiz-Heredia Y, Ortiz-Ruiz A, Samur MK, Garrido V, Rufian L, Sanchez R, Aguilar-Garrido P, Barrio S, Martín MA, Bolli N, *et al* (2021) Pathogenetic and prognostic implications of increased mitochondrial content in multiple myeloma. *Cancers (Basel)* 13: 3189

Ryu J, Kaul Z, Yoon AR, Liu Y, Yaguchi T, Na Y, Ahn HM, Gao R, Choi IK, Yun CO, *et al* (2014) Identification and functional characterization of nuclear mortalin in human carcinogenesis. *J Biol Chem* 289: 24832–24844

Sanjana NE, Shalem O & Zhang F (2014) Improved vectors and genome-wide libraries for CRISPR screening. *Nat Methods* 11: 783–784

Sarin V, Yu K, Ferguson ID, Gugliemini O, Nix MA, Hann B, Sirota M & Wiita AP (2020) Evaluating the efficacy of multiple myeloma cell lines as models for patient tumors via transcriptomic correlation analysis. *Leukemia* 34: 2754–2765

Seo JH, Rivadeneira DB, Caino MC, Chae YC, Speicher DW, Tang HY, Vaira V, Bosari S, Palleschi A, Rampini P, *et al* (2016) The Mitochondrial Unfoldase-Peptidase Complex ClpXP Controls Bioenergetics Stress and Metastasis. *PLoS Biol* 14: e1002507

Sheng Z, Li L, Zhu LJ, Smith TW, Demers A, Ross AH, Moser RP & Green MR (2010) A genome-wide RNA interference screen reveals an essential CREB3L2-ATF5-MCL1 survival pathway in malignant glioma with therapeutic implications. *Nat Med* 16: 671–677

Shou Y, Martelli ML, Gabrea A, Qi Y, Brents LA, Roschke A, Dewald G, Kirsch IR, Bergsagel PL & Kuehl WM (2000) Diverse karyotypic abnormalities of the c-myc locus associated with c-myc dysregulation and tumor progression in multiple myeloma. *Proc Natl Acad Sci U S A* 97: 228–233

Shpilka T & Haynes CM (2018) The mitochondrial UPR: mechanisms, physiological functions and implications in ageing. *Nat Rev Mol Cell Biol* 19: 109–120

Siegel RL, Miller KD & Jemal A (2016) Cancer statistics, 2016. *CA Cancer J Clin* 66: 7–30

Siira SJ, Spåhr H, Shearwood AMJ, Ruzzenente B, Larsson NG, Rackham O & Filipovska A (2017) LRPPRC-mediated folding of the mitochondrial transcriptome. *Nat Commun* 8: 1–11

Škrtić M, Sriskanthadevan S, Jhas B, Gebbia M, Wang X, Wang Z, Hurren R, Jitkova Y, Gronda M, Maclean N, *et al* (2011) Inhibition of Mitochondrial Translation as a Therapeutic Strategy for Human Acute Myeloid Leukemia. *Cancer Cell* 20: 674–688

Snider J, Wang D, Bogenhagen DF & Haley JD (2019) Pulse SILAC Approaches to the Measurement of Cellular Dynamics. *Adv Exp Med Biol* 1140: 575–583

Subramanian A, Tamayo P, Mootha VK, Mukherjee S, Ebert BL, Gillette MA, Paulovich A, Pomeroy SL, Golub TR, Lander ES, *et al* (2005) Gene set enrichment analysis: a knowledge-based approach for interpreting genome-wide expression profiles. *Proc Natl Acad Sci U S A* 102: 15545–50

Szalat R, Samur MK, Fulciniti M, Lopez M, Nanjappa P, Cleynen A, Wen K, Kumar S, Perini T, Calkins AS, *et al* (2018) Nucleotide excision repair is a potential therapeutic target in multiple myeloma. *Leukemia* 32: 111–119

Szczepanowska K, Maiti P, Kukat A, Hofsetz E, Nolte H, Senft K, Becker C, Ruzzenente B, Hornig-Do H, Wibom R, *et al* (2016) CLPP coordinates mitoribosomal assembly through the regulation of ERAL1 levels. *EMBO J* 35: 2566–2583

Szczepanowska K, Senft K, Heidler J, Herholz M, Kukat A, Höhne MN, Hofsetz E, Becker C, Kaspar S, Giese H, *et al* (2020) A salvage pathway maintains highly functional respiratory complex I. *Nat Commun* 11: 1643

Szczepanowska K & Trifunovic A (2021a) Mitochondrial matrix proteases: quality control and beyond. *FEBS J* doi:10.1111/febs.15964

Szczepanowska K & Trifunovic A (2021b) Tune instead of destroy: How proteolysis keeps OXPHOS in shape. *Biochim Biophys Acta - Bioenerg* 1862: 148365

Szklarczyk D, Gable AL, Lyon D, Junge A, Wyder S, Huerta-Cepas J, Simonovic M, Doncheva NT, Morris JH, Bork P, *et al* (2019) STRING v11: protein-protein association networks with increased coverage, supporting functional discovery in genome-wide experimental datasets. *Nucleic Acids Res* 47: D607–D613

Tan J, Grouleff JJ, Jitkova Y, Diaz DB, Griffith EC, Shao W, Bogdanchikova AF, Poda G, Schimmer AD, Lee RE, *et al* (2019) De Novo Design of Boron-Based Peptidomimetics as Potent Inhibitors of Human ClpP in the Presence of Human ClpX. *J Med Chem* 62: 6377–6390

Tellier J & Nutt SL (2019) Plasma cells: The programming of an antibody-secreting machine. *Eur J Immunol* 49: 30–37

Tian F, Wang C, Tang M, Li J, Cheng X, Zhang S, Ji D, Huang Y & Li H (2016) The antibiotic chloramphenicol may be an effective new agent for inhibiting the growth of multiple myeloma. *Oncotarget* 7: 51934–51942

Tigano M, Vargas DC, Tremblay-Belzile S, Fu Y & Sfeir A (2021) Nuclear sensing of breaks in mitochondrial DNA enhances immune surveillance. *Nature* 591: 477–481

Torres-Odio S, Lei Y, Gispert S, Maletzko A, Key J, Menissy SS, Wittig I, Auburger G & West AP (2021) Loss of Mitochondrial Protease CLPP Activates Type I IFN Responses through the Mitochondrial DNA-cGAS-STING Signaling Axis. *J Immunol* 206: 1890–1900

Vyas S, Zaganjor E & Haigis MC (2016) Mitochondria and Cancer. *Cell* 166: 555–566

Wadhwa R, Takano S, Kaur K, Deocaris CC, Pereira-Smith OM, Reddel RR & Kaul SC (2006) Upregulation of mortalin/mthsp70/Grp75 contributes to human

carcinogenesis. *Int J Cancer* 118: 2973–2980

Waldschmidt JM, Kloeber JA, Anand P, Frede J, Kokkalis A, Dimitrova V, Potdar S, Nair MS, Vijaykumar T, Im NG, *et al* (2021) Single-Cell Profiling Reveals Metabolic Reprogramming as a Resistance Mechanism in BRAF-Mutated Multiple Myeloma. *Clin Cancer Res* 27: 6432–6444

Walker BA, Wardell CP, Brioli A, Boyle E, Kaiser MF, Begum DB, Dahir NB, Johnson DC, Ross FM, Davies FE, *et al* (2014) Translocations at 8q24 juxtapose MYC with genes that harbor superenhancers resulting in overexpression and poor prognosis in myeloma patients. *Blood Cancer J* 4: e191

Wallace DC (2012) Mitochondria and cancer. *Nat Rev Cancer 2012 1210* 12: 685–698

Warburg O (1956) On the origin of cancer cells. *Science* 123: 309–314

Weinberg F, Hamanaka R, Wheaton WW, Weinberg S, Joseph J, Lopez M, Kalyanaraman B, Mutlu GM, Budinger GRS & Chandel NS (2010) Mitochondrial metabolism and ROS generation are essential for Kras-mediated tumorigenicity. *Proc Natl Acad Sci U S A* 107: 8788–8793

Weinhouse S (1956) On Respiratory Impairment in Cancer Cells. *Science (80-)* 124: 267–269

Wellen KE, Hatzivassiliou G, Sachdeva UM, Bui T V., Cross JR & Thompson CB (2009) ATP-citrate lyase links cellular metabolism to histone acetylation. *Science* 324: 1076–1080

Wong KS, Mabanglo MF, Seraphim T V., Mollica A, Mao YQ, Rizzolo K, Leung E, Moutaoufik MT, Hoell L, Phanse S, *et al* (2018) Acyldepsipeptide Analogs Dysregulate Human Mitochondrial ClpP Protease Activity and Cause Apoptotic Cell Death. *Cell Chem Biol* 25: 1017–1030

Xiang Y, Fang B, Liu Y, Yan S, Cao D, Mei H, Wang Q, Hu Y & Guo T (2020) SR18292 exerts potent antitumor effects in multiple myeloma via inhibition of oxidative phosphorylation. *Life Sci* 256

Xing L, Wang S, Liu J, Yu T, Chen H, Wen K, Li Y, Lin L, Hsieh PA, Cho SF, *et al* (2021) BCMA-Specific ADC MEDI2228 and Daratumumab Induce Synergistic Myeloma Cytotoxicity via IFN-Driven Immune Responses and Enhanced CD38 Expression. *Clin Cancer Res* 27: 5376–5388

Xu Y, Fulciniti M, Samur MK, Ho M, Deng S, Liu L, Wen K, Yu T, Chyra Z, Dereibal S, *et al* (2020) YWHAE/14-3-3e expression impacts the protein load, contributing to proteasome inhibitor sensitivity in multiple myeloma. *Blood* 136: 468–479

Yamada J, Kurata A, Hirata M, Taniguchi T, Takama H, Furihata T, Shiratori K, Iida N, Takagi-Sakuma M, Watanabe T, *et al* (1999) Purification, molecular cloning, and genomic organization of human brain long-chain acyl-CoA hydrolase. *J Biochem* 126: 1013–1019

Ye J, Kumanova M, Hart LS, Sloane K, Zhang H, De Panis DN, Bobrovnikova-Marjon E, Diehl JA, Ron D & Koumenis C (2010) The GCN2-ATF4 pathway is critical for tumour cell survival and proliferation in response to nutrient deprivation. *EMBO J* 29: 2082–2096

Yi X, Luk JM, Lee NP, Peng J, Leng X, Guan XY, Lau GK, Beretta L & Fan ST (2008) Association of mortalin (HSPA9) with liver cancer metastasis and prediction for early tumor recurrence. *Mol Cell Proteomics* 7: 315–325

Yun J & Finkel T (2014) Mitohormesis. *Cell Metab* 19: 757–766

Zhang H & Simon AK (2020) Polyamines reverse immune senescence via the translational control of autophagy. *Autophagy* 16: 181–182

Zhao Q, Wang J, Levichkin I V., Stasinopoulos S, Ryan MT & Hoogenraad NJ (2002) A mitochondrial specific stress response in mammalian cells. *EMBO J* 21: 4411–4419

Zhou D, Palam LR, Jiang L, Narasimhan J, Staschke KA & Wek RC (2008) Phosphorylation of eIF2 directs ATF5 translational control in response to diverse stress conditions. *J Biol Chem* 283: 7064–7073